# Microscopic View of Charge Transport in Molecular Organic Semiconductors

A thesis submitted for the degree of

*Doctor of Philosophy*

**Varsha Rani**

**School of Physical Sciences**

**Jawaharlal Nehru University**

**New Delhi, India**

**July, 2017**

*To my family...*

# Declaration

I hereby declare that the contents of this thesis entitled "Microscopic View of Charge Transport in Molecular Organic Semiconductors", are original and have not been submitted in whole or in part for consideration for any other degree, diploma, associateship or qualification in this or any other University. This thesis is the result of my own work, carried out in School of Physical Sciences, Jawaharlal Nehru University, New Delhi, under supervision of Prof. Subhasis Ghosh.

July, 2017

**Varsha Rani**

**Prof. Subhasis Ghosh**
Thesis Supervisor
School of Physical Sciences
Jawaharlal Nehru University
New Delhi - 110067

**Prof. Riddhi Shah**
Dean
School of Physical Sciences
Jawaharlal Nehru University
New Delhi - 110067

# Acknowledgements

After about six years of work on this thesis, It's a time to thank all the persons without whom it would have not been possible. First of all, I would like to express my sincere gratitude to my supervisor, Prof. Subhasis Ghosh for giving me the opportunity to work on charge transport properties of organic semiconductors and providing an excellent research laboratory. I am severely thankful to him for his guidance, motivational words and relevant support. I respect him from my heart for his knowledge and passion for research. He always encourages the students to go forward and to achieve their academic goals.

I would also like to thank all the other faculty members in the SPS, JNU for their co-operation and attention during my Ph.D days. Special thanks go to Prof. S. Sarkar, Prof. P. Mukhopadyay and Dr. N. Ray for their assistance in my research work. I am also thankful to Dr. T. Mohanty, Prof. A. Pandey, Prof. S. P. Das and Prof. S. Patnaik for teaching me during the course work of Ph.D. I would like to acknowledge the Advanced Instrumentation Research Facility (AIRF) staff, for providing experimental facility. I feel a great pleasure to acknowledge the simulation lab of AIRF where I ran some MD simulations and other programs.

I would like to express my regards to all the past and present members of SPS, JNU. Its a great pleasure to thank seniors of my lab, Dr. Budhi Singh, Dr. Akanksha Sharma, Dr. Sarita Yadav, Dr. Pawan Kumar Srivastava for their co-operation and help. They helped me several times with experiments during my early days of Ph.D. I would also thank to my senior Dr. Pramod Kumar for his help through emails. I am really impressed by dedication and strong determination of all the seniors towards getting some novel results in research. I would also like to thank Dr. Ravi Prakash and Dr Vishal Maurya alomg with all the other seniors of SPS for their help and co-opertion during my Ph.D. Tenure.

I also thank to my lab mates Dr. Chandrabhan, Premlata, Nasir, Jeetendra, Harish, Birendra, Dhirendra, Nirmal and Isha for their support and help. I cordially thank my all the batch mates, Anshu, Jyotsna, Nidhi, Girish, Prasenjit

for the memorizable moments, we spent together. It's a great pleasure to thank Jyoti, Him Shweta, Sudhir, Kalyan, Shravan, Yogendra, Renu, Jyoti, Prakriti and all the other students of SPS for their support and friendship. I would also like to thank Santosh for providing me nice tea, coffee and snacks.

I would like to pay my deepest regards to my family members for their unflagging love and support throughout my life; this thesis was simply impossible without them. Thanks to my mother, two sisters, brothers in law and my brother for their sacrifices and efforts towards my carrier. I really feel blessed to have such a kind hearted and supportive mother in law who always raised my enthusiasm and didn't let me miss my own mother at home. I can't forget the inspiration and patience that I got from my loving and caring husband, Abhay. I owe a special thank to Abhay for being a fantastic partner and wonderful person. I can't express in words what I feel for my father and father in law. I just wish that they would have been with me at this time.

Finally, I gratefully acknowledge the university grant commission (UGC), India for providing the financial support during the Ph.D. I also pay my regards to Department of Science and Technology (DST), India for providing me financial support to attend an international conference in USA.

# Publications

## Published

1. *"Understanding the dependence of transport parameters on carrier concentration within a Gaussian density of states in molecular organic semiconductors"* Akanksha Sharma, Pramod Kumar, **Varsha Rani**, Nirat Ray and Subhasis Ghosh, **Journal of Physics Condensed Matter 28**, 235802 (2016).

2. *"Controlled doping in graphene monolayers by trapping organic molecules at the graphenesubstrate interface"* Pawan Kumar Srivastava, Premlata Yadav, **Varsha Rani**, and Subhasis Ghosh, **ACS Applied Material & Interfaces 9**, 5375 (2017).

3. *"Morphology of self assembled monolayers using liquid phase reaction on silica and their effect on the morphology of adsorbed insulin"* Indu Sharma, Sudip K. Pattanayek, **Varsha Aggarwal** and Subhasis Ghosh, **Applied Surface Science 405**, 503 (2017).

4. *"Assorted morphosynthesis: access to multi-faceted nano-architectures from a super-responsive dual p-functional amphiphilic construct"* Deepak Asthana, Jyoti Shukla, Srikanta Dana, **Varsha Rani**, M. R. Ajayakumar, Kamla Rawat, Kalyanashis Mandal, Premlata Yadav, Subhasis Ghosh and Pritam Mukhopadhyay, **Chemical Communication 51**, 15237 (2015).

## Submitted

1. *"Charge transport mechanism in polycrystalline organic thin films with and without traps"* Varsha Rani, Akanksha Sharma, Pramod Kumar, Budhi Singh and Subhasis Ghosh, (In **Journal of Material Chemistry C**).

2. *"Field driven hopping to band-like transport in molecular organic semiconductors"* **Varsha Rani**, Pramod Kumar, Akanksha Sharma, Sarita yadav, Nirat Ray and Subhasis Ghosh ( In **Physical Review Letter**).

## Under Preparation

1. *"Microscopic origin of charge transport in pentacene."*
2. *"Role of microscopic molecular parameters on charge carrier mobility in phthalocyanines."*
3. *"How to determine diffusion coefficients in organic semiconductors?"*

# Conference Proceedings

1. "*What could be the Highest Hopping Mobility in Organic Thin-Film Transistors?*" **Varsha Rani**, Akanksha Sharma and Subhasis Ghosh, MRS Advances, 1, 2659-2664 (2016).

2. "*Determination of diffusion coefficient in disordered organic semiconductors*" **Varsha Rani**, Akanksha Sharma and Subhasis Ghosh, AIP Conference Proceedings 1728, 020265 (2016).

3. "*Charge Carrier Transport in Polycrystalline Organic Thin Film Based Field Effect Transistors*" **Varsha Rani**, Akanksha Sharma and Subhasis Ghosh, AIP Conf. Proc. 1731, 120027 (2016).

4. "*Organic Schottky Diode: Characterization of Traps*" **Varsha Rani**, Sarita Yadav and Subhasis Ghosh, AIP Conf. Proc. 1665, 120023 (2015).

5. "*What Decides the Mobility of Small Molecule-based Organic Semiconductors in Organic Thin Film Transistors?*" **Varsha Rani**, Sarita Yadav, Akanksha Sharma and Subhasis Ghosh, Proc. IEEEXplore, International Conference on Emerging Electronics, PP-1, 2014).

6. "*Pattern Formation in Organic Thin Films*" **Varsha Rani**, Akanksha Sharma and Subhasis Ghosh., Proc. IJERT, National Conference on Multifunctional Advanced Materials, 49(2013).

# Contents

# Chapter 1

# Introduction

Organic semiconductors have been continuously attracting the scientific communities due to their many potential applications such as large area display, light weight electronics, flexible and wearable electronic devices. In this chapter, we discuss the applications of organic electronics in commercial products, structure and characteristic features of organic semiconductors and mechanism of charge transport in them. Finally, organization of thesis has been discussed.

## 1.1 Background and motivation

After the demonstrations of first organic field effect transistor (OFET) in 1986 by A. Tsumara et al. [1] and first organic light emitting diode (OLED) in 1987 by Tang and Van Slyke [2], a new field of research, "organic electronics" emerged in front of scientific communities. Since then researchers of many fields have put great efforts towards understanding the physics and chemistry of organic semiconductors. Chemists investigated the chemical properties of organic semiconductors to identify the promising compounds and developed new synthetic routes to improve the efficiency of organic devices. Physicists also put their efforts towards increasing the device efficiency by investigating the mechanism of charge transport and introducing new concepts. These semiconductors could be successfully used in fabrication of a variety of electronic and optoelectronic devices such as transistors, diodes, sensors, solar cells, light emitting devices etc. Today, organic semiconductors have got a strong position in commercial world of electronic and optoelectronic devices. A wide range of products and technologies based on organic electronics which are used in todays electronic appliances are shown in Fig. 1.1. Some interesting properties of organic devices including solution-processability, mechanical flexibility, emission of different colors, transparency make them superior to inorganic devices. Nowadays, these properties have been used extensively in commercial products like wearable electronics [3], rollable [4] and e-paints. Transparent devices are also in progress. Applications of organic semiconductors have been shown in large number of electronic appliances by several companies such as Sony, Phillips, LG etc. Some recently developed products based on organic electronics have been summarized in Fig. 1.2. In 2007, Sony developed world's first OLED TV, named XEL-1 [5]. Front and side views of XEL-1 have been shown in Fig. 1.2(a). It is only 3 mm thick and has a screen size of 11". Fig. 1.2(b) shows thin, cheap and flexible device that can be used as a band aid plaster [6]. It can be easily attached to the skin. Applications of flexible and thin organic devices have been seen in medical field also. Recently, LG display declared that it got the success in developing a 77" flexible and transparent OLED display with a resolution of $3840 \times 2160$ and transparency of 40% [7]. Smart desk could be a future application of this display (Fig. 1.2(c) ). Further, Samsung developed a large flexible and bendable TV screen having the width of

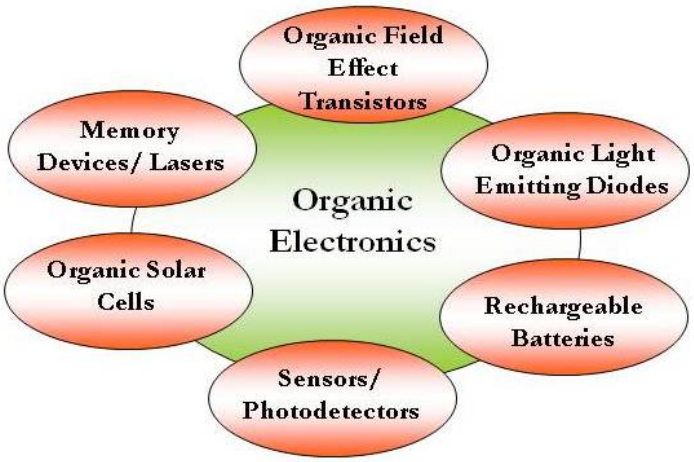


*Figure 1.1: Representation of the wide range of devices and technologies based on organic electronics*

105" (Fig. 1.2(d) ) [8]. As our lives are becoming more and more dependent on the electronic devices, electronic waste is an issue of concern. Stanford researchers developed a flexible and biodegradable organic semiconductor. Fig. 1.2(e) shows a biodegradable and flexible semiconductor that can also be appended to rough surfaces and can biodegrade to nontoxic products [9]. In Fig. 1.2(f), a pulse oximeter sensor based on organic optoelectronics has been shown [6]. It uses red and green OLEDs which are detected by organic photodiode.

In spite of spectacular research and developments in the field of organic electronics, our understanding of charge carrier transport in different organic systems remains incomplete and still a matter of debate and remains a bottle neck for development of organic based integrated circuits. For example, correlating chemical structure to charge transport is a missing link in the present understanding of charge carrier mobility in organic system. The motivation of this work is four folds: (i) to reduce the traps in organic thin films as much as possible in order to optimize the performance of two and three terminal based devices and further to investigate how mechanisms of charge transport get affected by trap in these devices. (ii) if optimized mobility is obtained in organic devices by engineering different growth parameters how it depends on microscopic molecular parameters in both localized and delocalized charge transport. (iii) to investigate the origin behind localization of charge carriers in organic semiconductors in tail of

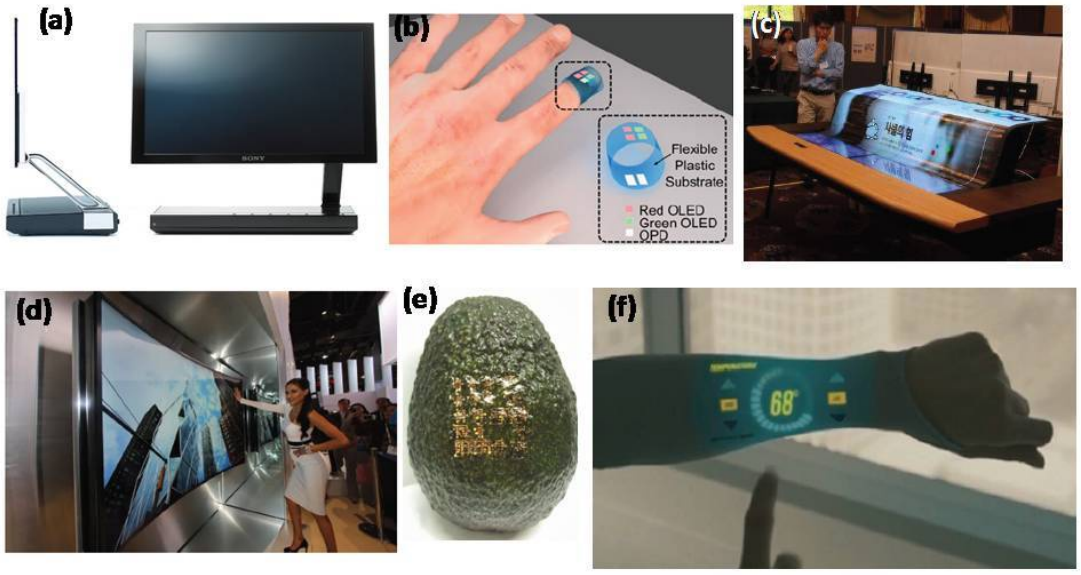


*Figure 1.2: Few examples of recent applications of organic electronics.*

the Gaussian density of states (GDOS) and how to get rid off this localization in order to get delocalized band-like transport, (iv) finally, we have studied the diffusion of charge carriers in disordered organic semiconductors. Diffusion of charge carriers in organic semiconductors is not investigated seriously and only drift of charge carriers is characterized with the assumption that only drift governs the charge transport in these systems.

## 1.2 Organic Semiconductors

Though, extensive discussion is available on the introduction of organic semiconductors however, for the essence of the work presented in this thesis, we also describe in brief. These materials consist of carbon atoms having single and double bonds in alternate. This conjugated nature of these materials results in their semiconducting properties. Ground state electronic configuration of carbon is: $1s^2, 2s^2, 2p^2$. Four electrons in outer cell (n = 2) can hybridize as: sp, $sp^2$ and $sp^3$. sp and $sp^2$ are significant in organic semiconductors as in $sp^3$ all the four electrons take part in hybridization and only sigma bonds form. In $sp^2$, three electrons in *s*, $p_x$ and $p_y$ orbitals participate in hybridization, forming sigma

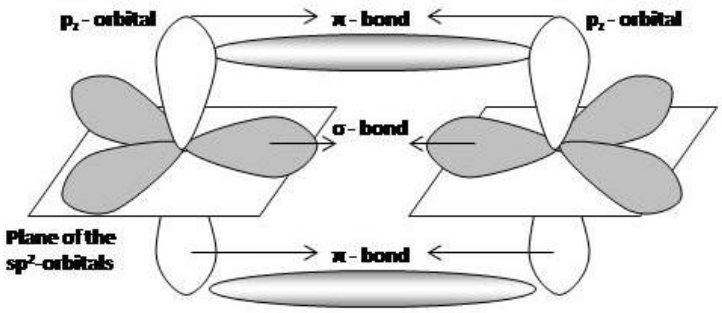


*Figure 1.3: Illustration of the $sp^2$ hybridization and formation of strong $\sigma$ and weak $\pi$ bond between two neighboring carbon atoms.*

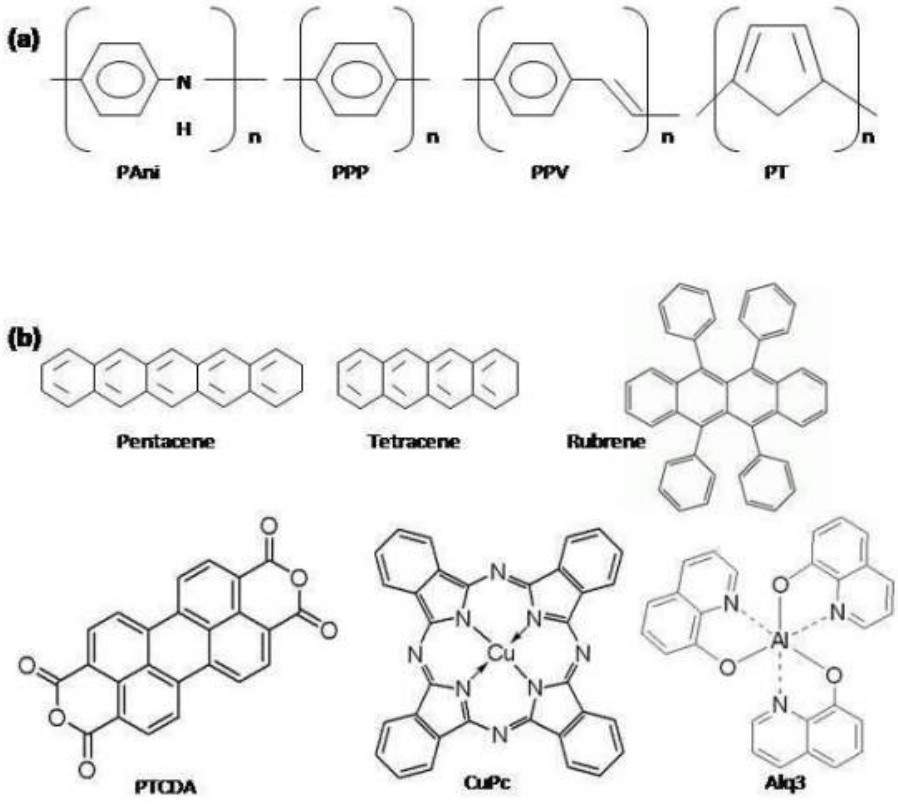


*Figure 1.4: Chemical structures of some widely used (a) organic polymeric semiconductors and (b) organic molecular semiconductors.*

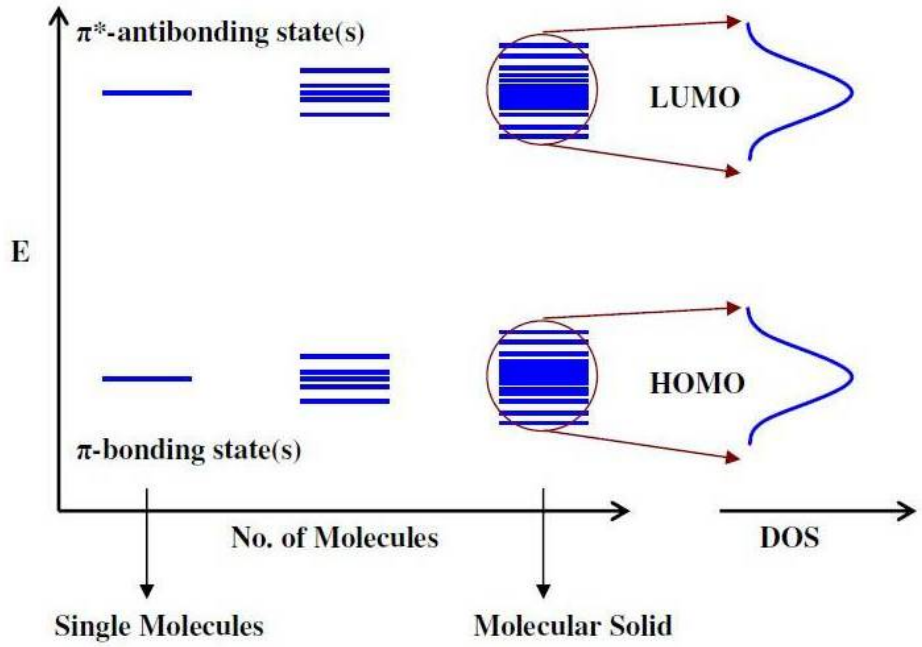


*Figure 1.5: Illustration of splitting of energy levels due to hybridization and formation of HOMO and LUMO with GDOS in organic semiconductors.*

bonds and an electron in remaining $p_z$ makes weaker $\pi$ bonds with the neighbor (Fig. 1.3). Most of the electronic and optical properties of these materials are decided by these $p_z$ electrons as these are delocalized.

Organic semiconductors are mainly divided into two groups; (i) low weight organic molecular semiconductors (OMS) and (ii) polymeric organic semiconductors, having a long chain of organic molecules. Thin films of OMSs are generally grown by vacuum evaporation whereas thin film of polymers are generally obtained by solution process. In Fig. 1.4, chemical structures of few relevant organic semiconductors have been presented. Fig 1.4 (a) shows the polymeric organic semiconductors and 1.4 (b) presents OMS.

## 1.3 Gaussian distribution of states (GDOS) in organic semiconductors

Broad distribution of localized states, exhibiting the shape of Gaussian is a characteristic feature of organic semiconductors [10, 11]. According to definition of hybridization, when two closely spaced atoms interact, their energy levels split into two new energy states. Lower lying state is completely occupied and called bonding orbital whereas higher energy state is empty and known as antibonding orbital. As the number of atoms increases, energy states also increase, correspondingly. An OMS contains several atoms, hence, there are large number of occupied and unoccupied states. All the occupied states collectively form highest occupied molecular orbital(HOMO) and unoccupied states form lowest unoccupied molecular orbital(LUMO). Same concept of hybridization and bonding and antibonding orbitals can be applied to molecules also. Hence, as the number of molecules increases, energy states in HOMO and LUMO increase, correspondingly. As interaction energy of a molecule with all the surrounding molecules is not identical, there is a large disorder in energies of the occupied as well as unoccupied localized states, leading to Gaussian distribution of density of states. Formation of GDOS in HOMO and LUMO has been shown in Fig. 1.5. Due to large disorder in HOMO and LUMO, these materials are also called disordered organic semiconductors.

After the structure and characteristic features of organic semiconductors, the next most important issue is mechanism of charge transport. Charge transport in organic semiconductors is a complex problem. Several theories and models have been proposed to explain the mechanism of charge transport in organic semiconductors. Here, we describe those in brief.

## 1.4 Charge transport in organic semiconductors

With respect to charge transport, organic semiconductors can be classified in three different classes depending upon the degree of crystallinity viz. organic single crystals, polycrystalline and amorphous thin films [12, 13]. Different scenarios of charge transport in organic semiconductors have been summarized in

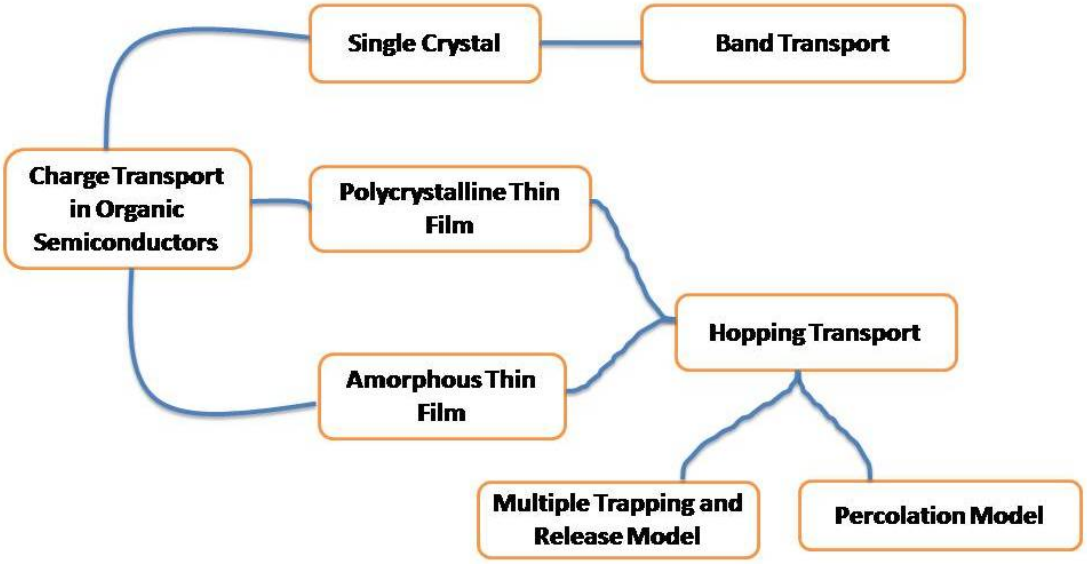


*Figure 1.6: Illustration of different charge transport mechanism, categorized on the basis of crystallinity of organic semiconductor.*

Fig. 1.6. For pure organic single crystals, band-like transport is assumed to dominate. In band transport charge carriers move as a delocalized wave in the periodic potential of the crystal and movement of these carriers is limited by the phonon scattering at room temperature. Band transport is characterized by the negative temperature coefficient of mobility [12].

To explain charge transport in polycrystalline and amorphous thin films, multiple trapping and release model (MTR) [14–16] and percolation model (PM) [17] based on variable-range-hopping [18, 19], respectively are generally used. As, both of these models are based on the thermal activation of charge carriers, mobility shows positive temperature coefficient in both the mechanisms. In MTR model [16], a distribution of localized energy states is assumed to exist between HOMO and LUMO and most of the charge carriers induced by the external bias are trapped in these localized states. Then depending on some parameters like temperature, trap depth and carrier concentration in organic thin film, charge carriers jump into HOMO or LUMO by some thermal activation process. This model is generally used to study charge transport in polycrystalline thin film based OFETs i.e. when charge transport is studied parallel to surface of the thin film. Mechanism of charge transport along the perpendicular to the film may be

different.

In PM, charge carriers are localized in GDOS and move to neighboring sites by phonon assisted tunneling. It is based on Mott's VRH [19]. Several theories have been suggested to estimate the rate of charge transfer in hopping regime, each starting from Miller-Abraham approach and Bassler's Gaussian disorder model [10] and putting some modifications in them.

Though, there is a different theory of charge transport for each class of organic semiconductors however, this classification is not realized in experiments. Negative temperature coefficient as well as high magnitude ($> 10\text{cm}^2/\text{Vs}$) of mobility has been observed in polycrystalline thin film based devices also [20–23]. Hence, classification of different charge transport mechanism on the basis of degree of crystallinity of organic semiconductors, doesn't seem appropriate and a generalized theory based on the degree of localization of charge carriers should be developed. For this, the fundamental cause behind the localization of charge carriers in polycrystalline and amorphous thin films should be investigated. Most probably, position of Fermi level in the tail of GDOS leads to localization of charge carriers, due to very low density of states in the tail. As the Fermi level moves towards the center of GDOS, density of accessible sites increases. This explains the carrier concentration dependence mobility in organic devices.

After discussing basic charge transport mechanisms in different organic semiconductors, we discuss how charge transport in these systems can be investigated. In this thesis, we are interested in charge transport mechanism in small organic molecules based thin films which are generally polycrystalline. Charge transport in organic semiconductors is investigated with two contrasting points of view: macroscopic and microscopic.

### 1.4.1 Macroscopic view of charge transport

The key parameter deciding the efficiency of charge transport in organic semiconductors is the charge carrier mobility. In the macroscopic view, mobility in organic devices is affected by different parameters such as surface morphology and crystalline quality of thin films, metal/organic interface and dielectric/organic interface etc. Typically, orientation of organic molecules on the substrate i.e. surface morphology and crystalline quality are believed to strongly affect mo-

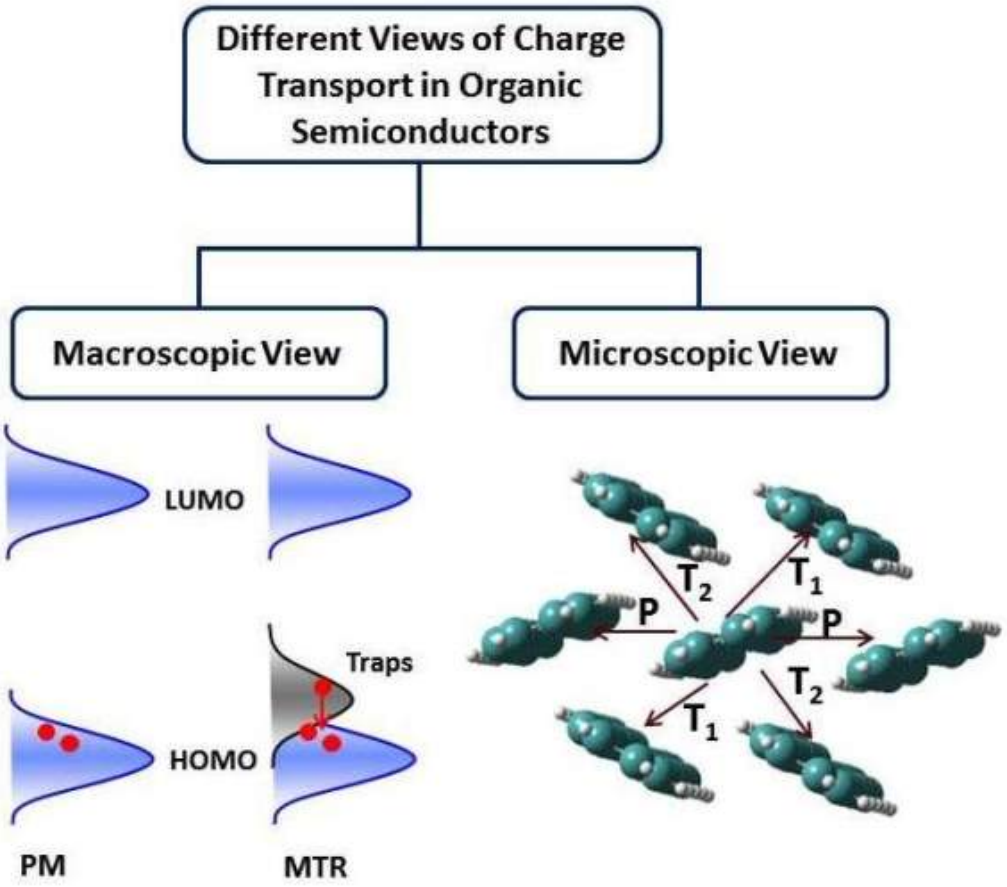


*Figure 1.7: Schematic representation of macroscopic and microscopic charge transport in organic semiconductors.*

bility in organic devices however, this doesn't answer several questions. First, why large difference in mobility is observed in the devices fabricated in different configuration with the same organic film? Second, if surface morphologies and X-ray diffraction patterns are same for more than one organic thin film then what decides the efficiency of charge transport? In this thesis, we will show that only macroscopic view of charge carrier transport is skewed and sometimes misleading in organic semiconductors.

### 1.4.2 Microscopic view of charge transport

Microscopically, charge transport in organic semiconductors is treated as a self-exchange reaction process between two organic molecules and the rate of this reaction depends on the relative strength of overlapping between the orbitals of the molecules (transfer integral) and of the coupling of external charge carrier with the vibration of the molecule (reorganization energy). These two parameters further depend on the molecular structure and their packing in solid-state. Hence, this theory correlates the charge transport with microscopic molecular parameters. Both of these aspects of charge transport have been schematically represented in Fig. 1.7 and explored in forthcoming chapters of this thesis.

## 1.5 Organization of the thesis

In this thesis, we have presented systematic experimental and theoretical studies in order to investigate origin of charge transport in organic semiconductors and tried to establish a correlation between macroscopic and microscopic charge transport parameters. Macroscopic parameters are obtained by fabricating devices in different configuration whereas microscopic parameters are estimated by performing first principle density functional theory (DFT) calculations. This thesis contains six chapters. In this chapter, starting from the importance of organic semiconductors in modern electronics and optoelectronics, we discuss in brief about basic structure of organic semiconductors and present scenario of charge transport in them.

In Chapter 2, we present an investigation on how the structural disorder induced traps in polycrystalline organic thin films can be reduced substantially. Generally, thin films based on small organic molecules are polycrystalline. Grain boundaries in polycrystalline thin films are main cause of structural disorders and trap the charge carriers in thin film based devices. Hence, engineering of different growth parameters is essential in order to minimize the grain boundaries in organic thin films. Further, how mechanism of charge transport in polycrystalline thin films gets affected when grain boundaries are negligible, has also been discussed in this chapter. In Chapter 3, we investigate the charge transport in a variety of molecules from both macroscopic and microscopic view and examine

what microscopic parameters decide the charge transport in organic devices when growth conditions are optimized. Though, it is accepted that inherent disorders in polycrystalline thin films lead to the localization of charge carriers in the tail of GDOS, resulting in low values of mobility in comparison to their pure single crystals however, evidences of negative temperature coefficients of mobility in polycrystalline thin films led us to think what is the fundamental cause of the localization of charge carriers in organic thin films and how we can get rid off the localization of charge carriers? In Chapter 4, we have discussed this issue in details.

Generally, efficient charge transport in organic devices means large carrier mobilities however, diffusion of charge carriers is another crucial phenomenon taking place during charge transport in organic semiconductors and has not been discussed in these semiconductors. Due to the localization of charge carriers in the tail of the GODS, non uniform charge density distribution exist which further leads to the diffusion of charge carriers. In Chapter 5, we have tried to estimate diffusion coefficient by employing the simple two terminal sandwiched devices based on organic thin films.

Finally, Chapter 6 presents a comprehensive summary of all the problems investigated in this thesis along with the future scope of this study.

# Bibliography


[1] A. Tsumara, H. Koezuka, T. Ando, Appl. Phys. Lett. **49**, 1210 (1986).

[2] C. W. Tang, and S. A. Van Slyke, Appl. Phys. Lett. **51**, 913 (1987).

[3] A. Bonfiglio, D. De Rossi, T. Kirstein, I. R. Locher, F. Mameli, R. Paradiso, and G. Vozzi, IEEE Transactions on Information Technology in Biomedicine **9**, 319 (2005).

[4] http://www.teleread.org/blog/?p=3519.

[5] M.Ebling, C. Mark. Pervasive Computing, IEEE **7**, 8 (2008).

[6] www.linkedin.com/pulse/organic-electronics-future-flexible-graham-jones.

[7] www.oled-info.com/lgd-developed-77-flexible-and-transparent-oled-display.

[8] www.theverge.com/2014/9/4/6105033/samsungs-105-inch-bendable-tv-has-arrived.

[9] http://news.stanford.edu/2017/05/01/flexible-organic-biodegradable-new-wave-electronics.

[10] H. Bassler, Phys. Status Solidi B **175**, 15 (1993).

[11] I. N. Hulea, H. B. Brom, A. J. Houtepen, D. Vanmaekelbergh, J. J. Kelly and E. A. Meulenkamp, Phys. Rev Lett. **93**, 166601(1996).

[12] M. Gershenson, V. Podzorov, and A. Morpurgo, Reviews of modern physics **78**, 973 (2006).

[13] C. Liu, K. Huang, W. T. Park, M. Li, T. Yang, X. LIU, L. Liang, T. Minari and Y. Noh, Mater. Horiz., **4**, 608 (2017).

[14] B. Hartenstein, H. Bassler, A. Jakobs, and K. W. Kehr, Phys. Rev. B **54**, 8574 (1996).

[15] A. Salleo, T. W. Chen, A. R. Volkel, Y. Wu, P. Liu, B. S. Ong, and R. A. Street, Phys. Rev. B **70**, 115311 (2004).

[16] G. Horowitz, Adv. Mater. **10**, 365 (1998).

[17] M. C. J. M. Vissenberg and M. Matters, Phys. Rev. B **57**, 12964 (1998).

[18] S. D. Baranovskii, physica status solidi (b) **251**, 487 (2014).

[19] N. F. Mott, Can. J. Phys. **34**, 1356 (1956).

[20] A. Troisi and G. Orlandi, Phys. Rev. Lett. **96**, 086601, (2006).

[21] S. Fratini and S. Ciuchi, Phys. Rev. Lett. **103**, 266601 (2009).

[22] T. Sakanoue and H. Sirringhaus, Nat. Mater. **9**, 736 (2010).

[23] Yu Yamashita, Felix Hinkel, Tomasz Marszalek, Wojciech Zajaczkowski, Wojciech Pisula, Martin Baumgarten, Hiroyuki Matsui,*, Klaus Mullen,*, and Jun Takeya, Chem. Mater. **28**, 420, (2016).

# Chapter 2

# How to reduce defects in organic thin film?

Defects in organic thin films is a main issue that affects the performance of organic devices and hence limits their applications in integrated circuits, displays and memory devices requiring fast processing. Points defects and structural disorder induced defects are two main varieties of defects which are responsible for trapping of charge carriers in organic thin film based devices. Point defects can be eliminated by repeated sublimation of material. However, structural disorders are induced during thin film growth. As thin films based on small organic molecules are polycrystalline, grain boundaries in these films trap the charge carriers and limit the charge transport in them. Generally, multiple trapping and release (MTR) model is a widely used mechanism to explain the charge transport in polycrystalline thin film based organic field effect transistors without emphasizing the origin of trap. In this chapter, we have investigated the charge transport mechanism in polycrystalline thin films of copper phthalocyanine (CuPc) with and without traps. Thin films with or without traps have been obtained, by carefully engineering the different growth parameters. It appears that mechanism for charge transport in polycrystalline thin films with traps is completely different than that in polycrystalline thin films without traps. We find that interface states at grain boundaries in polycrystalline grainy thin films act as traps for charge carriers.

## 2.1 Introduction

Although, organic semiconductors are continuously attracting the commercial world of electronics in the field of large area display such as flat screens of computers and televisions, flexible devices such as rollable displays etc. [1–3] however, defects are very prone to exist in organic semiconductors and limit their application in integrated circuits, displays and memory devices [4]. Predominantly, there are two types of defects viz. point defects and structural disorder induced defects. [4–6]. Point defects are mostly due to impurities incorporated during the material synthesis and can be reduced by subliming the organic material repeatedly whereas the structural disorder induced defects arise during thin film growth due to the polycrystalline nature of thin films based on small organic molecules [7, 8]. Grain boundaries in polycrystalline organic thin films (OTFs) generate multiple barriers for carriers and act as trap, hence limit the charge carrier transport in OTF based devices. Compared to inorganic materials, it is more difficult to characterize structural defects in organic semicoductors due to the inherent disorder. Further, to get rid of traps at grain boundaries in polycrystalline thin films is also a difficult task, however these traps can be reduced substantially if the growth conditions are optimized. This is highly required since the exact role of intrinsic parameters (microscopic) on the performance of organic devices will be misunderstood and misguided, unless the role of extrinsic parameters are optimized.

It has already been shown [9–11] that grain boundaries play a significant role in deciding the efficiency of charge transport in OTFs and a vast improvement in the performance of organic thin film based devices can be achieved if grain boundaries are reduced substantially. However, there appears to be little investigation on how mechanism of charge transport in polycrystalline organic thin films gets affected when (i) density of grain boundaries is varied (ii) shape of the grains is varied and (iii) interface traps at the interface of grain boundaries are varied. Several models either analytical or based on simulation have been developed to investigate the charge transport mechanism in organic semiconductor thin film based devices [12, 13]. Currently, two widely used models to explain the charge transport mechanism in organic field effect trasistors (OFETs) are; multiple trapping and release (MTR) [14–16] model and percolation model (PM) [17].

PM, based on variable- range- hopping (VRH) [18] within the energetic states in the GDOS of highest occupied molecular orbital (HOMO) or lowest unoccupied molecular orbital (LUMO), usually accounts for the carrier transport in amorphous films. Organic polymer thin films which are otherwise amorphous consist of low density of trap states. [19] However, the carrier transport in polycrystalline thin films is usually described by the ubiquitous model known as MTR. According to this model, [20, 21] charge transport is controlled by traps which are energetically located between HOMO and LUMO. Most of the charge carriers reside at traps and temporarily get released to HOMO or LUMO, depending upon the position of the trap level and temperature. Surprisingly, the most important aspect of this model i.e. trap is always casually treated without emphasizing where the trap is or what is the origin of the trap in polycrystalline thin films? Though, there are several studies [15, 22] proposing MTR model to be most suitable to explain charge transport in polycrystalline OTFs. However there have been some issues which have no clear evidence of how the applicability of MTR model is affected if the grain boundaries are reduced and if PM could be valid in case of polycrystalline thin films with less grain boundaries which is otherwise valid in amorphous thin films.

In this chapter, we have studied the charge transport mechanism in polycrystalline copper phthalocyanine (CuPc) thin films having different surface morphologies i.e different concentration of interface states by using a combination of two terminal and three terminal devices. In two terminal devices, charge transport occurs along the perpendicular to the film surface whereas in three terminal devices, charge transport is two dimensional and is parallel to the film surface. We show that charge transport mechanism in two terminal and three terminal devices based on polycrystalline CuPc thin films with and without traps are completely different.

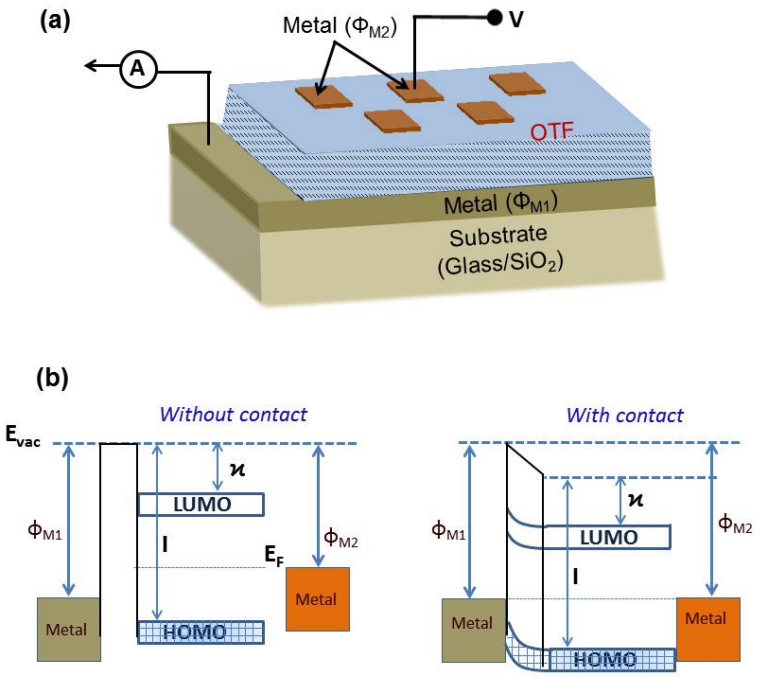


*Figure 2.1: Schematic representation of (a) a metal/organic/metal based two terminal device and (b) energy level diagram at metal/organic interface without contact (left panel) and with contact (right panel). According to vacuum level alignment injection barrier for holes and electrons at metal ($\Phi_{M1}$)/organic interface are $\Phi_{Bh} = I - \Phi_{M1}$ and $\Phi_{Be} = \Phi_{M1} - \chi$ respectively, where $\Phi_{M1}$ is work function of metal electrode which makes Schottky contact with organic and I and $\chi$ are the ionization potential and electron affinity of the organic semiconductor respectively.*

## 2.2 Geometries and working principles of two and three terminal based organic devices

### 2.2.1 Two terminal devices

To study the charge transport in polycrystalline OTFs, we use the most fundamental device structure i.e. metal/organic/metal based single carrier device. In this configuration an OTF is sandwiched between two metal electrodes, either having the same or different work functions. One of them is known as injecting electrode at which voltage is applied and the other is as extracting or blocking electrode and is grounded (Fig. 2.1(a)). The barrier at metal/organic interface plays an important role in deciding the charge injection mechanism from metal

to organic semiconductor. According to Mott-Schottky vacuum level alignment (VLA) [23], at metal ($\Phi_{M1}$)/organic interface, the energy barrier for holes ( $\Phi_{Bh}$) and electrons ($\Phi_{Be}$) are estimated as, $\Phi_{Bh} = I - \Phi_{M1}$ and $\Phi_{Be} = \Phi_{M1} - \chi$ respectively, where $\Phi_{M1}$ is the work function of the metal electrode which exhibits a significant barrier at metal/organic interface and $I$ and $\chi$ are the ionization potential and electron affinity of the organic semiconductor respectively, schematically shown in Fig. 2.1(b). If the difference between the work function of metal and HOMO or LUMO (in case of hole and electron transport, respectively) of the organic semiconductor is less than 0.2-0.3 eV, contact is Ohmic i.e. it is able to inject more charge carriers than those can be extracted at the other electrode. In Fig. 2.1, metal($\Phi_{M2}$)/organic interface provides Ohmic contact. If there is a large barrier at metal/organic interface then it behaves as a Schottky contact. Hence, two terminal devices can be mainly fabricated in two configurations: (i) single carrier devices where both the contacts are Ohmic. It is generally used when charge transport mechanism has to be studied and (ii) organic Schottky diodes where a barrier is introduced at one of the metal/organic interface, are generally required for capacitive measurements. Figure 2.1(b) and (c) show the energy band diagram at metal/organic interface without and with contact respectively, when organic layer is sandwiched between two metal electrodes. When a metal and organic semiconductor are brought into contact, charges flow from either metal to organic or organic to metal until Fermi levels on both sides are equalized. This results into a potential barrier at the interface.

### 2.2.2 Three terminal devices

OFETs are the three terminal devices consisting of: a gate electrode ($G$) isolated by a dielectric from the organic semiconducting layer and two metallic electrodes, source ($S$) and drain ($D$) which are in the direct contact with the semiconductor layer. There are two preferred configurations in which OFETs are generally studied i.e. top contact OFET and bottom contact OFET. Figure 2.2 shows the schematic diagram of the OFETs in top and bottom contact configurations. It has been shown in several reports [24–26] that in bottom contact configuration OFETs show larger contact resistance in comparison to that in top contact configuration mainly due to the poor packing of the organic molecules at

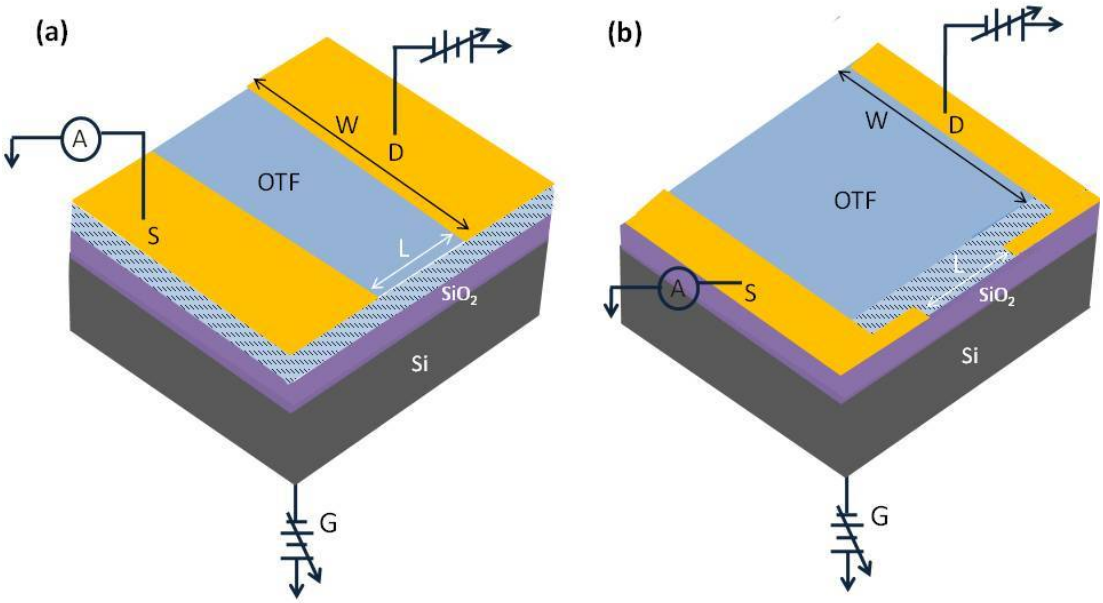


*Figure 2.2: Schematics of device geometry and circuit diagram of a p-type OFET in (a) top-contact ad (b) bottom contact configuration.*

the source/drain contact edge [24]. Hence, OFETs have been fabricated in top contact configuration for our study.

Lets discuss the working principle of a p-type OFET in brief. Initially, when gate voltage ($V_G$) = 0 V, OFET is in turned-off state and there is a minimum conduction between source and drain electrodes. A negative $V_G$, attracts the holes towards organic/dielectric interface and accumulates a layer of holes. When $V_G$ exceeds the threshold voltage ($V_T$), conduction established between source and drain. Hence $V_T$ is the minimum value of $V_G$ required to make the OFET active. When no voltage is applied at drain i.e potential difference between source and drain is zero, concentration of the holes accumulated at the interface is uniform throughout the channel and depends on the applied $V_G$ and the dielectric constant of the insulator. Then device can be treated as a metal-insulator-semiconductor (MIS) diode. There exist three different operating regimes, depending on the sign of $V_G$. Figure 2.3 shows the energy band diagram for a *p*-type MIS diode, corresponding to different regimes.

(i) Accumulation regime:- when a negative $V_G$ is applied in case of p-type

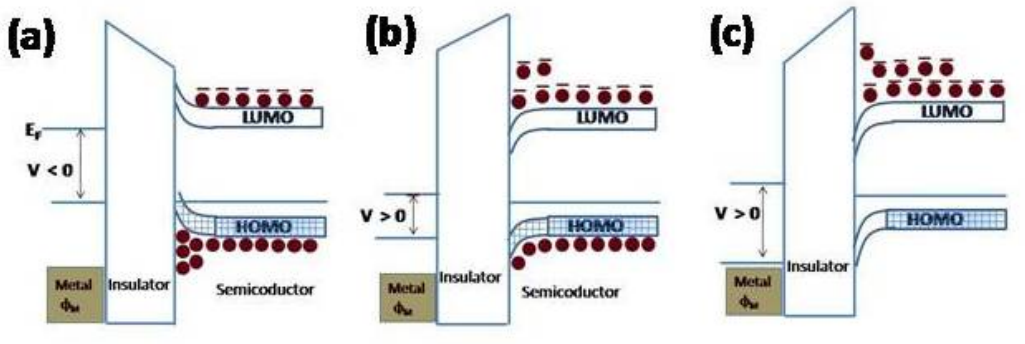


*Figure 2.3: Energy band diagram of a MIS device in (a) accumulation regime (b) depletion regime and (c) inversion regime.*

OFETs, band edges bend upward and come closer to the Fermi level at the insulator-semiconductor interface resulting an accumulation layer of holes at interface (Fig. 2.3(a)).

(ii) Depletion regime:- When a positive instead of negative $V_G$ is applied, Band edges bend downwards and density of holes gets depleted (Fig. 2.3(b)).

(iii) Inversion regime:- When gate is made more positive, band edges bend downward so significantly that intrinsic Fermi level crosses the Fermi level $E_F$ and electron density exceeds the hole density (Fig. 2.3(c)).

OFETs normally operate in the accumulation regime in which a negative $V_G$ is required in order to get a layer of mobile holes at the semiconductor/dielectric interface. Conventionally, source is kept grounded and negative voltage is applied at drain. As a result, charge carriers are injected at source and move towards drain. So there is a linear charge density gradient from source to drain.This corresponds to the linear $I_{DS} - V_{DS}$ characteristics of the OFETs at small $V_{DS}$ (Fig. 2.4(a)). As $V_{DS}$ increases, flow of charge carriers from source to drain also increases, resulting the decrease in charge density near the drain. When $V_{DS}$ is increased further and becomes equal to $V_G - V_T$, source is unable to inject sufficient charge carriers to flow throughout the channel and depletion region forms due to the pinch-off the channel near the drain (Fig. 2.4(b)). Beyond pinch-off, applied $V_{DS}$ does not increase $I_{DS}$ anymore rather extends the deletion region inside the channel and saturation region is observed (Fig. 2.4(c)). Thus two regions: linear and saturation are observed while studying the $I_{DS} - V_{DS}$

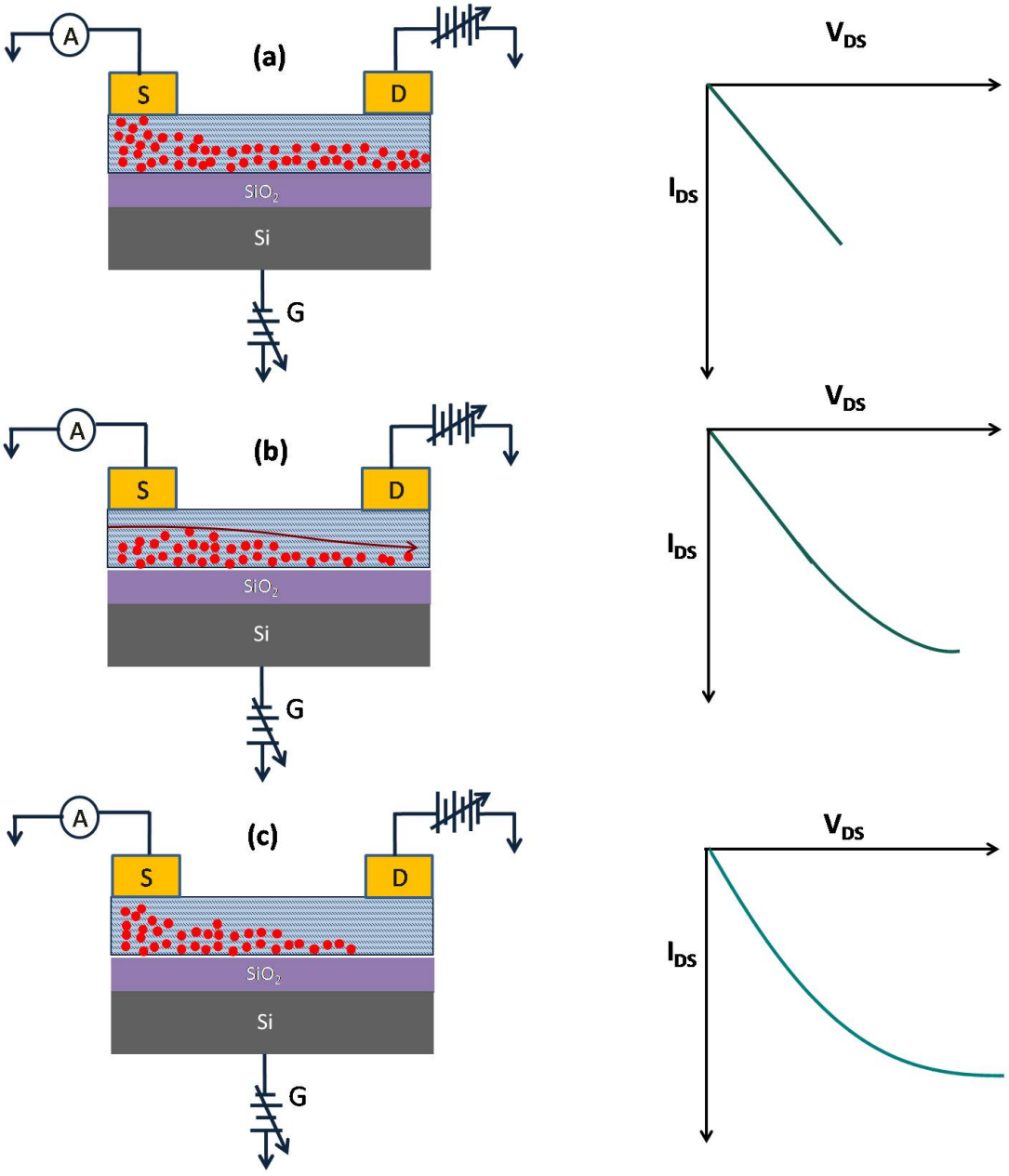


*Figure 2.4: Schematics of the working of a p-type OFET with respect to applied voltage for (a) linear region where* $V_{DS} << V_G$ *(b) start of depletion region due to pinch-off when* $V_{DS} \sim V_G$ *and (c) saturation region when* $V_{DS} > V_G$.

characteristics of an OFET.

(i) Linear region:- In the linear region, $V_{DS} < V_T$ and $I_{DS}$ can given as [23]

$$I_{DS} = \mu \frac{W}{L} C_i \left[ (V_G - V_T) V_{DS} - \frac{V_{DS}^2}{2} \right] \tag{2.1}$$

where $C_i$ is the dielectric capacitance per unit area, $W$ is the channel width, $L$ is the channel length and $V_T$ is the threshold voltage.

(ii) Saturation region:- In saturation region, $I_{DS}$ increases proportional to the square of the gate voltage and can be given as [23]

$$I_{DS} = \mu \frac{W}{2L} C_i (V_G - V_T)^2 \tag{2.2}$$

Output characteristics in linear and saturation regions are used to estimate several parameters that govern the performance of the OFETs as follow.

(1) Mobility ($\mu$): $\mu$ is the most important parameter and decides the speed of charge carriers in the OFETs. It is estimated by fitting the $I_{DS} - V_{DS}$ characteristics in the linear region according to the Eq. 3.44; [23]

(2) Threshold voltage ($V_T$): $V_T$ arises due to the interface states at metal/dielectric interface and is equal to the minimum gate volatge required to make the channel active. It is estimated by fitting the transfer $I_{DS} - V_G$ characteristics according to the Eq. 2.2 [23].

(3) Subthreshold swing ($S$): $S$ may be defined as the gate voltage required for an increament of one decade in $I_{DS}$ and is estimated from the slope of $\log_{10}$ ($I_{DS}$) vs $V_G$ plot as [27],

$$S = \left( \frac{\log_{10} I_{DS}}{V_{DS}} \right)^{-1} \tag{2.3}$$

(4) ON-OFF ratio ($r$): $r$ is given as the ratio of maximum and minimum drain current and is estimated from the $I_{DS} - V_{GS}$ curve.

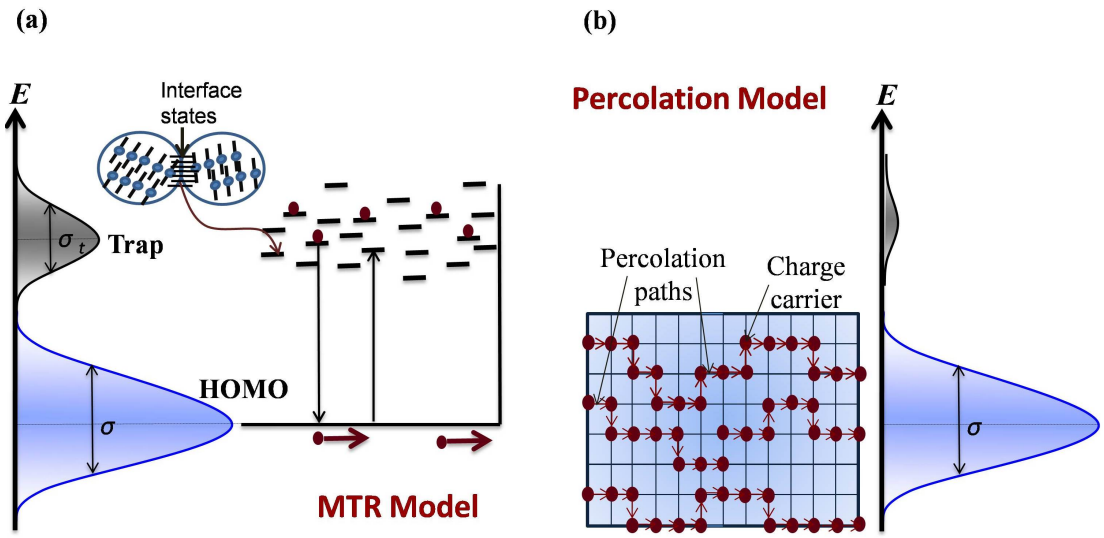


*Figure 2.5: Schematic representation of (a) trap limited charge carrier transport in polycrystalline organic thin films. Traps are energetically localized between HOMO and LUMO and (b) charge transport according to the percolation model within the GDOS of HOMO.*

## 2.3 Different models for charge transport in OFETs

In contrast to inorganic semiconductors in which charge carriers move as a delocalized wave in broad valence or conduction band, charge transport in organic semiconductors is described by the hopping through the localized states in GDOS [23]. In organic semiconductors charge carriers are localized due to the spatial and energetic disorder within the GDOS and by absorbing a phonon they make a jump from one site to other neighboring site. Following two models have been widely discussed while studying the charge transport in thin film based OFETs.

### 2.3.1 MTR model

MTR model is generally used to explain charge transport in OFETs based on polycrystalline organic thin films. It presumes that a distribution of localized energy levels exist between HOMO and LUMO, however the origin of these localized levels has not been emphasized in this model. According to this model,

most of the charge carriers induced by gate bias are trapped in the localized levels i.e. these levels act as trap for charge carriers and limit the charge transport in devices. Then depending on the trap depth, temperature and background carrier concentration i.e. $V_G$ in the device, the carriers temporarily get released by thermally activated process to HOMO (hole transport) or LUMO (electron transport), as schematically shown in Fig. 2.5(a). In this model, $\mu$ strongly depends on the $V_G$ as [21],

$$\mu^{MTR} = \mu_0^{MTR} \left[ \frac{C_i \left( V_G - V_T \right)}{qN_t} \right]^{\frac{T_{MTR}}{T} - 2} \tag{2.4}$$

where $\mu_0^{MTR}$ is weakly temperature dependent prefactor, $T_{MTR}$ is the characteristics temperature which defines the width of energetic distribution of traps ($\sigma_t$) as $\sigma_t = k_B T_{MTR}$.

### 2.3.2 PM

In PM [17], charge carriers move due to phonon assisted tunneling within the localized states distributed energetically in GDOS , as shown schematically in Fig. 2.5(b). This model considers that any two sites (*i,j*) in GDOS are correlated to each other by a conductance ($G_{ij}$). $G_{ij}$ is large enough if sites, *i, j* are two nearest neighbor. Vissenberg and Matters used the concept of VRH [17] i.e. a carrier may either hop over a small distance with a high activation energy or hop over a long distance with a low activation energy and developed a mathematical expression for the percolation model of hopping. According to them, in hopping regime, dependence of  on carrier concentration is presented as [17, 28],

$$\mu^{PM} = \mu_0^{PM} \left[ \frac{(C_i V_G)^2}{2 k_B T_{PM} \epsilon_s} \right]^{\frac{T_{PM}}{T} - 1} \tag{2.5}$$

where $\mu_0^{PM}$ is weakly temperature dependent prefactor, $T_{PM}$ is the characteristic temperature which represents the width of HOMO or LUMO as $\sigma_{PM} = k_B T_{PM}$ and $\epsilon_s$ is the dielectric constant of organic semiconductor.

## 2.4 Experimental details

CuPc, a co-planar organic molecule, has been chosen for this study for two reasons, (i) its exceptional thermal and chemical stability and (ii) different surface morphologies, required to have thin films with and without intrinsic traps. For this, the planar organic molecules having two dimensional extended aromatic systems are required and CuPc is an ideal choice for this. High purity ($> 99.999\%$), triple sublimed CuPc, procured from Sigma Aldrich Chemical Co. USA has been used for this study to avoid any chemical impurity induced traps. For two terminal devices, 200 nm single layer of CuPc is sandwiched between ITO and Au or Al and Au. Thin films are deposited in oil free evaporation system at a base pressure of $5 \times 10^{-6}$ mbar. For OFETs, the heavily doped Si wafers with 300 nm $SiO_2$ layer have been used as substrate. 100 nm thick CuPc films are deposited on the substrate with a deposition rate of 0.1 Å/s and at different substrate temperatures ($T_G$). Finally, Au was deposited on the organic layer to form the source and drain contacts. The devices have an identical channel width of 3 mm and channel lengts of 20$\mu$m.

As discussed earlier, thin films based on organic molecules are polycrystalline with large number of grains and grain boundaries. The grain boundaries in polycrystalline thin films are difficult to characterize, as the grains are too small to allow for measurements across individual grain boundaries. In case of Poly-Si thin film transistors (TFTs), several methods have been employed to characterize traps due to grain boundaries. For example, in doping method the activation energy of sheet resistance is measured with various dopant concentrations [29, 30], in conductance method the frequency dependence of the conductance is measured [31], in deep level transient spectroscopy method, the change in capacitance due to trapping and de-trapping is measured. [32] All of these methods examined poly-Si TFT structures to correlate the grain boundary trap state densities with the transfer characteristics of TFTs. Unfortunately, none of these methods can be applied in polycrystalline OTFs for their high resistivity and low carrier mobility. In view of these problems, techniques based on steady state or quasi-static measurements are desirable for the characterizations of defects in organic devices. [33] The electrical characterizations of two terminal devices and OFETs were carried out in rough vacuum ($10^{-2}$ mbar) using Keithley picoammeter and

Keithley voltage sources. The capacitance measurements were performed using Wayne Kerr LCR meter and Keithley voltage sources under rough vacuum ($10^{-2}$ mbar) and at room temperature. Surface morphology of thin films was studied using Park system XE 70 atomic force microscope (AFM). Crystalline quality of thin films were examined by studying the X-ray diffraction (XRD) pattern using a PANalytical X-ray diffractometer.

In case of organic semiconductors, separation of bulk conduction known as space charge limited conduction (SCLC), which dominates when there is either no or small barrier at metal/organic interface from contact limited conduction known as injection limited current (IJL) which dominates when there exists a barrier at metal/organic interface is extremely important. We have considered two sandwiched devices, based on CuPc (ITO/CuPc/Au and Al/CuPc/Au). CuPc is a hole transport material with HOMO and LUMO at 4.8 eV and 3.0 eV, respectively [34]. The work functions of Al, ITO and Au are 4.2 eV, 4.8 eV and 5.2 eV, respectively. There would be either no or very small barrier for holes at Au/CuPc and ITO/CuPc interfaces, but a barrier of 0.6 eV exists at Al/CuPc interfaces [23, 34].

## 2.5 Growth of organic thin films with and without traps

Predominantly, there are two sources of traps in organic thin films, impurities related traps and structural disorder induced traps. Repeatedly sublimed organic materials are used to grow thin films in order to diminish the impurity related traps. However, to reduce the effect of traps arising due to structural disorder, engineering of different growth parameters such as $T_G$ and evaporation rate ($F_G$) is essential [35]. Generally, low $F_G$ results in reducing the effect of structural disorder induced traps in thin films [11]. At low $F_G$, molecules can spend enough time in finding out a preferred orientation which results thin film with reduced structural disorders. There is another parameter which can also induce disorder in thin films i.e. $T_G$. Figure 2.6 shows the surface morphology of CuPc thin films fabricated on $SiO_2$ with a fixed low evaporation rate of 0.1 Å/s but $T_G$ varying from 30$^o$C to 120$^o$C. Size and shape of the grains gradually change,

having isotropic at low $T_G$ and nano-wire like anisotropic structure at higher $T_G$ (120$^o$C). At 30$^o$C CuPc thin films exhibit nucleation growth, resulting into isotropy grainy structure. Grains start showing elongation at 60$^o$C and transform to connected rod-like lamellae at 120$^o$C. At low $T_G$ (30$^o$C) molecules don't have sufficient kinetic energy to migrate and meet the other existing islands and get settled at random positions on the substrate, resulting into nucleation growth. Hence, at low $T_G$ thin films exhibit polycrystalline grainy structure with almost equal sized grains (40-60 nm) and a large number of grain boundaries. These grain boundaries create barriers for charge carriers while moving from source to drain [11], hence charge transport in organic thin films affected due to grain boundaries whether the charge transport is studied parallel or perpendicular to the film surface. As $T_G$ increases kinetic energy of the molecules also increases and molecules get sufficient time to diffuse on the substrate and stick to the other existing grains. Hence, at high $T_G$, lateral growth due to larger sticking coefficient in a preferred direction i.e. along the $\pi - \pi$ interactions in adjacent molecules takes place. Hence, low $F_G$ and high $T_G$ are appropriate for anisotropic nano-wire like morphology of CuPc thin films. Hence CuPc thin films with and without traps can be achieved by varying the growth conditions appropriately.

## 2.6 Arrangement of CuPc molecules in thin films

Figure 2.7(a) shows the XRD pattern of CuPc thin film grown at 120$^o$C. The XRD pattern exhibits a strong peak at $2\theta \sim 6.8^o$ which is due to (100) plane confirming $\alpha$-phase triclinic structure. [36] From XRD, it can be concluded that bc-plane lies parallel to the substrate and is relevant for charge transport in OFET. Figure 2.7(b) shows the arrangement of CuPc molecules in OFET geometry. In this plane, CuPc molecules adopt stacking along b-axis. Figure 2.7(c) shows the arrangement of CuPc molecules perpendicular to the substrate i.e. along a-axis which is relevant for charge transport along perpendicular to bc-plane *i.e.* in two terminal sandwiched devices. The XRD pattern of CuPc thin films grown at 30$^o$C is identical, except the intensity of peak is less than that in thin film grown at 120$^o$C.

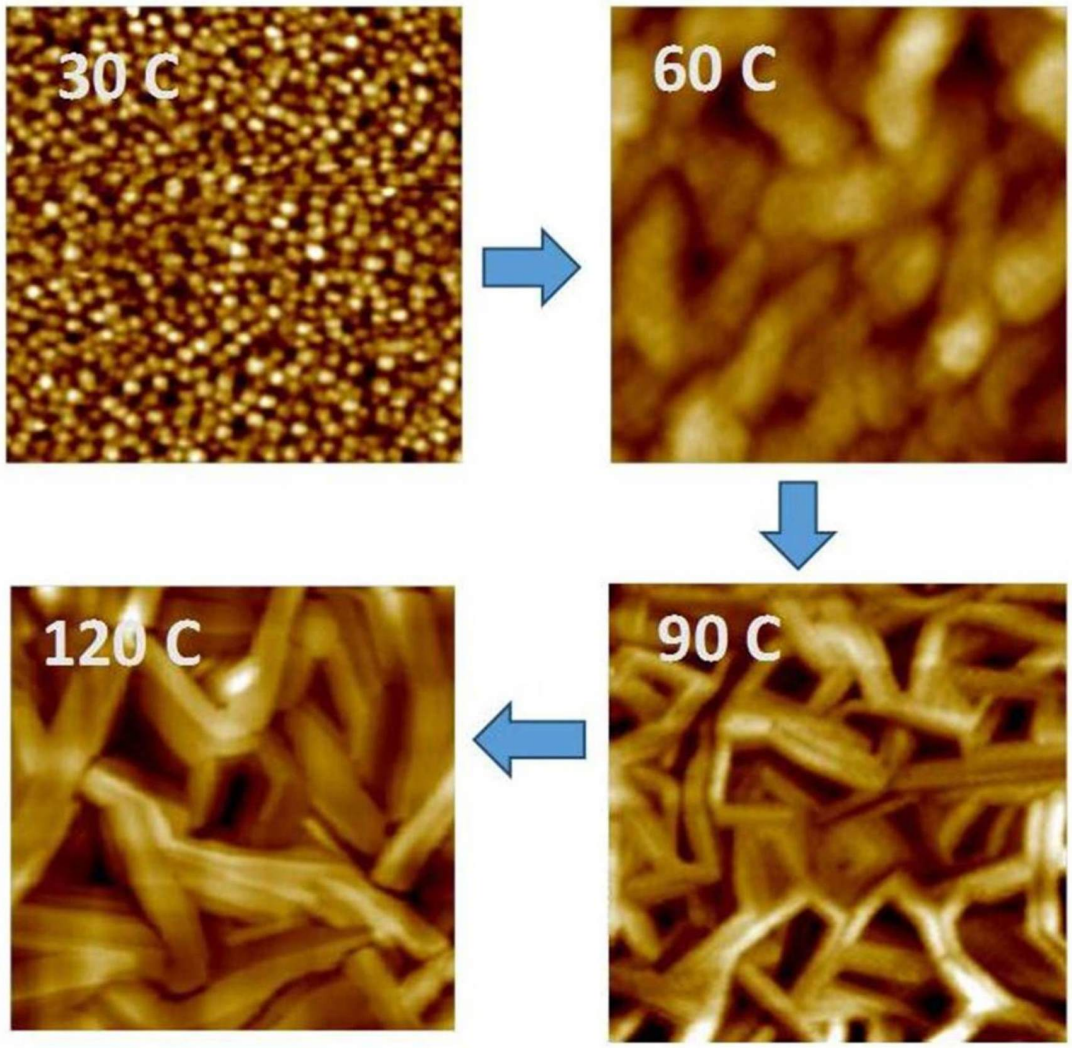


*Figure 2.6: AFM topographic (1 $\mu$m $\times$ 1$\mu$m) images of CuPc thin films grown at substrate temperatures ($T_G$) varied from 30°C to 120°C.*

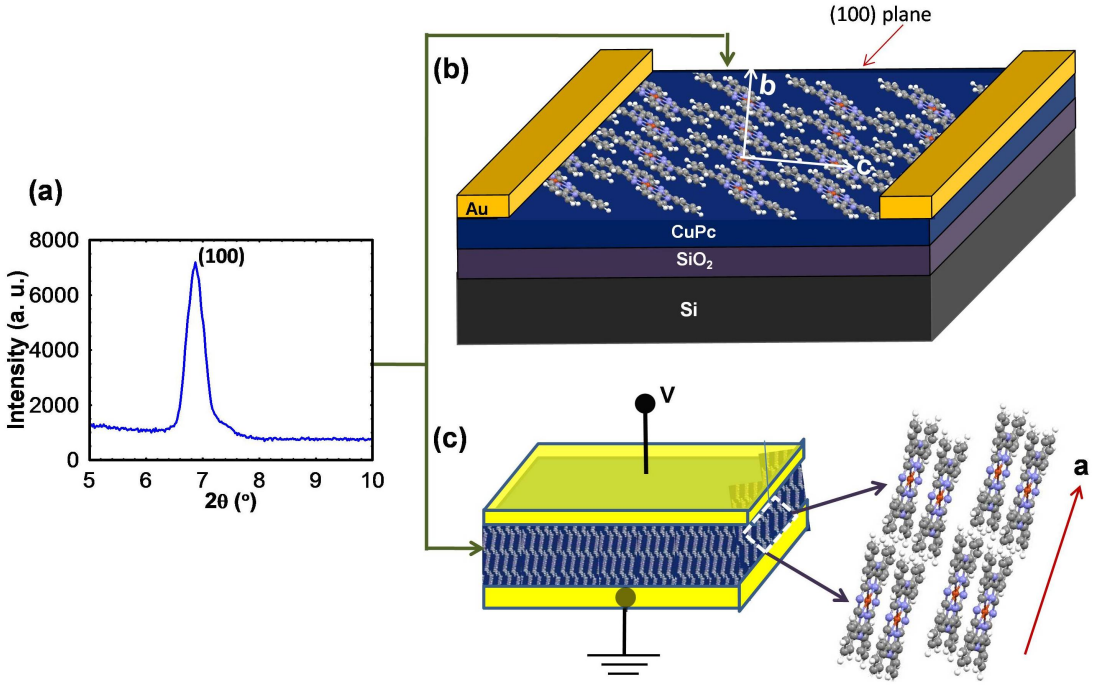


*Figure 2.7: XRD pattern of CuPc thin film grown at* $T_G = 120^oC$ *on* $SiO_2$ *substrate. Schematic representation of arrangement of CuPc molecules in a plane (b) parallel to the substrate and relevant for charge transport in three terminal devices and (c) perpendicular to the substrate and relevant for charge transport in two termial devices.*

## 2.7 Charge transport along the direction, perpendicular to (100) plane

In two terminal devices, dominant charge transport occurs along the perpendicular to the film surface and mechanism of charge transport depends on the concentration of traps in polycrystalline organic thin films. Space charge limited conduction (SCLC) [37] is generally observed when the concentration of traps in organic thin films is significantly low. However, in the case of higher density of traps in thin films, charge carriers get captured by these traps and charge transport in two-terminal devices described by trap charge limited conduction (TCLC) [38,39]. Conduction mechanism in OTF based two terminal devices can be decided by the nature of the $J$-$V$ characteristics of the devices.

### 2.7.1 SCLC

Charge transport mechanism in organic semiconductors is much more complex than in their inorganic counterparts as transport properties in organic semiconductors are generally affected by the structure of individual molecular entity due to weak van der Waals interactions between them. Further due to the absence of long range order, charge carriers are localized in the tail of the GDOS of HOMO or LUMO in case of hole or electron transport, respectively and need some activation energy to hop to the neighboring sites, leading to low value of mobility in these materials. Hence, charge transport mechanism in these materials depends on the concentration of free carriers in the semiconductor. In two terminal sandwiched devices, at low bias, intrinsic free carrier density is lower than the injected density and carriers injected from one electrode redistribute themselves in such a way that they replace the holes flowing out at the other. Hence charge transport is contact limited and current flowing through the device is governed by the thermally generated free charge carriers in the device, leading to Ohmic conduction. Density of injected charge carriers increases with bias and at high bias, injected carrier density is too high to be replaced by the holes flowing out at the other electrode. Accumulation of holes takes place at high bias. These excess holes create a space charge and current shows non-linear behavior with source-drain bias. Hence nonlinear behavior of $I_{DS}$ at high bias can be explained on the basis

of SCLC. In SCLC regime, slope starts from 2 and eventually increases with bias due to the field dependent carrier mobility $\mu(\mathrm{F},\mathrm{T})$ as proposed by Bassler et. al. [40]

$$\mu\left(\mathrm{F},\mathrm{T}\right)=\mu\left(0,\mathrm{T}\right)\exp\left[\gamma\left(\mathrm{T}\right)\sqrt{\mathrm{F}}\right] \tag{2.6}$$

where $\mu(0,\mathrm{T})$ is the zero field charge carrier mobility and $\gamma(\mathrm{T})$ is the field activation factor.

### 2.7.2 TCLC

TCLC would be the mechanism of charge transport in two terminal devices if there are large number of traps, mainly due to the structural disorders in polycrystalline thin films. Due to the large number of traps in thin film, most of the charge carriers get captured. Then, current in two terminal devices is controlled by the trapped charge and not by the free charge. In this case, at low bias Ohmic region is observed due to thermally generated free charge carrier same as in trap free devices, however the magnitude of the current can be lower. At higher bias, current increases rapidly with the applied voltage with a slope in the range of 5-10 due to the variation in ratio of free to total carrier concentration [41].

## 2.8 *J-V* and *C-T* characteristics of devices with and without traps

Figure 2.8(a) and (b) represent the current-voltage *J-V* characteristics of ITO/CuPc/Au based two terminal devices in which CuPc thin films were grown at $\mathrm{T_G}$ = 30$^{\mathrm{o}}$C and 120$^{\mathrm{o}}$C, respectively. In Fig. 2.8(a), initially, Ohmic region due to thremally generated charge carriers is observed (J $\sim$ V) . As the bias increases, current increases rapidly with more than fourth power of voltage due to TCLC, following J $\propto \mathrm{V}^{\mathrm{l}+1}(\mathrm{l} > 1)$ [38, 39]. This is generally attributed to the exponential or Gaussian distribution of traps [39, 42] . Upper inset shows capacitance-temperature *(C-T)* characteristics obtained from thermally stimulated capacitance (TSCAP) [43] for the Al/CuPc/Au based Schottky diodes. We observe a clear step at 230 K in *C-T* curve which is a direct proof of the existence

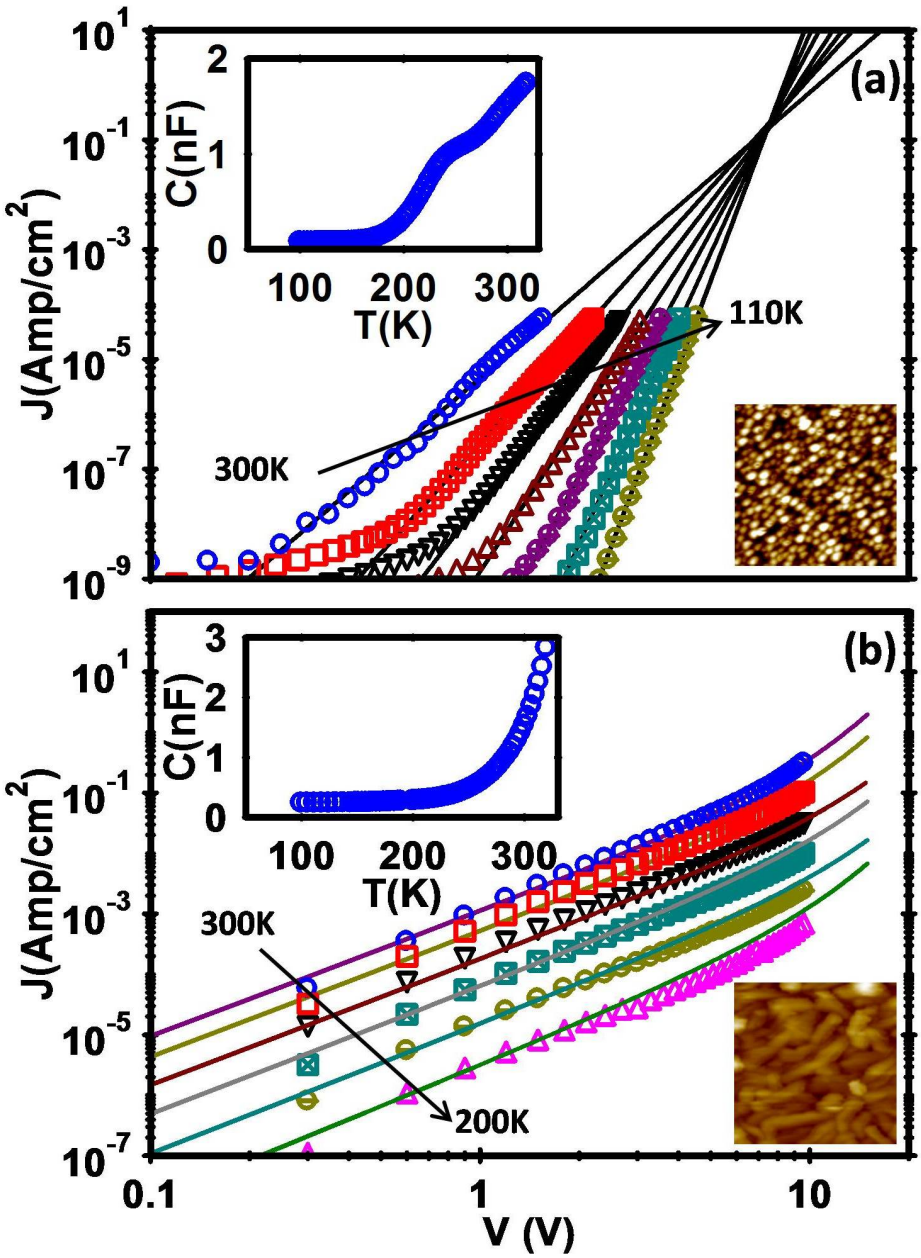


*Figure 2.8: Temperature dependent J-V characteristics of ITO/CuPc/Au devices in which CuPc thin films were grown at* $T_G$ *of (a) 30 °C and (b) 120 °C. Solid lines represent the theoretical fitting with (a) TCLC [Eq. 2.7] and (b) SCLC with field dependent mobility [Eq. 2.6], respectively. Upper insets show TSCAP measurements of Al/CuPc/Au based sandwiched devices with heating rate of 5 K/min in which CuPc thin films were grown at* $T_G$ *of (a) 30 °C and (b) 120 °C. Lower insets show the AFM images* ($1\mu m \times 1\mu m$) *of the CuPc thin films grown at* $T_G$ *of (a) 30 °C and (b) 120 °C.*

of traps in thin films grown at low $T_G$. This step is observed due to combined effect of two processes; one generation of carriers with temperature and other loss of carriers due to trapping. The midpoint of the step has been used to determine the trap level (Et), given by, [43] $E_t = k_B T_m \ln(\alpha T_m^4/\beta)$, where $T_m$ is the midpoint of the step, $k_B$ is the Boltzmann's constant, $\alpha \sim 1K^{-3}s^{-1}$ and $\beta$ is the heating rate which is maintained at 5 *K/min* during *C-T* measurement. $E_t$ calculated in this way has been found to be at $0.5 \pm 0.05\ eV$ . Hence deep traps exist in CuPc thin films grown at low $T_G$. In TCLC regime, *J-V* characteristics of two terminal devices, can be written as [42, 44]

$$J = q^{1-l}\mu N_V \left(\frac{2l+1}{l+1}\right)^{l+1} \left(\frac{l}{l+1}\frac{\epsilon_s}{N_{tot}}\right)^{l} \frac{V^{l+1}}{d^{2l+1}} \tag{2.7}$$

where $q$ is the elementary charge, $N_V$ is the effective density of the states (DOS) in the HOMO of CuPc, $\mu$ is the mobility of charge carriers, $N_{tot}$ is the density of trap states, $d$ is the thickness of the thin film. The value of l can be obtained directly from the slope of log (J) vs. log (V). The Eq. 2.7 can be written in the Arrhenius form as,

$$J = \left(\frac{\mu N_V q V}{d}\right) f(l) \exp\left[-l \ln\left(\frac{q N_{tot} d^2}{2\epsilon_s}\right)\right] \tag{2.8}$$

where $f(l) = 2^{-l}\left(\frac{2l+1}{l+1}\right)^{l+1}\left(\frac{l}{l+1}\right)^{l} \simeq 0.5$ when $l > 2$. Further from Fig. 2.8(a), it can be seen that the current is temperature independent at a particular voltage $V_c$, where $E_a$ must be zero. So one gets from Eq. 2.8,

$$V_c = \frac{q N_{tot} d^2}{2\epsilon_s} \tag{2.9}$$

By extrapolating, log $(J)$-log $(V)$ characteristics at various temperatures, $V_c$ and $N_{tot}$ are found to be $\sim$ 8 V and 5.8 x $10^{16}$ $cm^{-3}$, respectively. $N_{tot}$ is actually the concentration of interface states at grain boundaries, as will be shown below.

Figure 2.8(b) shows the *J-V* characteristics of ITO/CuPc/Au based two terminal devices in which CuPc thin films were grown at $T_G = 120^oC$. At low bias, *J-V* characteristics exhibit Ohmic behavior i.e. current increases linearly with bias but as bias increases, current exhibits the power law dependence on voltage

where slope starts from 2 due to the SCLC mechanism [37, 45] and eventually increases with bias due to the field dependent SCLC. Experimental *J-V* characteristics have been simulated by solving the Poissons equation describing the relationship between the electric field $F$ and the local charge density *p(x)* and continuity equation, $J(x) = qp(x)\mu[F(x), T]F(x)$, simultaneously [40]. Upper inset of Fig. 2.8(b) shows the TSCAP measurements of the corresponding device. No step in *C-T* characteristics has been observed. SCLC and absence of step further confirms that there are no deep traps in CuPc thin films grown at high $T_G$. Lower insets in Fig. 2.8(a) and (b) show the surface morphology of CuPc thin films grown on ITO at $T_G = 30^oC$ and $120^oC$, respectively. As discussed earlier, thin films at low $T_G$ show nearly uniform distribution of isotropic grains and hence large number of in-plane interface states at grain boundaries. Charge carriers injected from ITO can be initially trapped by these large number of in-plane interface states, resulting in the TCLC along the perpendicular to the film. However, thin films at high $T_G$ show rod like elongated nanowires providing very few soft grain boundaries, hence in-plane interfacial area is significantly reduced. There is a very less possibility of charge carriers injected from ITO to get trapped by the in-plane interfacial states and charge transport occurs by the SCLC. We can conclude that charge transport, perpendicular to the film grown at low and high $T_G$ takes place by two completely different mechanisms.

## 2.9 Characterization of traps from *C-f* measurements

Figure 2.9(a) shows the capacitance-frequency (*C-f*) characteristics of Al/CuPc/Au Schottky diodes, fabricated at $30^oC$ and $120^oC$, respectively. Initially, the capacitance decreases with frequency but beyond a certain frequency capacitance becomes independent of frequency. At higher frequency carriers are no longer able to follow the ac signal and contribution due to diffusion capacitance diminishes [46]. A step in *C-f* characteristics of the device with deep traps has been observed around $\sim$ 1kHz due to traps whereas this peak is absent in diodes without traps. In case of reverse bias, the capacitance is mainly determined by the depletion capacitance in low frequency region and remains

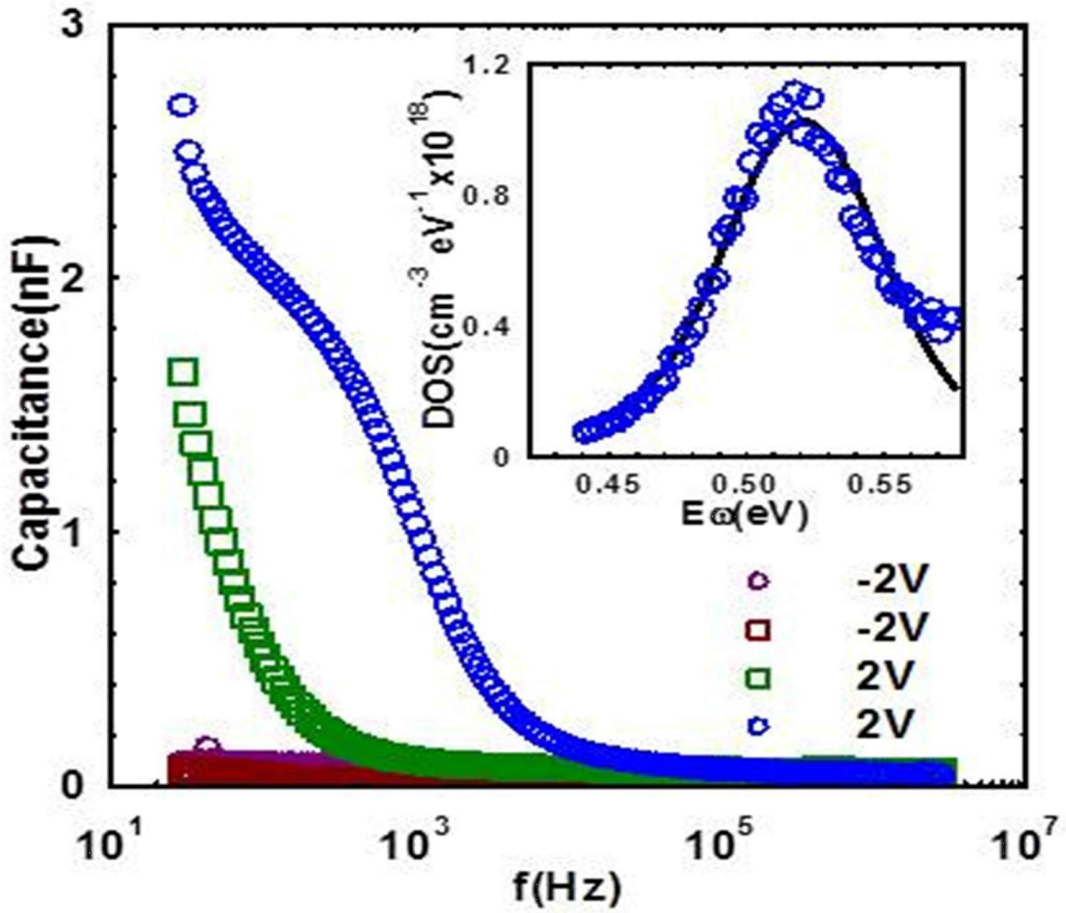


*Figure 2.9: C-f characteristics of Al/CuPc/Au based Schottky diodes in which CuPc thin films were grown at substrate temperature of 30 °C (empty circles) and 120 °C (empty squares). Insets show the energetic distribution of trap states obtained from C-f characteristics of the devices grown at 30 °C. Traps are absent in thin films grown at 120°C. Solid line is fit with Gaussian [Eq. 2.12].*

unresponsive at high frequency regions, for both the devices with and without traps. Hence, under reverse bias, *C-f* characteristics of the diodes with and without traps are quite similar. In the forward bias, *C-f* characteristics over a wide range of frequency have been used to determine the energetic position and density of trap states [46]. At low frequency, all the traps are filled whereas at high frequency only those traps below certain demarcation energy ($E_\omega$) will be filled and contribute to capacitance. $E_\omega$ is given by [47, 48].

$$E_\omega = k_B T \ln\left(\frac{\nu}{\omega}\right) \tag{2.10}$$

$\nu$ denotes an attempt-to-escape frequency, which is typically of the order of $10^{12} s^{-1}$ and $\omega = 2\pi f$, the angular frequency of the ac signal. So by varying the frequency, we can obtain the density of traps as a function of trap level. Following this approach, the traps distribution can be related to the derivative of the capacitance with respect to frequency and given by [46]

$$N_t(E_\omega) = -\frac{V_{bi}}{qWk_BT}\frac{dC(\omega)}{d\ln\omega} \tag{2.11}$$

where W is the width of the depletion region and $V_{bi}$ is the built-in potential due to different work functions of metal electrodes [14]. Insets of Fig. 2.9 show the energetic distribution of trap states obtained by differentiating the *C-f* characteristics of Al/CuPc/Au based Schottky diodes. Traps are absent in thin films grown at high $T_G$ whereas Gaussian energetic distribution of traps has been observed in devices in which thin films of CuPc were grown at low $T_G$. Width of energetic distribution of traps and position of the trap level with respect to HOMO has been obtained by fitting the experimental data with Gaussian distribution of trap states $N_t(E)$ centered at $E_t$ as [49]

$$N_t = \frac{N_{tot}}{\sqrt{2\pi}\sigma}\exp\left(-\frac{(E_\omega - E_t)^2}{2\sigma_t^2}\right) \tag{2.12}$$

Inset of Fig. 2.9 shows the trap density of states as a function of energy along with fitting with Eq. 2.12, resulting $\sigma_t$ to be 0.04 eV and the trap level at around 0.50 eV. The value of $E_t$ matches well with those obtained independently from C-T measurement for devices fabricated at low $T_G$. Thus *C-f* characteristic also

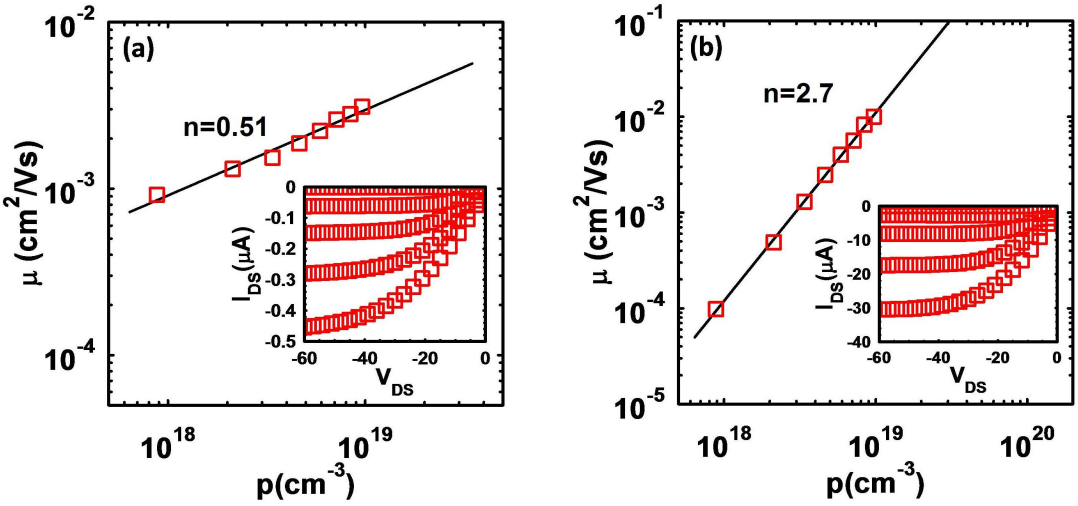


*Figure 2.10: Dependence of room temperature charge carrier mobility ($\mu$) on charge carrier concentration ($p$) in CuPc based OFETs fabricated at substrate temperature of (a) 30 °C and (b) 120 °C. Insets show the room temperature* $I_{DS}-V_{DS}$ *characteristics of respective OFETs at* $V_G$ *varying from 0 V to -80 V with a step of 20 V. Solid lines are power law fit* $\mu \propto p^n$*, where* $n = T_{MTR}/T - 2$ *or* $T_{PM}/T - 1$*, according to Eq. 2.4 and 2.5, respectively.*

corroborates the existence of deep traps in devices in which thin films were grown at low $T_G$.

## 2.10 Charge transport mechanism in OFETs with and without traps

In this section, a comparative study on charge transport mechanism in OFETs based on CuPc thin films with and without trap have been carried out. Figure 2.10(a) and (b) show the $\mu$ as a function of carrier concentrations ($p$) for the OFETs based on CuPc thin film with and without traps, respectively. Insets in Fig. 2.10(a) and (b) show the ($I_{DS}-V_{DS}$) of the OFETs with and without trap, respectively. Mobilities at different $p$ have been calculated from the linear region of the output characteristics ($I_{DS}$–$V_{DS}$) using the Eq. [23]. $p$ at different $V_G$ have been calculated using the relation, $p = C_i(V_G - V_T)/qt$, $t$, being the thickness of the accumulation layer and has been taken 10 nm. The linear relation in the $\mu$-$p$

on log-log scale suggests the power law dependence of $\mu$ on $p$ i.e. $\mu \sim p^n$, where $n$ is the temperature dependent parameter and appropriate model for charge transport in OFETs is decided by its magnitude. After fitting the $\mu - p$ curves shown in Fig. 2.10(a) and (b), $n$ for the OFETs with and without traps have been found to be 0.51 and 2.7, respectively. Putting these $n$ in MTR model (Eq. 2.4) [21], characteristic temperatures defining the width of trap distribution, $T_{MTR}$ have been found to be 753 K and 1410 K for the OFETs with and without traps, respectively and the corresponding width of the energetic distribution of trap states are found to be 61 meV and 130 meV respectively. The width of energetic distribution of traps ($\sim$ 60 meV) obtained from MTR model for CuPc thin films grown at low $T_G$ matches well with the value obtained from *C-f* characteristics but the value obtained for thin films grown at high $T_G$ is more than that of HOMO (100 meV) [50]. Moreover, MTR model estimates, the width of energetic distribution of traps to be larger for the OFETs without traps than for the OFETs with traps which is contradicted. Hence charge transport in organic thin films having traps is governed by MTR model but the same model is not applicable for thin films without deep traps. However, same data can be analyzed by PM. Putting the values of $n$ in PM (Eq. 2.5), we get $T_{PM}$ to be 453 K and 1110 K in the devices with and without traps respectively and the corresponding width of the DOS are found to be 45 and 95 meV, respectively. The calculated width of the DOS for OFETs without traps is $\sim$ 100 meV which is the typical width of the HOMO or LUMO in organic semiconductors [50]. The unusually low value of width of DOS with traps indicates that PM which is otherwise successful [51] in case of OFETs without traps, is not suitable for OFETs having traps.

Further, larger values of $n$ for the OFETs without traps compared to those with traps can be explained as follows. Upon increasing $V_G$, the injected carriers fill the interface states and lower energy states at the edge of the HOMO or LUMO in the organic semiconductors and any additional charges will start to fill higher energy states towards the center, resulting low activation energy to hop away to the neighboring sites, with higher $\mu$ with increasing $V_G$ i.e. with increasing $p$. Hence for OFETs with traps, most of the charge carriers are captured by the interface states at grain boundaries i.e. grain boundaries impose significant barriers and prevent the charge carriers from reaching to transport level. Whereas for OFETs without traps, injected carriers easily fill the interface states and

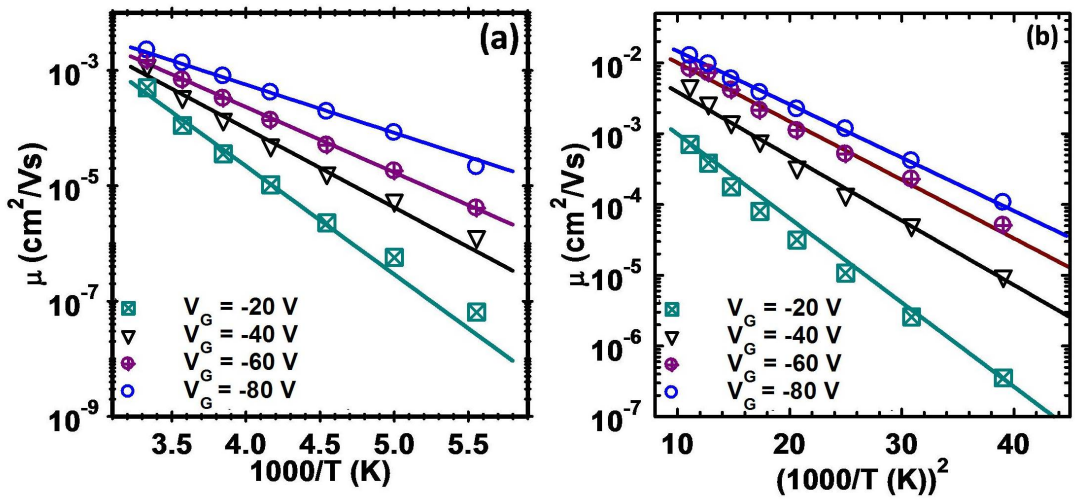


*Figure 2.11: Temperature dependence of μ, measured at different* $V_G$ *for CuPc thin film based OFETs (a) with and (b) without traps. Solid lines in (a) and (b) represent the fitting according MTR model and PM, respectively.*

additional carriers occupy higher energy states in the GDOS, resulting a sharp increase in mobility. In a recent study, similar effect of grain boundaries on the current modulation with gate bias has been observed [28].

Next, to investigate the impact of the interface states on the charge transport mechanism in quantitative way, we have estimated the maximum surface density of interfacial traps ($N_s$) for OFETs fabricated at low and high $T_G$. Subthreshold swing ($SS$) is an important OFET parameter that can be used to estimate the density of these traps as, [9,52] $N_s = [\mathrm{Slog(e)}k_BT/q{-}1]Ci/q2$. $S$ itself is estimated as, [9] $S = [\mathrm{dlog}(I_{DS})/dV_G] - 1$. $S$ for the OFETs fabricated at low and high $T_G$ have been found to be 9.8 V/decade and 4.89 V/decade, respectively. Then $N_s$ calculated form $S$ have been found to be 1.04 $\times 10^{13}$ $cm^{-2}$ $eV^{-1}$ and 5.18 $\times 10^{12}$ $cm^{-2}$ $eV^{-1}$, for the OFETs at low and high $T_G$, respectively. It means that high density of grain boundaries creates additional interfacial traps in the CuPc thin films at low $T_G$.

## 2.11 Temperature dependence of $\mu$ for OFETs with and without traps

To justify our arguments on the charge transport mechanism in the OFETs with and without traps, temperature dependence of $\mu$ at different $V_G$ have also been investigated. As can be seen in Fig. 2.11(a), $\mu$ at different $V_G$ in OFETs with traps follow Arrhenius temperature dependence, $\ln\mu \sim 1/T$. Arrhenius like temperature dependence of $\mu$ interprets that MTR model should be able to successfully explain the charge transport in OFETs with traps [52]. However, non-Arrhenius -like temperature dependence of $\mu$, ($\ln\mu \sim 1/T^2$) has been observed in the OFETs without traps (Fig 2.1(b)) which is a direct consequence of the hopping transport within the GDOS in organic semiconductors, as discussed in correlated Gaussian disorder model (CGDM) [18, 53]. VRH model, itself is an extended form of the hopping model [18]. Hence, PM, based on VRH seems to be applicable to explain charge transport in OFETs without traps.

## 2.12 Thermally stimulated current analysis for OFETs with traps

To reveal the nature of traps and their resulting impact on charge carrier transport in disordered organic semiconductors, temperature dependence of $I_{DS}$ at two different $V_G$ of 60 V and 90 V for OFETs based on CuPc thin films having traps has been shown in Fig. 2.12(a). Initially, $I_{DS}$ decreases with decreasing temperature but at around 75 K and 65 K for $V_G = 60$ V and 90 V, respectively, current increases abruptly by several orders of magnitude and then remains almost constant. This anomalous behavior in current-temperature ($I_{DS}$–T) characteristics can be explained on the basis of grain boundary controlled charge carrier transport in CuPc thin film with traps [34].

Figure 2.12(b) shows the energy-level diagram including band-bending due to the trapping of positive charge at the grain boundary interface in CuPc thin films. High density of localized energy levels inside the band gap of the semiconductor exists due to the interface states lying between grain boundaries in polycrystalline thin films with traps. [34, 55] The levels which lie below the Fermi

level $E_F$, are filled, at thermal equilibrium. Consequently, a negative charge at the interfaces and space-charge regions on the both sides, of grain boundaries are generated. Positive charge, trapped at the grain-boundary interface creates a potential barrier for charge carrier transport and the height of this barrier ($E_B$) can be estimated as [34, 55]

$$E_B = \frac{q^2 (n_T)^2}{8\epsilon_s N_A} \tag{2.13}$$

where $N_A$ is the acceptor concentration inside the grain, $n_T$ is the density of occupied traps at grain boundary interface. $n_T$ depends on the Fermi level, hence on $T$ and for a Gaussian distribution of trap in organic semiconductors, $n_T$ can be given by [34]

$$n_T = \int_0^\infty \frac{N_{tot}}{\sqrt{2\pi}\sigma} \frac{\exp\left[-\frac{((E-E_{T0})^2}{4\sigma^2}\right]}{1+\exp\left[\frac{(E-E_F)}{k_B T}\right]} dE \tag{2.14}$$

where $E_T$ represents the maximum height of the Gaussian distribution. $E_F$ is given by

$$E_F(T) = k_B T \ln[N_V/p] \tag{2.15}$$

$I_{DS}$, in polycrystalline thin films with large number of grains is controlled by the rate of charge carrier jumps across the grain boundary as [56]

$$I_{DS} = I_0 \exp[-E_B/k_B T] \tag{2.16}$$

Theoretical fit with Eq. 2.13-2.17 along with the experimental data has been shown in Fig. 2.12(a). It is interesting to note that in low temperature region (around 60 K and 50 K for $V_G = 60$V and 90 V, respectively), $I_{DS} - T$ characteristics can be excellently fitted with Eq. 2.13-2.16. However, at high temperature fitting is not good because of the contribution to barrier due to hopping conduction at high temperature. After including the barrier for hopping transport ($\Delta$), Eq. 2.17 can be written as

$$I_{DS} = I_0 \exp[-(E_B + \Delta)/k_B T] \tag{2.17}$$

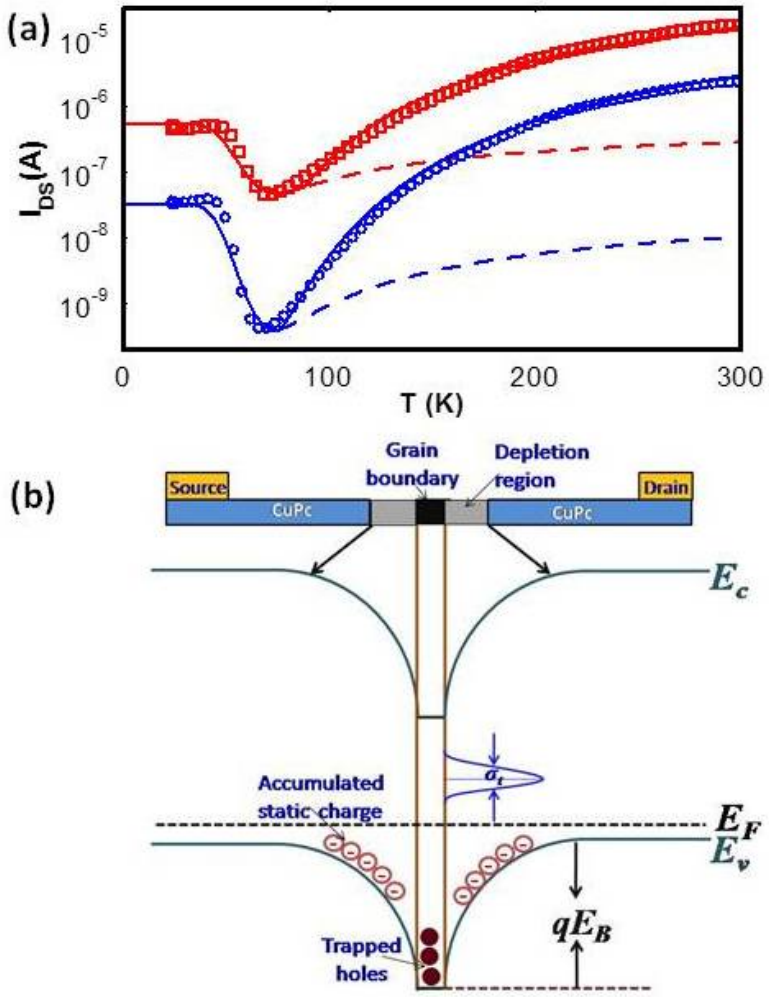


*Figure 2.12: (a) Temperature dependence of* $I_{DS}$ *at* $V_G$ *= 60 V (open circle) and* $V_G$ *= 90 V (open square) for OFETs based on CuPc thin films with traps. Abrupt increase in* $I_{DS}$ *at* $\sim$ *75 K for* $V_G$ *= 60 V and at* $\sim$ *65 K for* $V_G$ *= 90 V has been observed. Dashed lines represent the theoretical fitting according to Eq. 2.16, without inclusion of hopping barrier (*$\Delta$*) i.e.* $\Delta$ *= 0 whereas solid lines represent the theoretical fitting with a finite value of* $\Delta$*. (b) The schematic representation of energy-level diagram including band-bending at grain-boundary interface in CuPc thin films.* $E_c$ *and* $E_v$ *represent the LUMO and HOMO edges, respectively and* $E_f$ *is the equilibrium Fermi level. At thermal equilibrium some of energy levels below the Fermi level are occupied by carriers giving rise to a negative interface charge at the grain boundaries and space-charge regions on both sides of the boundary.* $E_B$ *corresponds to the height of the potential barrier due to the trapped charges at the grain-boundary interface.*

In high temperature region, $I_{DS}$–T characteristics could be excellently fitted with Eq. 2.13, 2.14, 4.23 and 2.17 as shown in Fig. 2.12(a). From fitting $\Delta$ has been found to be 82 meV and 43 meV for $V_G$ = 60V and 90 V, respectively. The anomalous temperature dependence of current can be understood as follows: At low temperature the Fermi level will be close to the HOMO and traps will be neutral. This situation results in a vanishing band bending at the grain boundaries resulting in high conductivity. With increasing temperature the Fermi level moves toward the middle of the band gap resulting in a potential well. When the well depth is about the order of $k_BT$ or higher, the charge carriers will be trapped by the potential well. For conduction, the charge carriers have to overcome the barrier thermally. As a result, conductivity decreases drastically. At higher temperatures, when all the traps are negatively charged, potential well $E_B$ remains constant. A further increase in temperature leads to a higher probability for the charge carriers to escape from the well, resulting in an increase in conductivity.

## 2.13 Conclusion

In conclusion, charge transport mechanism in polycrystalline organic thin films of CuPc has been investigated, in great detail. Trap density in thin films has been controlled by engineering different growth conditions. CuPc thin films grown at low $T_G$ exhibited high concentration of traps and *J-V* characteristics of two terminal devices fabricated at low $T_G$ could be well fitted to TCLC. *C-f* and *C-T* characteristics also demonstrate the presence of traps in CuPc thin films grown at low $T_G$. Width of the trap distribution from MTR model is in agreement with that obtained independently from *C-f* characteristics of CuPc based organic Schottky diodes. Hence MTR model can be applied to explain the charge carrier transport in polycrystalline organic thin films with isotropic grainy structure. Charge carriers trapped by interface states at grain boundaries cannot hop to HOMO or LUMO unless they get sufficient energy to be released because trapped charges at the grain-boundary interfaces lead to the formation of a potential barrier for charge transport process. Polycrystalline thin films grown under favorable growth conditions to achieve anisotropic morphology with fewer grain boundaries seem to be providing a percolative passage for the carrier transport.

It is extremely important to investigate the traps and their role on charge transport thoroughly, because to investigate the role of microscopic parameters (presented in next chapter) on the charge transport would be a futile exercise unless the thin films have negligible amount of traps.

# Bibliography


[1] M.Ebling, C. Mark. Pervasive Computing, IEEE **7**, 8 (2008).

[2] J. A. Rogers and Z. Bao, J. Polym. Sci A: Polym. Chem. **40**, 3327 (2002).

[3] www.theverge.com/2014/9/4/6105033/samsungs-105-inch-bendable-tv-has-arrived.

[4] T. P. Nguyen, Phys. Stat. Sol. (a) **205**, 162 (2008).

[5] A. Sharma, P. Kumar, B. Singh, S. R. Chaudhuri, S. Ghosh, Appl. Phys. Lett. **99**, 023301 (2011).

[6] H. Sirringhaus, Adv. Mater. **21**, 3859 (2009).

[7] H. Sirringhaus, Adv. Mater. **17**, 2411 (2005).

[8] D. Braga, G. Horowitz, Adv. Mater. **21**, 1473 (2009).

[9] V. Kalihari, E. Tadmor, G. Haugstad, C. D. Frisbie, Adv. Mater. **20**, 4033 (2008).

[10] J. Rivnay, L. H. Jimison, J. E. Northrup, M. F. Toney, R. Noriega, S. Lu, T. J. Marks, A. Facchetti, A. Salleo, Nat. mater. **8**, 952 (2009).

[11] P. Kumar, A. Sharma, S. Yadav, S. Ghosh, Org. Electron. **14**, 1663 (2013).

[12] Q. Wei,K. Hashimoto, K. Tajima, ACS Appl. Mater. Interfaces **3**, 139 (2011).

[13] R. J. Chesterfield, J. C. McKeen, C. R. Newman, P. C. Ewbank, D. A. da S. Filho, J. L. Bredas, L. L. Miller, K. R. Mann, C. D. Fris-bie, J. Phys. Chem. B **108**, 19281 (2004).

[14] B. Hartenstein, H. Bssler, A. Jakobs, K. W. Kehr, Phys. Rev. B **54**, 8574 (1996).

[15] A. Salleo,T. W. Chen, A. R. Vlkel, Y. Wu, P. Liu, B. S. Ong, R. A. Street, Phys. Rev. B **70**, 115311 (2004).

[16] G. Horowitz, Adv. Mater. **10**, 365 (1998).

[17] M. C. J. M. Vissenberg, M. Matters, Phys. Rev. B **57**, 12964 (1998).

[18] S. D. Baranovskii, Phys. Stat. sol. (b) **251**, 487 (2014).

[19] R. Hausermann, K. Willa, B. Blulle, T. Morf, A. Facchetti, Z. Chen, J. Lee, B. Batlogg, Org. Electron. **28**, 306 (2016).

[20] D. Guo, T. Miyadera, S. Ikeda, T. Shimada, K. Saiki, J. Appl. Phys. **102**, 023706 (2007).

[21] Z. Bao, J. Locklin, Organic field-effect transistors; CRC press, 2007.

[22] L. Wang, D. Fine, D. Basu, A. Dodabalapur, J. Appl. Phys. **101**, 054515 (2007).

[23] S. M. Sze, K. K. Ng., Physics of Semioconductor Devices, 3rd edition.; Wiley-Interscience, 2006.

[24] K.-D. Jung, Y. C. Kim, H. Shin, B.-G. Park, J. D. Lee, E. S. Cho, and S. J. Kwon, Appl. Phys. Lett. **46**, 96 (2010).

[25] F. Gamier, F. Kouki, R Hajlaoui, G. Horowitz, MRS Bull **22**, 52 (1997).

[26] I. Kymissis, C.D. Dimitrakopoulos, S. Purushothaman, IEEE Trans. Electron Dev. **48**, 1060 (2001).

[27] W. L. Kalb, B. Batlogg, Phys. Rev. B **81**, 035327 (2010).

[28] L. Li, G. Meller, H. Kosina, Synt. Met., **157**, 243 (2007).

[29] H. de Graaff, M. Huybers, J. de Groot, Solid-St. Electron, **25**, 67 (1982).

[30] C. H. Seager, T. G. Castner, J. Appl. Phys. **49**, 3879 (1978).

[31] S. Hirae, M. Hirose, Y. Osaka, J. Appl. Phys. **51**, 1043 (1980).

[32] J. R. Ayres, J. Appl. Phys. **74**, 1787 (1993).

[33] W. Zhu, T. Low, Y.-H. Lee, H. Wang, D. B. Farmer, J. Kong, F. Xia, P. Avouris, Nat. Commun. **5**, 3087 (2014).

[34] A. K. Mahapatro, S. Ghosh, Appl. Phys. Lett. **80**, 4840 (2002).

[35] Y. Zhihao, et al. Nat. Commun. **5**, 5290 (2014).

[36] A. Hoshino, Y. Takenaka, and H. Miyaji, Acta Crystallogr. Sect. B **59**, 393 (2003).

[37] M. A. Lampert and P. Mark, Current injection in solids, Electrical science series (Academic Press, 1970)

[38] B. Ramachandhran, H. G. A. Huizing, R. Coehoorn, Phys. Rev. B **73**, 233306 (2006).

[39] M. M. Mandoc, B. de Boer, P. W. M. Blom, Phys. Rev. B **73**, 155205 (2006).

[40] H. Bassler, Phys. Stat. Sol. (b), **175**, 15 (1993).

[41] S. C. Jain, A. K. Kapoor, W. Geens, J. Poortmans, R. Mertens, M. J. Willander, Appl. Phys. **92**, 3752 (2002).

[42] G. Paasch, S. Scheinert, J. Appl. Phys. **106**, 084502 (2009).

[43] D. K. Schroder, Semiconductor Material and Device Characterization, 3rd ed.; John Wiley & Sons, Inc., Hoboken, New Jersey, 2006.

[44] V. Kumar, S. Jain, A. Kapoor, J. Poortmans, R. Mertens, J. Appl. Phys. **94**, 1283 (2003).

[45] R. Agrawal, P. Kumar, S. Ghosh, A. K. Mahapatro, Appl. Phys. Lett., **93**, 073311 (2008).

[46] A. Sharma, S. Yadav, P. Kumar, S. Ray Chaudhuri, S. Ghosh, Appl. Phys. Lett. **102**, 143301 (2013).

[47] S. S. Hegedus, E. A. Fagen, J. Appl. Phys. **71**, 5941 (1992).

[48] J. Bhattacharya, R. W. Mayer, M. Samiee, V. L. Dalal, Appl. Phys. Lett. **100**, 193501 (2012).

[49] J. Steiger,R. Schmechel, H. von Seggern, Synth. Met. **129**, 1 (2002).

[50] C. Tanase, E. J. Meijer, P. W. M. Blom, D. M. de Leeuw, Phys. Rev. Lett. **91**, 216601 (2003).

[51] C. Tanase, P. Blom, D. de Leeuw, Phys. Rev. B **70**, 193202 (2004).

[52] J. A. Letizia, J. Rivnay, A. Facchetti, M. A. Ratner, T. J. Marks, Adv. Funct. Mater. **20**, 50 (2010).

[53] S. V. Novikov, D. H. Dunlap, V. M. Kenkre, P. E. Parris, A. V. Vannikov, Phys. Rev. Lett. **81**, 4472 (1998).

[54] A. K. Mahapatro, N. Sarkar, S. Ghosh, Appl. Phys. Lett. **88**, 162110 (2006).

[55] J. W. Orton, M. J. Powell, Rep. Prog. Phys. **43**, 1263 (2000).

[56] S. Verlaak, V. Arkhipov, P. Heremans, Appl. Phys. Lett. **82**, 745 (2003).

# Chapter 3

# Microscopic origin of charge transport in pentacene and phthalocyanine thin film

In this chapter, we investigate the charge transport properties of pentacene and phthalocyanines, by a joint experimental and theoretical study. Experimentally, current-voltage characteristics of both two and three terminal devices based on polycrystalline thin films have been used to estimate the charge carrier mobility. Theoretically, the importance of chemical structure of molecules and their arrangement in unit cell has been discussed in determining charge transport properties on the basis of electronic structures of isolated molecules and in their solid state, estimated using density functional theory (DFT). Anisotropy of charge transport in organic semiconductors has also been studied using both experimental and theoretical approaches. We observe a strong correlation between chemical structure, molecular packing and charge carrier mobility.

## 3.1 Introduction

Understanding the elementary processes occurring during charge transport within the organic semiconductors is a primary task because efficiency of charge transport in organic devices fabricated under optimized conditions further depends on the microscopic parameters such as chemical structure of the molecules and their arrangement in the solid-sate packing [1]. Charge transport in narrow band organic semiconductors has been widely described in terms of hopping of charge carriers between localized states in Gaussian density of states (GDOS) [2–4]. Although several theories have been discussed to estimate the transfer rate of charge carriers, starting from Miller-Abraham approach [4–7] but, it has to be settled how macroscopic charge transport properties are correlated with microscopic molecular parameters. Typically, charge carrier mobility is believed to be the most crucial parameter that decides the efficiency of charge transport in organic devices [8]. Hence, microscopic model needs to be established by correlating mobility with molecular parameters. Appreciable efforts have been gone into towards improving the mobility in organic thin film based devices by correlating efficiency of charge transport with surface morphology and crystalline quality [9–11] and without any doubt this has improved our understanding of charge transport, substantially. However, engineering of surface morphology and crystalline quality of organic thin films to get higher mobilities is not sufficient, because complex microstructure exists within the grains [12]. Moreover, similar surface morphologies and X-ray diffraction (XRD) patterns are also possible for different molecules with different charge transport properties. Furthermore, the efficiency of charge transport sometimes is interpreted by single parameter, i.e. width of GDOS. It is natural to ask how a single parameter can scale the charge carrier mobility in such wide class of materials. Hence, knowledge of microscopic parameters responsible in determining the efficiency of charge transport is essential.

Generally, Marcus theory [6, 7] is used to study hopping transport in organic semiconductors. Within this approach, hopping transport in organic semiconductors is modeled as an intermolecular self-exchange reaction and two microscopic parameters reorganization energy ($\lambda$) [13], arising due to the relaxation of the geometry of a molecule during charge transfer and transfer integral ($t_{ij}$) [14],

measuring the strength of electronic coupling between molecular orbitals, are considered the key parameters, deciding the efficiency of charge transport in organic semiconductors. Although, Marcus theory has been proved successful in predicting the intrinsic mobility in organic semiconductors however, there have been some issues. These are: (i) large difference in the magnitudes of mobility in devices fabricated with same organic thin film but with different device structures like two terminal and three terminal based devices, (ii) difference in mobilities in devices fabricated in same configuration but with different organic thin films having identical surface morphology and crystalline quality and (iii) while moving from hopping to band-like transport, what microscopic parameters decide the charge transport in organic semiconductors.

Though, $\lambda$ and $t_{ij}$ are considered relevant parameters to explain charge transport in hopping regime but, $\lambda$ is an intrinsic property of the molecule and hence not applicable in band-like picture of charge transport. There are some approaches to estimate $t_{ij}$ from band structure using tight-binding approximation (TBA) [15]. Though hopping is believed to be the dominant mechanism of charge transport in organic thin films due to the inherent disorder but, evidences on the band-like transport with higher magnitudes of mobility in pure organic single crystal led us to consider whether delocalization of charge carriers is also possible in organic thin film. And if it is possible what would be the charge transport governing parameters and how these parameters depend on the microscopic molecular parameters. To resolve all these issues, systematic experimental and theoretical studies are to be pursued for a variety of molecules.

In this chapter, we present a detailed and systematic investigation on the charge transport in anisotropic (pentacene) and isotropic (phthalocyanines) molecules and tried to establish a correlation between experimentally observed macroscopic and theoretically estimated microscopic charge transport parameters. Here, for our study we have chosen five different organic molecules due to the following reasons. (i) Pentacene has been chosen for this study due to its linear and simple chemical structure, intrinsic anisotropy, relatively high carrier mobility in thin film and single crystal form and wide applications in large area and flexible displays [16]. (ii) Four phthalocyanine (Pc) molecules are chosen because; (a) they are exceptionally thermally and chemically stable [17–19], (b) Pcs exhibit significant photophysical properties and uniform surface morphology

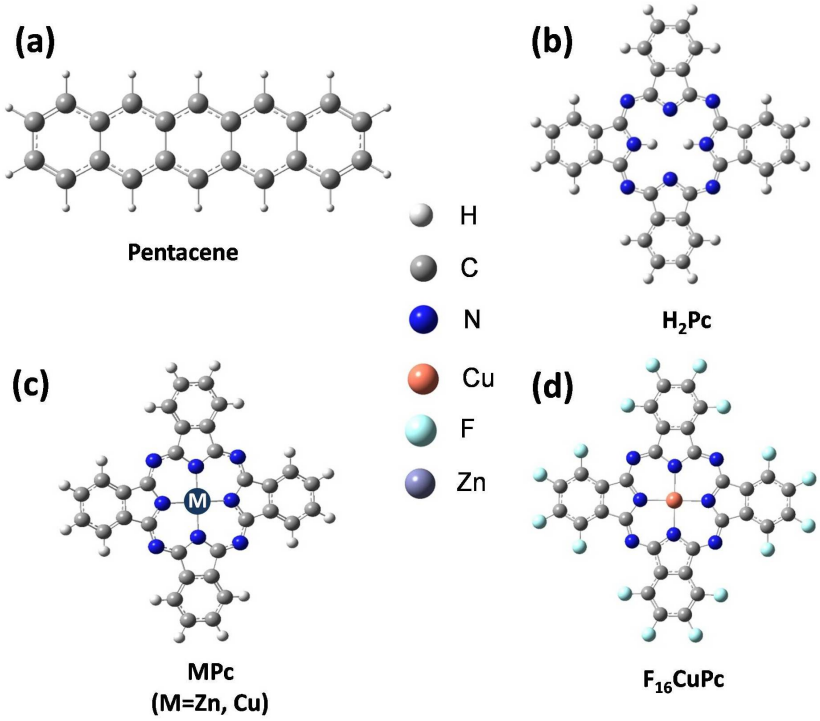


*Figure 3.1: Chemical structures of different organic molecules, optimized using Gaussian 09 [20]*

at optimized growth parameters are important molecules for organic field effect transistors (OFETs) and organic solar cells (OSCs) [17], (c) a range of metal ions can be placed in the central cavity of Pc macrocycle, consisting of four iminoisoindoline units and the central metal ion may also influence the charge transport properties of the molecule due to difference in the occupation of d-orbitals by central metal ion, (d) different substituents at the ligand of the Pcs may also affect the charge transport properties due to the modulation of molecular energy levels near Fermi level i.e. highest occupied molecular orbital (HOMO) and lowest unoccupied molecular orbital (LUMO). We choose different p-type phthalocyanines as; metal free phthalocyanine ($H_2Pc$), zinc phthalocyanine (ZnPc) and copper phthalocyanine (CuPc) to carry out our studies in the view of difference in occupation of d-orbital by central metal ion ($H_2Pc$; no metal, ZnPc; $d^{10}$ and CuPc; $d^9$) and n-type $F_{16}CuPc$ in order to see the effect of modulation of molecular orbitals. Chemical structures of these molecules, optimized using Gaussian 09 [20]

are shown in Fig. 3.1.

## 3.2 Different regimes of charge transport in semiconductors

Two most important charge transport mechanisms are band transport, generally observed in inorganic semiconductors and hopping transport, in disordered organic semiconductors, as schematically shown in Fig. 3.2. Lets discuss these mechanisms separately in brief.

(1) **Band Transport:**

It is generally observed in systems with long-range ordering. Due to the covalent bonding between the atoms in inorganic semiconductors overlapping between the orbitals of neighboring atoms is large. This leads to broad valence and conduction band in inorganic semiconductors. Charge carrier then moves like a delocalized plane wave within broad valence or conduction band, with some probability of finding at any location, resulting into coherent transport. In this regime, charge transport is limited by different scattering i.e. phonon scattering, impurity scattering etc [21]. Electronic structure calculations in solid state are required to characterize the delocalized charge transport. Calculation of electronic structure of solids is based on the band theory [22]. Mobility, limited by phonon scattering increases as the temperature decreases, following the relation, $\mu \propto T^{-n}$, n $\simeq$ 1.5 for inorganic semiconductors [21], due to a decrease in number of phonons at low temperature.

**(2) Hopping transport:**

In organic semiconductors, though covalent bonds bind the atoms within a molecule but, weak van der Waals bind among the neighboring molecules within organic solid. Hence, overlapping between adjacent molecules is weak, leading to narrow highest occupied molecular orbital (HOMO) or lowest unoccupied molecular orbital (LUMO) band with Gaussian distribution of localized states. Hence, charge carriers get trapped within the randomly distributed localized states and charge transport is described by the thermally activated hopping among neighboring sites. As energy of the carriers increases with temperature, it can hop to neighboring site easily. Hence, mobility increases with temperature following

the Arrhenius law ($\mu \propto \exp(-E_a/k_BT)$), $E_a$ being the activation energy). Generally, Marcus theory of self exchange reaction is used to investigate the charge transport in this regime and mobility is estimated using Einstein relation as [23], $\mu = eD/k_BT$.

## 3.3 Different aspects to study charge transport in organic semiconductors

### 3.3.1 Experimental techniques

Experimentally, charge transport in organic semiconductors is investigated by fabricating the devices based on thin films or single crystals. The most common device configurations are; OFETs, OLEDs and organic solar cells (OSCs). For investigating charge transport parallel to the substrate, OFETs are fabricated and characterized. However, by characterizing two terminal devices, charge transport along the perpendicular of the substrate can be investigated. Geometry and Working of two and three terminal devices based on organic thin films have been discussed in Chapter 2 in detail.

### 3.3.2 Theoretical methods

#### 1.3.2.1 Hopping regime

It is well known that charge transport in organic semiconductors is characterized by the discrete hopping events within the localized states in GDOS and these hops are assisted by the vibrations of the lattice. Several theories have been proposed so far to model the charge transport in hopping regime. Initially, Bassler formulated the hopping transport in disordered organic semiconductors using variable-range-hopping [2, 24]. He proposed that due to static and energetic disorder in the localized states in GDOS, Miller-Abrahams approach [4, 5] can be used to estimate the charge transfer rate ($k_{ij}$) between two sites (*i, j*). This formalism is known as Gaussian disorder model (GDM) [2]. According to Miller-Abrahams, $k_{ij}$ is estimated as [5],

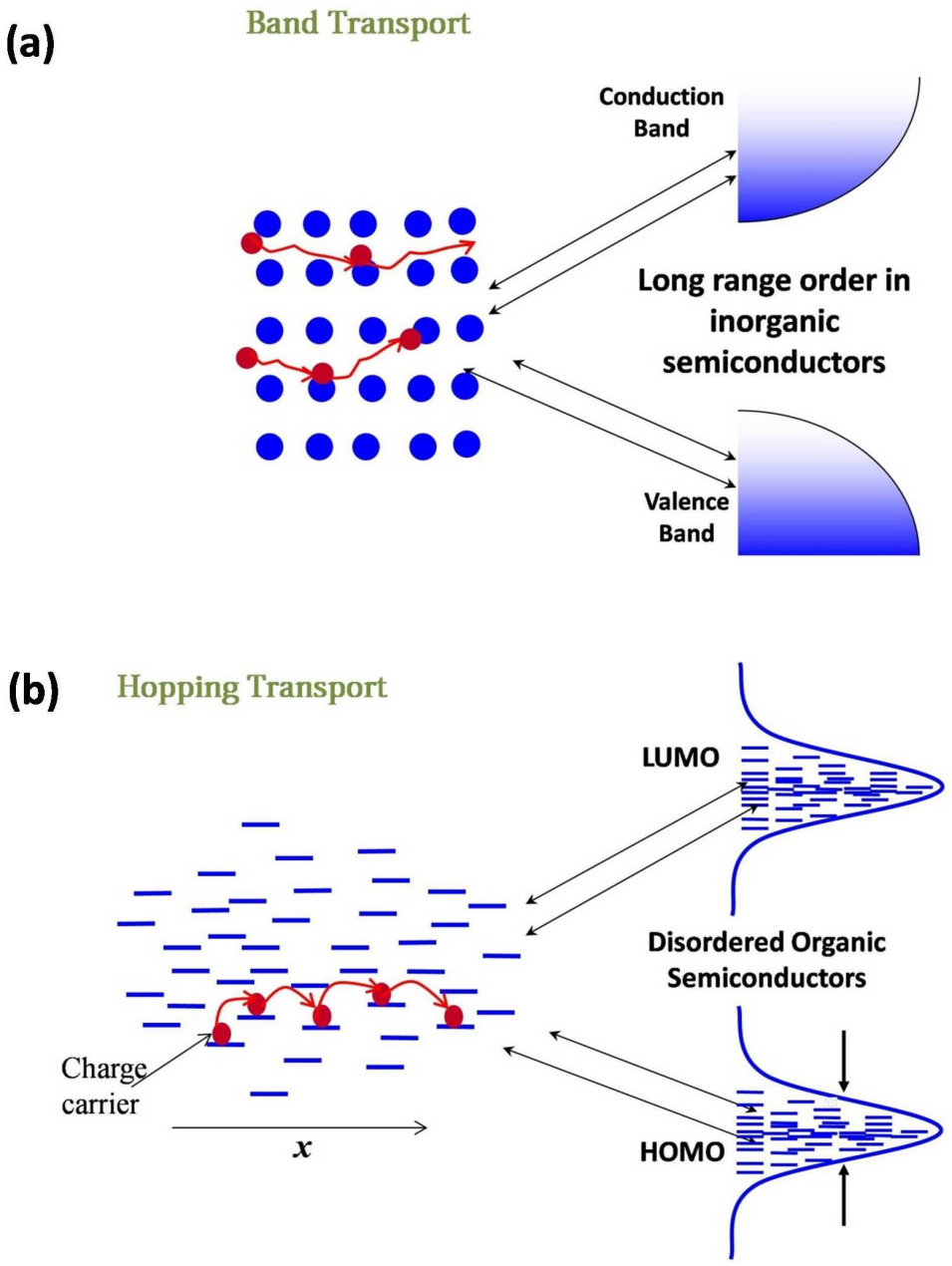


*Figure 3.2: Schematic representation of typical charge transport mechanisms in (a) inorganic semiconductors with long range order and (b) highly disordered organic semiconductors.*

$$k_{ij} = \nu_0 exp(-2\gamma|x_i - x_j|) \begin{cases} exp\left(-\frac{E_j - E_i}{k_B T}\right); & E_j > E_i \\ 1; & E_j < E_i \end{cases} \tag{3.1}$$

where, $\nu_0$ is the attempt frequency to hop, $E_i$ is the energy of the occupied site $i$ and $E_j$ of the initially unoccupied site $j$, and $\gamma$ is the inverse localization radius of the charge carriers. Here, $|E_i - E_j| \geq k_B T$ has been assumed. First exponential term represents the probability of tunneling between sites, $i$ and $j$ and second term accounts for the activation energy for hop.

In GDM, coupling of charge carrier with lattice vibration has been considered as perturbation only, however, in case of organic semiconductors this approximation breaks down, moreover, polaronic effects should be taken into account. Marcus took the strong charge carrier-phonon interaction into account and considered the charge transfer as a self exchange reaction with the transfer rate $k_{ij}$ as [6, 7],

$$k_{ij} = \frac{t_{ij}^2}{\hbar}\sqrt{\frac{\pi}{4\lambda k_B T}}\, exp\left(-\frac{\lambda}{k_B T} - \frac{E_j - E_i}{2k_B T} - \frac{(E_j - E_i)^2}{16 k_B T \lambda}\right) \tag{3.2}$$

where $\lambda$ represents the strength of coupling of the charge with the lattice phonon and is known as reorganization energy, $t_{ij}$ is the transfer integral, representing the strength of overlapping between neighboring sites. Hence, according to Marcus theory, in order to calculate $k_{ij}$, two parameters $t_{ij}$ and $\lambda$ have to be determined separately.

#### 1.3.2.2 Reorganization energy ($\lambda$)

As, external charge carrier interacts with the vibrations of the organic molecules, geometry of the molecule as well as the surrounding medium changes. Total $\lambda$ consists of two parts (i) internal and (ii) external. External part of $\lambda$ can be neglected due to the low polarity of most of the organic semiconductors and only internal part is significant. Internal reorganization energy is totally intrinsic property of the molecule and can be represented as [13],

$$\lambda = [(E_{\pm}^{'} - E_{\pm}) + (E^{'} - E)] \tag{3.3}$$

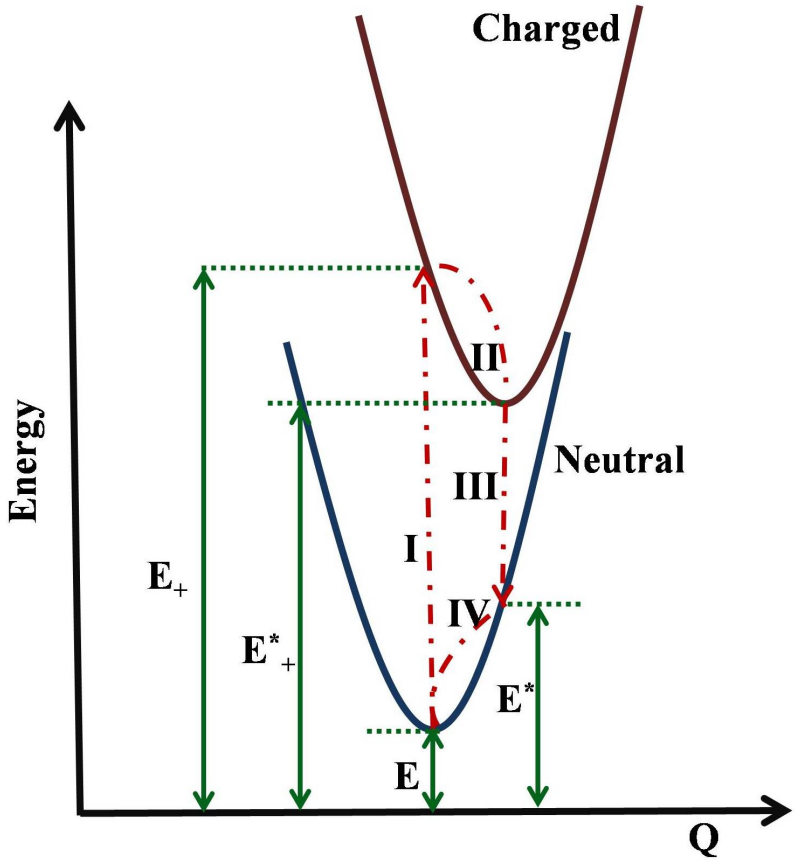


*Figure 3.3: The potential energy surfaces of the neutral and the charged monomer. After charging or discharging, molecules relax their nuclear coordinates. Different energies contributing to reorganization energy during charge transfer have also been represented.*

where $E$ and $E_{\pm}$ are the ground state energies of the molecule in the neutral state and in the ionic state respectively. $E^{'}$ is the energy of the neutral molecule in the optimized geometry of the charged molecule and $E^{'}_{\pm}$ is the energy of the charged molecule in the optimized geometry of the neutral molecule (Fig. 3.3). For efficient charge transport, $\lambda$ is required to be small.

#### 1.3.2.3 Transfer integral ($t_{ij}$)

Efficiency of charge transport also depends on the extent of overlapping between the neighboring molecules and $t_{ij}$ is a quantitative measure of the overlapping. Various numerical methods exist to estimate transfer integral and have

been reviewed in literatures extensively [1]. In a most popular approach, transfer integral for hole transport can be given as the half of the difference of HOMO and [HOMO-1] levels of the equivalent molecular dimmers in neutral state and this method is kown as energy splitting in dimer (ESD) method. In case of electron transport, difference between LUMO and LUMO + 1 is considered. In this chapter, we will discuss hole transport only. As frontier orbitals of monomers forming dimer are not orthonormal, ESD method is not able to predict accurate values of $t_{ij}$ and full wave function treatment is required.

Another method named dimer projection (DIPRO) method [25] has been used successfully to estimate $t_{ij}$. This method is based on the projection of monomer orbitals on the dimer orbitals. In this method, $t_{ij}$ is given by

$$t_{ij} = \frac{J_{ij} - 1/2(e_i + e_j)S_{ij}}{1 - S_{ij}^2} \tag{3.4}$$

where $J_{ij}$ is the electronic coupling element and given as, $J_{ij} = \langle \phi^i | H | \phi^j \rangle$, $H$ being the Hamiltonian for a dimer and is not orthonormal. $e_i(e_j)$ is site energy of a hole located on a monomer, *i(j)* with $e_{i(j)} = \langle \phi^{i(j)} | H | \phi^{i(j)} \rangle$ and $S_{ij} = \langle \phi^i | \phi^j \rangle$ is the element of some overlapping matrices $S$. Further $H$ and $S$ have the form,

$$H = \begin{bmatrix} e_i & J_{ij} \\ J_{ij} & e_j \end{bmatrix}$$

$$S = \begin{bmatrix} 1 & S_{ij} \\ S_{ij} & 1 \end{bmatrix}$$

and a secular equation representing this dimer system is as follows

$$(H - ES)\, C = 0 \tag{3.5}$$

$C$, is expansion coefficient. Now, as monomer orbitals are not orthonormal, $J_{ij}$ cannot provide accurate values of transfer integral and suitable transformation is required in order to make the $H$ orthonormal and Eq. 3.5 takes a form;

$$\left(\mathrm{H}^{'} - \mathrm{E}\right) \mathrm{C} = 0 \tag{3.6}$$

where $\mathrm{H}' = \mathrm{S}^{-1/2}\mathrm{H}\mathrm{S}^{1/2}$ and has the form

$$\mathrm{H}' = \begin{bmatrix} \epsilon_{\mathrm{i}} & \mathrm{t}_{\mathrm{ij}} \\ \mathrm{t}_{\mathrm{ij}} & \epsilon_{\mathrm{j}} \end{bmatrix}$$

with

$$\epsilon_{\mathrm{i(j)}} = \frac{1}{2}\frac{1}{1 - \mathrm{S}_{\mathrm{ij}}^2}\left((\mathrm{e}_{\mathrm{i}} + \mathrm{e}_{\mathrm{j}}) - 2\mathrm{j}_{\mathrm{ij}}\mathrm{S}_{\mathrm{ij}}(\mathrm{e}_{\mathrm{i}} - \mathrm{e}_{\mathrm{j}})\sqrt{1 - \mathrm{S}_{\mathrm{ij}}^2}\right) \tag{3.7}$$

Hence, to study intrinsic charge transport in organic semiconductors, electronic structure of isolated molecules and molecular solids need to be estimated. Many quantum-chemical methods are used to study the electronic structure of organic semiconductors. Each method discusses the solution of a Hamiltonian for a many body system by introducing some approximations, because analytical solution of the Hamiltonian for such a large and correlated system is impossible.

## 3.4 Approximations for evaluating electronic structures

Generally, to obtain the solution of a Hamiltonian for a stationary system, time independent Schroedinger equation needs to be solved and for a many body system this equation is written as

$$\mathrm{H}\Psi\left(\mathrm{R};\mathrm{r}\right) = \mathrm{E}\Psi\left(\mathrm{R};\mathrm{r}\right) \tag{3.8}$$

where $H$ is the Hamiltonian of the system, containing the kinetic and potential energy operators; $E$ is the energy of the system; $\Psi\left(\mathrm{R};\mathrm{r}\right)$ is the wavefunction of the system; $R$ are the positions of the nuclei, and $r$ are the variables that describe the coordinates of the electrons. If we consider a system with $M$ nuclei and $N$ electrons, total $H$ in terms of different components of kinetic and potential

energies can be written as,

$$H = T_e + T_N + V_{eN} + V_{ee} + V_{NN} \tag{3.9}$$

where $T_e$, $T_N$, $V_{eN}$, $V_{ee}$ and $V_{NN}$ represent the kinetic energy of the electrons, kinetic energy of the nuclei, attractive interactions between nuclei and electrons, repulsive interactions among the electrons and repulsive interactions among the nuclei, respectively. Each of theses terms can be written separately as,

$$T_e = -\sum_i \frac{\hbar^2}{2m_e} \bigtriangledown r_i^2 \tag{3.10}$$

$$T_N = -\sum_I \frac{\hbar^2}{2m_N} \bigtriangledown R_I^2 \tag{3.11}$$

$$V_{eN} = -\sum_{iI} \frac{Z_I e^2}{|R_I - r_i|} \tag{3.12}$$

$$V_{ee} = \frac{1}{2} \sum_{i \neq j} \frac{e^2}{|r_i - r_j|} \tag{3.13}$$

$$V_{NN} = \frac{1}{2} \sum_{I \neq J} \frac{Z_I Z_J e^2}{|R_I - R_J|} \tag{3.14}$$

($4\pi\epsilon_0$ has been take to be 1 in all the potetial energy terms.)
Exact solution of the Schroedinger equation for such a large system containing several atoms and electrons seems impossible as motions of electrons and nuclei are correlated. Many approximations are used to determine the eigen values and wave functions for such a large system. Here, we give a brief description of some important and widely applied approximations.

### 3.4.1 Born-Oppenheimer Approximation

In Born-Oppenheimer Approximation, nuclei are assumed to be fixed due to their much larger (approx. 2000 times) mass than that of electrons. Hence kinetic energy term for nuclei in the Hamiltonian should be omitted and $\Psi(R; r)$ can be replaced by $\Psi(r)$. Then electrons are assumed to move in the field of the fixed

nuclei and rearrange themselves instantaneously after any movement of atoms. Within this approximation, Hamiltonian for a many body system can be given as

$$\mathrm{H} = \mathrm{T_e} + \mathrm{V_{eN}} + \mathrm{V_{ee}} + \mathrm{V_{NN}} \tag{3.15}$$

Though, $H$ has been simplified to some extent by applying the Born-Oppenheimer approximation, analytical solution of $H$ is still different due to the correlated motion of electrons. Hence some other approximations should also be applied in order to get more simplified form of $H$ but, solution should be as accurate as possible.

### 3.4.2 Hartree-Fock approximations

Lets first discuss the Hartree approximation and then come to Hartree-Fock approximations. Hartree assumed the $N$ electrons in the system as non-interacting particles and wrote $\Psi(\mathrm{r})$ in terms of $N$ orthonormal wavefunctions, corresponding to $N$ non-interacting electrons as

$$\Psi^{\mathrm{H}}(\mathrm{r}) = \phi_1(\mathrm{r}_1)\phi_2(\mathrm{r}_2).....\phi_{\mathrm{N}}(\mathrm{r}_{\mathrm{N}}) \tag{3.16}$$

Now, as electrons are Fermi particles with half-integral spin, in order to satisfy the asymmetry principle when two electrons exchange the coordinates, $\Psi(\mathrm{r})$ must be expressed in form of a slater determinate as,

$$\Psi^{\mathrm{HF}}(\mathrm{r}) = \frac{1}{\sqrt{\mathrm{N!}}} \begin{vmatrix} \phi_1(\mathrm{r}_1) & \phi_1(\mathrm{r}_2) & \dots & \phi_1(\mathrm{r}_{\mathrm{N}}) \\ \phi_2(\mathrm{r}_1) & \phi_2(\mathrm{r}_2) & \dots & \phi_2(\mathrm{r}_{\mathrm{N}}) \\ \dots & \dots & \dots & \dots \\ \dots & \dots & \dots & \dots \\ \phi_{\mathrm{N}}(\mathrm{r}_1) & \phi_{\mathrm{N}}(\mathrm{r}_2) & \dots & \phi_{\mathrm{N}}(\mathrm{r}_{\mathrm{N}}) \end{vmatrix} \tag{3.17}$$

This is called Hartree-Fock approximation. In this approach, total energy of the system $\mathrm{E^{HF}}$ is give as,

$$\mathrm{E^{HF}} = \langle \Psi^{\mathrm{HF}} | \mathrm{H} | \Psi^{\mathrm{HF}} \rangle \tag{3.18}$$

In this approach, solution of Hamiltonian is obtained by the use of variational principle which states that when a trial normalized wave function is used in Schrodinger equation, estimated enrgy ($E_e^{HF}$)is always higher than the actual ground state energy ($E_0^{HF}$). If the trial wave function matches with the actual ground state wave function then both the energies are equal i.e.

$$E_e^{HF} \geq E_0^{HF} \tag{3.19}$$

Although HF theory is able to give an approximate solution for ground state energy, improvements are needed in order to get a solution much closer to the exact one. Main difference between the estimated and exact energy is attributed to the fact that in this theory, electrons are supposed to move in an average field created by all other elctrons. It does not take into account the intrinsic electron correlation.

## 3.5 Density Functional Theory (DFT)

DFT is the most efficient tool to predict the ground state properties of many-body systems. It relies on the density of particles in the ground state of the system. Within this approach, particle density ($\rho(r)$) rather than the wave function, $\Psi(r)$ is taken as a variable and the two are related to each other through the relation

$$\rho(r) = N \int dr_1 dr_2 ....dr_{N-1} |\Psi(r_1, r_2 ... r_N)|^2 \tag{3.20}$$

This approach is favorable as problem of many body Schroedinger equation changes into a single particle density. To understand the basics of DFT in more details two fundamental theorems need to be discussed.

### 3.5.1 First Hohenberg-Kohn theorem

According to First Hohenberg-Kohn theorem, if there is a system of interacting particles under an external potential V(r), a unique functional of density $\rho(r)$ exists by which the ground state properties of the system can be determined. Hence, total energy of the system in ground state can be written as

$$E_0 = \langle \Psi | H | \Psi \rangle = \langle \Psi | T_e + V_{ee} + V_{eN} | \Psi \rangle \tag{3.21}$$

or in terms of $\rho_0$

$$E_0(\rho_0) = T_e(\rho_0) + E_{ee}(\rho_0) + E_{eN}(\rho_0) \tag{3.22}$$

Here, $T_e$, $E_{ee}$ and $E_{eN}$ represent the contribution to the total energy by the kinetic energy of electrons, electrostatic interaction among electron-electron and nuclear-electron term. In their original paper [26], Hohenberg and Kohn defined a functional $F[\rho]$, consisting of the sum of following two terms

$$F[\rho] = T_e(\rho) + E_{ee}(\rho) \tag{3.23}$$

and energy functional takes the form

$$E(\rho) = F[\rho] + E_{Ne}(\rho) \tag{3.24}$$

The main task in DFT is to find a appropriate form of $F(\rho)$.

### 3.5.2 Second Hohenberg-Kohn theorem

Second theorem is somewhat analogous to Hartree-Fock approximation and it also employs the variation principle but a functional of density instead of a wavefunction is used. This theorem tells that any trial density functional ($F[\rho]$) provides the lowest energy i.e. actual ground state energy if input density in density functional provides the true density of the ground state, $\rho_0$. Otherwise, energy is always larger than the ground state energy i.e.

$$E(\rho) \geq E(\rho_0) \tag{3.25}$$

In summary, DFT can be successfully applied to estimate the ground state properties of correlated system. Although variational principle can be used to estimate ground state energy and wave functions, more approximations have been proposed and may be more accurate.

### 3.5.3 Kohn-Sham equations

Kohn and Sham utilized the theory of Hohenberg and Kohn, originally proposed for an inhomogeneous system of interacting electrons and developed approximations in order to estimate the form of $F[\rho]$ [27]. They suggested that complex system with interacting electrons can be considered equivalent to some other non interacting system and a functional of density named exchange-correlation functional ($E_{XC}$) can be introduced that contains all the extra difficult terms of interacting system. Further, they proposed that this non interacting reference system is under effective local potential ($V_{eff}$). Hence, Hamiltonian ($H_s$) for a $N$ electron system is

$$H_s = T_s + V_s \tag{3.26}$$

where $T_s = \sum_i T_i$ is kinetic energy of the reference system and $V_s = \sum_i V_{eff}(r_i)$ is the local effective potential. But $H_s$ does not represent the true interacting system. Hence Kohn and Sham defined the functional $F[\rho]$ as

$$F[\rho] = T_s[\rho] + I[\rho] + E_{XC}[\rho] \tag{3.27}$$

$I[\rho]$ accounts for the electron-electron interaction for non interacting system and $E_{XC}[\rho]$ has the form

$$E_{XC}[\rho] = (T[\rho] - T_s[\rho]) + (E_{ee}[\rho] - I[\rho]) \tag{3.28}$$

$T[\rho]$ and $E_{ee}$ being the same energy term for true system. Now the problem of large interacting system is simplified to a problem of estimating the form of $E_{XC}[\rho]$. Different approaches have been developed to estimate the form of $E_{\chi C}$ as accurate as possible. some of the popular approximations are: local density approximation (LDA), general gradient approximation (GGA) and hybrid functionals.

## 3.6 Electronic structure calculation for molecular solid

DFT calculations are used in some different manner to estimate the electronic structure of crystalline molecular solids from those employed for individual molecules. As crystalline solids possess large density of electrons and ions ($\approx 10^{24}/\mathrm{cm}^3$), it seems impossible to write a Hamiltonian of the type as proposed by Kohn and Sham for individual molecules. Crystallines solids have periodic structures hence, problems based on such a large systems can be reduced to one that can be solved by the knowledge of the minimum unit cell of the solid. Hence periodicity of the lattice must be taken into account while writing the Kohn-Sham Hamiltonian for the solids. Periodicity means effective potential $\mathrm{V_{eff}}$ used in Kohn-Sham equation for individual molecules should also have a periodic form as

$$\mathrm{V_{eff}} = \mathrm{V_{eff}}(\mathrm{r} + \mathrm{R}) \tag{3.29}$$

R, being the lattice vector. To write an acceptable form of wavefunction for the Hamiltonian with periodic potential, Bloch's theorem is used. According to this theorem, a wavefunction should have the form as,

$$\psi^{\mathrm{k}}(\mathrm{r}) = \sum_{\mathrm{n}} \mathrm{e}^{\mathrm{ik.R}} \phi_{\mathrm{nk}}(\mathrm{r}) \tag{3.30}$$

where $\phi_{\mathrm{nk}}(\mathrm{r})$ is written as,

$$\phi_{\mathrm{nk}}(\mathrm{r}) = \mathrm{e}^{\mathrm{ik.r}} \mathrm{u_{nk}}(\mathrm{r}) \tag{3.31}$$

here $\mathrm{e}^{\mathrm{ik.r}}$ represents a plane wave and $\mathrm{u_{nk}}$ is a periodic function of the form

$$\mathrm{u_{nk}}(\mathrm{r}) = \mathrm{u_{nk}}(\mathrm{r} + \mathrm{R}) \tag{3.32}$$

and energy eigenvalue should exhibit the form,

$$\mathrm{E_n}(\mathrm{k}) = \mathrm{E_n}(\mathrm{k} + \mathrm{G}) \tag{3.33}$$

$G$, being the translation vector in reciprocal space.

## 3.7 Software packages used

To estimate the electronic structure of isolated molecules or molecular solids, different softwares are available. Each of them has its advantages as well drawbacks. Here, we give the description of the softwares used in this thesis.

### 3.7.1 Gaussian 09

Gaussian 09 (G09) is a computer program, generally used for computational chemistry [20]. It is able to predict several properties such as optimized geometry, energy, electronic structure, vibrational frequencies, charge density etc., for different organic and inorganic systems. It utilizes various computational modeling methods such as molecular mechanics, density functional theory (DFT), ab-initio and many hybrid methods. A visualization software, Gauss View is used in conjunction with G09 in order to build the molecules, to set up the Gaussian jobs and to view the results after the completion of the job.

### 3.7.2 Votca

VOTCA stands for Versatile Object oriented Toolkit for Coarse-graining Applications and CTP represents its "Charge Transport" toolkit [28]. Use of VOTCA-CTP simplifies the charge transport simulation in an organic semiconductor. It consists of different programs written in modular C++ code and several scripts also. A program in VOTCA-CTP is run by a command which executes a specific task. All the data generated by the output of a program is stored in the database file (state.sql) in sqlite3 format, which is used for further calculations.

### 3.7.3 Quantum Espresso

ESPRESSO stands for opEn-Source Package for Research in Electronic Structure, Simulation, and Optimization [29]. It allows one to execute electronic structure calculations within density functional theory (DFT) using plane wave basis set and pseudopotentials. It consists of many core packages: PWscf, CP, PWneb, PHonon, PostProc, PWcond, XSPECTRA, TD-DFPT etc..

## 3.8 Methodology

### 3.8.1 Experimental Details

Starting materials are triple sublimed 99.999% pure to reduce the chemical impurities as much as possible. Thin films based on different organic molecules such as pentacene and Pcs have been fabricated on the substrates; $SiO_2$/Si and ITO/glass substrate. The devices used in this study are two terminal hole only devices and three terminal based devices i.e OFETs. For hole only devices, 200 nm thick single layer of organic molecules is sandwiched between two metal electrodes. For OFETs, organic thin films as active layers are fabricated on $n^{++}Si/SiO_2$ substrate. Au source and drain contacts are deposited on organic layers using shadow mask. The channel length and width are fixed at 20 $\mu$m and 3 mm, respectively. Each layer is deposited in a vacuum chamber at a rate of 0.1 Å/s using an oil free deposition system. Controlling mechanism of growth to get desired morphology depends upon the balancing between diffusion of the molecules on the substrate ($D_s$) and deposition flux ($F_G$). Slower deposition rate results thin film growth close to equilibrium conditions since incoming molecules get enough time to locate a favorable orientation resulting lesser number of nucleation sites and as a consequence larger grains. All organic layers and metal electrodes are grown at a base pressure of $2 \times 10^{-6}$ Torr. Thin film morphology has been analyzed using Park Systems Atomic Force Microscopy (AFM) in non-contact mode. Crystallinity of thin films have been investigated by performing grazing incidence XRD using PANalytical Xpert Pro syetem. The electrical measurements were performed in rough vacuum ($10^{-2}$ mbar) using Keithley picoammeter and voltage sources.

### 3.8.2 Computational Details

Monte Carlo simulations have been performed, to study the evaluation of surface morphology of pentacene thin film. Marcus theory [6] has been employed to study charge transport in hopping regime. To estimate different charge transport parameters in hopping regime, we have used Gaussian 09. All parameters for hopping mobility have been calculated, by employing ground state energy calculations on pentacene monomer and dimers on the B3LYP (Becke, three- parameter, Lee-Yang-Parr) [11, 30] functional and 631-G (d,p) basis set [31]. To estimate $\lambda$,

geometries of neutral and ionic molecules are optimized and the single point energy are run on optimized geometries. Transfer integrals $t_{ij}$ have been calculated from the output of Gaussian calculations using versatile Object-oriented Toolkit for Coarse-graining Applications (VOTCA) package [28]. VOTCA takes the non-orthonormality of monomer orbitals into account and estimates $t_{ij}$ by projecting monomer orbitals on the dimer orbital.

Periodic DFT calculations have also been performed in order to estimate the electronic structure and charge transport parameters of molecular solid. The different transport parameters in this regime have been estimated using Quantum Espresso [29]. To study different transport parameters, experimentally determined lattice parameters of pentacene bulk phase have been taken as initial point. Atomic coordinates have been relaxed on $4 \times 4 \times 3$ MonkhorstPack k-mesh. Non scf calculation for density of states have been performed on denser k mesh of $6 \times 6 \times 4$. We use generalized gradient approximatin (GGA) with the Perdew-Burke-Ernzerhol (PBE) [32] exchange correlation function and ultrasoft pseudopotentials. Dispersion interactions between organic molecules have been taken into account by using London type pairwise empirical atomic interactions as implemented by DFT-D2 method [33, 34].

## 3.9 Evaluation of surface morphology of pentacene thin film

Orientation of the organic molecules on the substrate i.e. surface morphology of organic thin films has strong influence on the charge carrier transport. Hence, growth physics of thin film in monolayer and mulitlayer should be studied which may be useful in investigating charge transport parallel and perpendicular to the film surface. Figure 3.4 shows the evaluation of surface morphology of pentacene thin film from monolayer (0.2 nm) to multilayers (10 nm). Upper panel in Fig. 3.4 shows the surface topographic images of pentacene thin films, grown on $SiO_2$ at room temperature with a very slow rate of 0.1Å/s. At very low thickness of 0.2 nm, the film shows small islands uniformly distributed on the surface (Fig. 3.4(a)). With increasing film thickness the islands grow across the surface meeting other existing nuclei exhibiting fractal shape (Fig. 3.4). As the thickness of

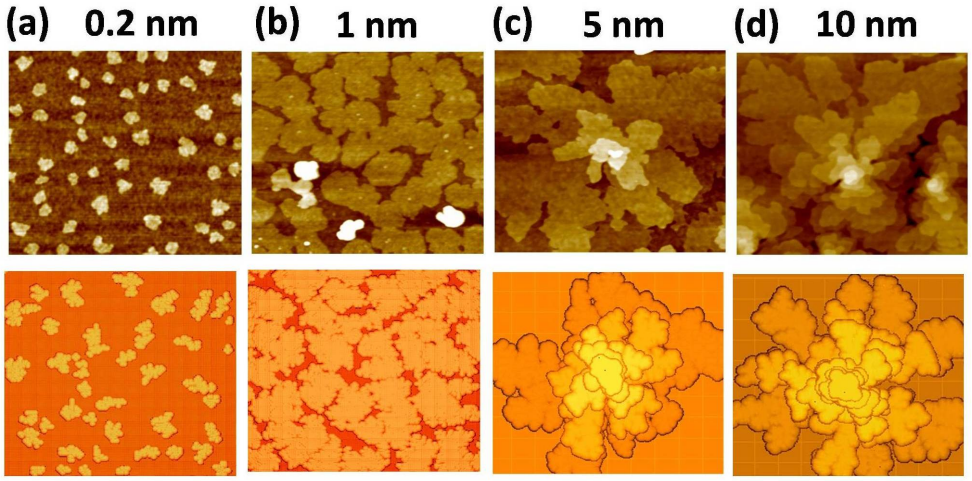


*Figure 3.4:* ***Growth dynamics of pentacene thin film:*** *upper panel shows the AFM topographic images (size 2 $\mu$m $\times$ 2 $\mu$m) of pentacene thin films with thickness of (a) 0.2 nm (b) 1nm (c) 5 nm and (d) 10 nm. Lower panel shows the corresponding morphologies generated by Monte Carlo simulation. Inclusion of Schwoebel barrier in DLA mechanism could reproduce the surface morphology of pentacene multilayer thin films.*

the film increases, islands also become larger in size but second layer nucleation occurs before the first monolayer covers the complete surface by the coalescence of individual islands in first monolayer. Same process repeats for subsequent layers, resulting into fractal-mound growth. To study the evaluation of surface morphology of pentacene thin film for different coverage, we have used Monte Carlo simulations with the results shown in lower panel of Fig. 3.4. Simulated morphological patterns resemble the real surface morphologies of pentacene thin films, acquired by AFM, closely. In simulation, initially a few number of lattice sites are randomly distributed. A monomer is added to the lattice one at a time, which is then allowed to diffuse randomly until it hits a binding position. Compact islands at very low coverage can be attributed to the growth perpendicular to the branch axis. Due to the perpendicular growth, space between branches within a single island is filled, resulting into coalescence of neighboring branches and formation of compact islands. Hence, for an individual two dimensional island, the shape is a result of competition between two kinetic processes: edge diffusion and monomer incorporation [35]. Edge diffusion is characterized by the time it takes a monomer diffusing along the island edge to find an energetically fa-

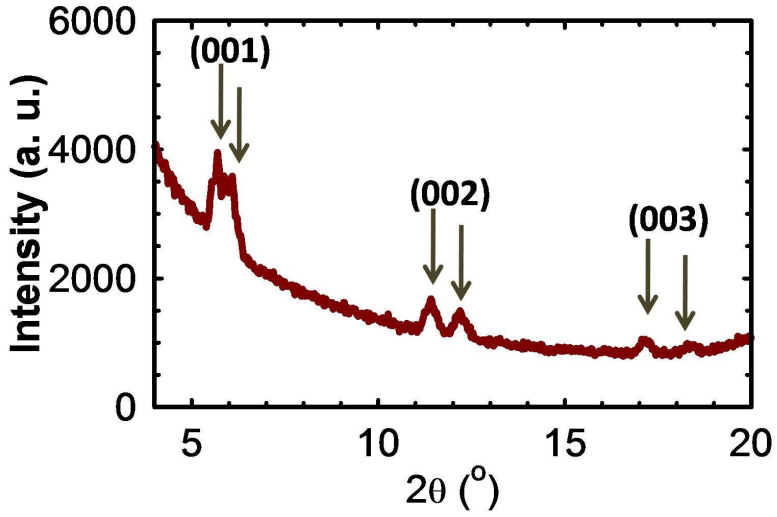


*Figure 3.5: X-ray diffraction (XRD) pattern of pentacene thin film grown at room temperature on $SiO_2$.*

vorable binding site; monomer incorporation is characterized by the average time interval between two successive monomer incorporation events. As the surface coverage increases, growth of pentacene in submonolayer regime can be characterized by diffusion limited aggregation (DLA) [12, 36]. In DLA, incident molecules first move on the surface to meet other already existing nuclei. When a critical number of molecules four in case of Pentacene meet they form a stable nuclei which further grows on subsequent deposition [37]. DLA mode is obtained when monomer incorporation is made faster than edge diffusion in simulation. To simulate the fractal-mound growth for higher thickness of pentacene thin film, a term, "Schwoebel barrier" [38] is taken into account in simulation. Schwoebel barrier is a potential barrier which prevents the molecules incident on the top of the first layer to hop downward and new nucleation center forms on the first monolayer. In this way density of monomers increases in second monolayer and subsequently, stable islands form in second monolayer. Mechanism repeats for further monolayers and results into horizontal DLA plus vertical mound growth.

## 3.10 Orientation of pentacene molecules on substrate surface

Figure 3.5 shows the X-ray diffraction (XRD) pattern of pentacene thin film grown at room temperature on $SiO_2$. XRD pattern of pentacene exhibits three diffraction peaks at $2\theta = 5.7^{o}$, $11.4^{o}$ and $17.25^{o}$ corresponding to the plane (001), (002) and (003) [39]. It means that ab-plane lies parallel to the substrate and charge transport in OFETs should be governed by this plane. Whereas c-axis that lies almost perpendicular to the substrate should be main direction of charge transport in two terminal sandwiched devices. Further, average interplanar spacing has been estimated to be 1.54 nm, consistent with the c-axis of unit cell of pentacene in thin film phase [39]. However, other low intensity peaks at $2\theta = 6.09^{o}$, $12.2^{o}$ and $18.4^{o}$ results the interplanar spacing to be $\sim 1.45$ nm, consistent the bulk phase of pentacene [40, 41]. Hence, pentacene thin film exhibits the contributions due to both phase i.e thin film and bulk phase. However, thin film phase dominates the bulk phase.

As is clear from the structural characterization, growth of pentacene thin films along the parallel and perpendicular to the substrate takes place by two different mechanisms i.e DLA and mound growth, respectively. Mechanism of charge transport may also be different along these directions.

## 3.11 Directional dependence charge transport in pentacene thin film

### 3.11.1 Arrangement of molecules in two terminal devices

To investigate the charge transport along the perpendicular to the film surface, we have sandwiched 200 nm thick film of pentacene between ITO and Au. Figure 3.6(a) shows the arrangement of pentacene molecules in two terminal sandwiched devices. Pentacene is a hole transport material with HOMO at 5.0 eV and LUMO at 3.1 eV. The work functions of Au and ITO are 5.2 eV and 4.8 eV, respectively [42]. There would be no barrier at Au/Pentacene interface, and a very small barrier of 0.2 eV exists for hole at ITO/Pentacene interface. The current-voltage

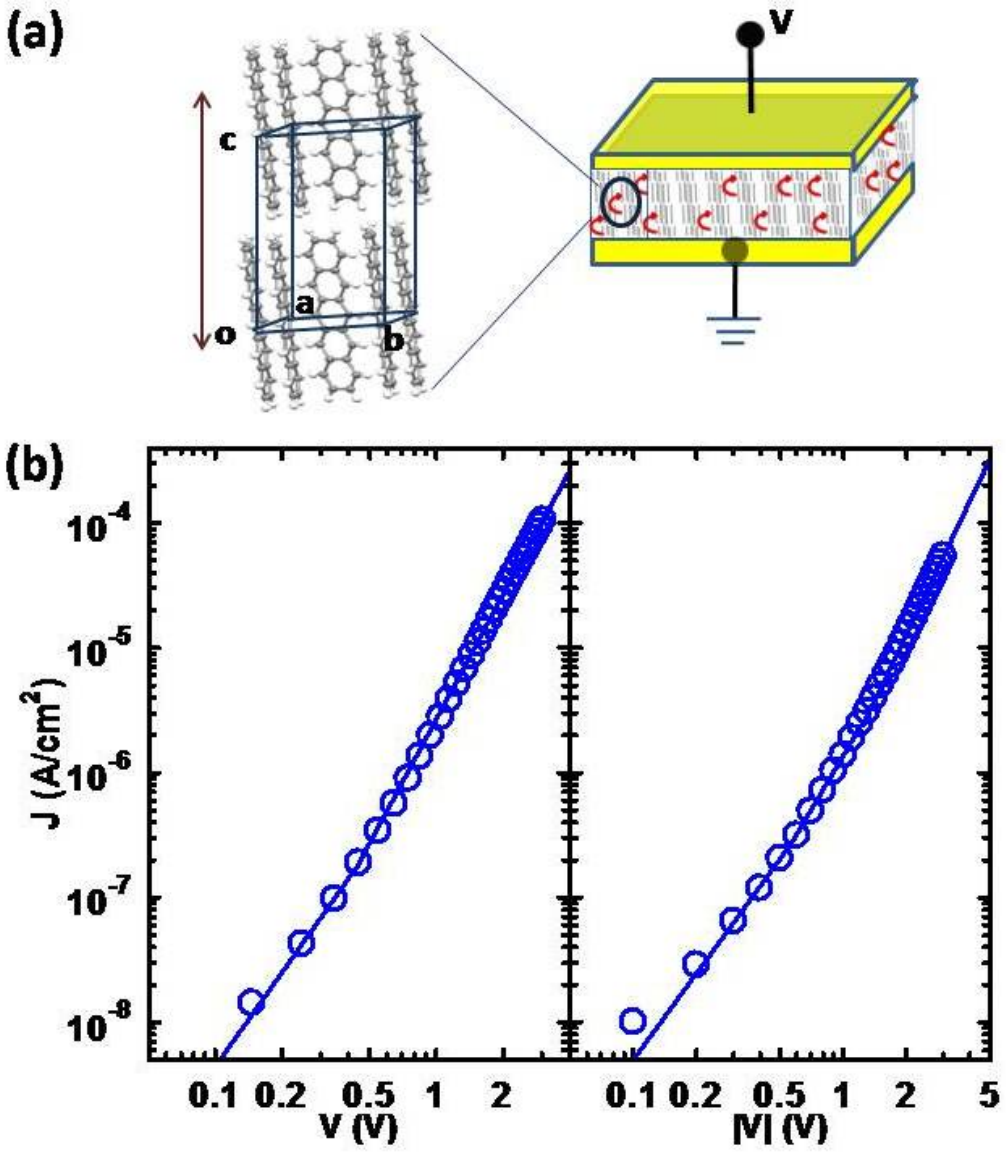


*Figure 3.6: (a) Schematic representation of unit cell of pentacene (left) and the arrangement of molecules in a two terminal device (right) and (b)J-V characteristics of ITO/pentacene/Au based two terminal device in forward (left) and reverse bias (right) on a log-log plot. Solid lines show theoretical fittings with field and carrier concentration dependent mobility.*

($J$-$V$) characteristics of a hole only ITO/Pentacene/Au based two terminal device is shown in Fig. 3.6(b). The current due to the hole injection from positively biased Au was measured (left panel of Fig. 3.6(b)) and then the current due to hole injection from ITO was measured by reversing the polarity of the bias voltage V (right panel of Fig. 3.6(b)). $J$-$V$ characteristics of ITO/Pentacene/Au devices display weak asymmetric behavior. The current injected from Au electrode is more than that from ITO electrode. Current in both cases i.e either injected from Au or from ITO shows non linear dependence on $V$. Hence, SCLC should be the mechanism of charge transport in forward as well as reverse bias. $J$-$V$ characteristics shown in Fig. 3.6(a) exhibit square law at very low bias but beyond that slope increases gradually hence, Mott-Gurneys square law, given by [43],

$$\mathrm{J} = \frac{9}{8}\epsilon_{\mathrm{s}}\mu\frac{\mathrm{V}^2}{\mathrm{d}^3} \tag{3.34}$$

is not applicable to model the $J$-$V$ characteristics. Here, $\epsilon_{\mathrm{s}}$ is the dielectric constant of organic semiconductors and $d$ is the thickness of the organic thin film. Enhancement in reverse and forward currents from square law have been explained on the basis of field dependent mobility ($\mu[\mathrm{T},\mathrm{F}]$) as proposed by Bassler *et. al.* [2] and field and carrier concentration dependent mobility ($\mu[\mathrm{T},\mathrm{p},\mathrm{F}]$) as proposed by Pasveeer *et. al.* [44], respectively. $J$-$V$ characteristics in forward bias were also tried to fit with field dependent mobility however, simulated data was not consistent with the experimental data. In reverse bias, $J$-$V$ characteristics have been simulated, by solving the following set of equations self consistently,

$$\mathrm{J} = \mathrm{ep}\,(\mathrm{x})\,\mu\,[\mathrm{T},\mathrm{F}\,(\mathrm{x})]\,\mathrm{F}\,(\mathrm{x}) \tag{3.35}$$

$$\frac{\mathrm{dF}\,(\mathrm{x})}{\mathrm{dx}} = \mathrm{e}\frac{\mathrm{p}\,(\mathrm{x})}{\epsilon_{\mathrm{s}}} \tag{3.36}$$

$$\mathrm{V_{DS}} = \int_0^{\mathrm{L}} \mathrm{F}\,(\mathrm{x})\,\mathrm{dx} \tag{3.37}$$

where, *p(x)* is the density of charge carriers at a distance $x$ from the injecting electrode. In reverse bias $J$-$V$ characteristics could be fitted to the field dependent mobility as shown by solid line in Fig. 3.6(b) (right) whereas in forward bias, $J$-$V$ characteristics are simulated, by solving the following set of equations self

consistently [44].

$$J = ep(x)\,\mu[T, p, F(x)]\,F(x) \tag{3.38}$$

$$\frac{dF(x)}{dx} = e\frac{p(x)}{\epsilon_s} \tag{3.39}$$

$$V_{DS} = \int_0^L F(x)\,dx \tag{3.40}$$

As suggested by Pasveer *et. al.* [44], field and carrier concentration dependence of mobility is represented by the following Eqs.

$$\mu(F, p, T) = \mu(p, T)g(F, T) \tag{3.41}$$

$$\mu(p, T) = \mu_0 c_1 e^{(-c_2\widehat{\sigma}^2)} e^{\left[\frac{1}{2}(\widehat{\sigma}^2-\widehat{\sigma})(2pa_0^3)^{\delta}\right]} \tag{3.42}$$

$$g(F, T) = \left\{0.44\left(\widehat{\sigma^2}-\widehat{\sigma}\right)\left[\sqrt{1+0.8\left(\frac{Fea_0}{\sigma}\right)^2}-1\right]\right\} \tag{3.43}$$

where $\mu(p, T)$ and $g(F, T)$ are the mobility components for electric field $F$ and the charge carrier density $p$, respectively. $\mu_0 = \frac{a_0^2\nu_0 e}{\sigma}$, is the charge carrier mobility at infinite temperature, $a_0$ is the lattice constant, $\delta = 2\frac{\ln(\widehat{\sigma}^2-\widehat{\sigma})}{\widehat{\sigma}^2}$, $\widehat{\sigma} = \sigma/k_B T$, $\sigma$ is the width of GDOS, $c_1 = 1.8 \times 10^{-9}$ and $c_2 = 0.42$. The excellent fit of the experimental data in forward bias (solid line in the left figure in FIg. 3.6(b)) using this approach shows that at higher applied bias, the current mechanism is controlled by more complex interplay between the field and charge carrier density. There are three fitting parameters $\mu_0(T)$, $\sigma$ and $a_0$ and have been found to be 5.4 $\times 10^{-6}$ $cm^2/Vs$, 0.11 eV and 1.6 nm, respectively. Hence pentacene molecules on ITO lie almost perpendicular to the substrate.

### 3.11.2 Arrangement of pentacene molecules in three terminal devices

Figure 3.7(a) shows structure of OFET used for study the charge transport in plane parallel to the film surface with the arrangement of pentacene molecules in that plane i.e ab-plane. In right side, different dimers governing the charge transport have also been shown. Fig. 3.7(b) shows the room temperature output

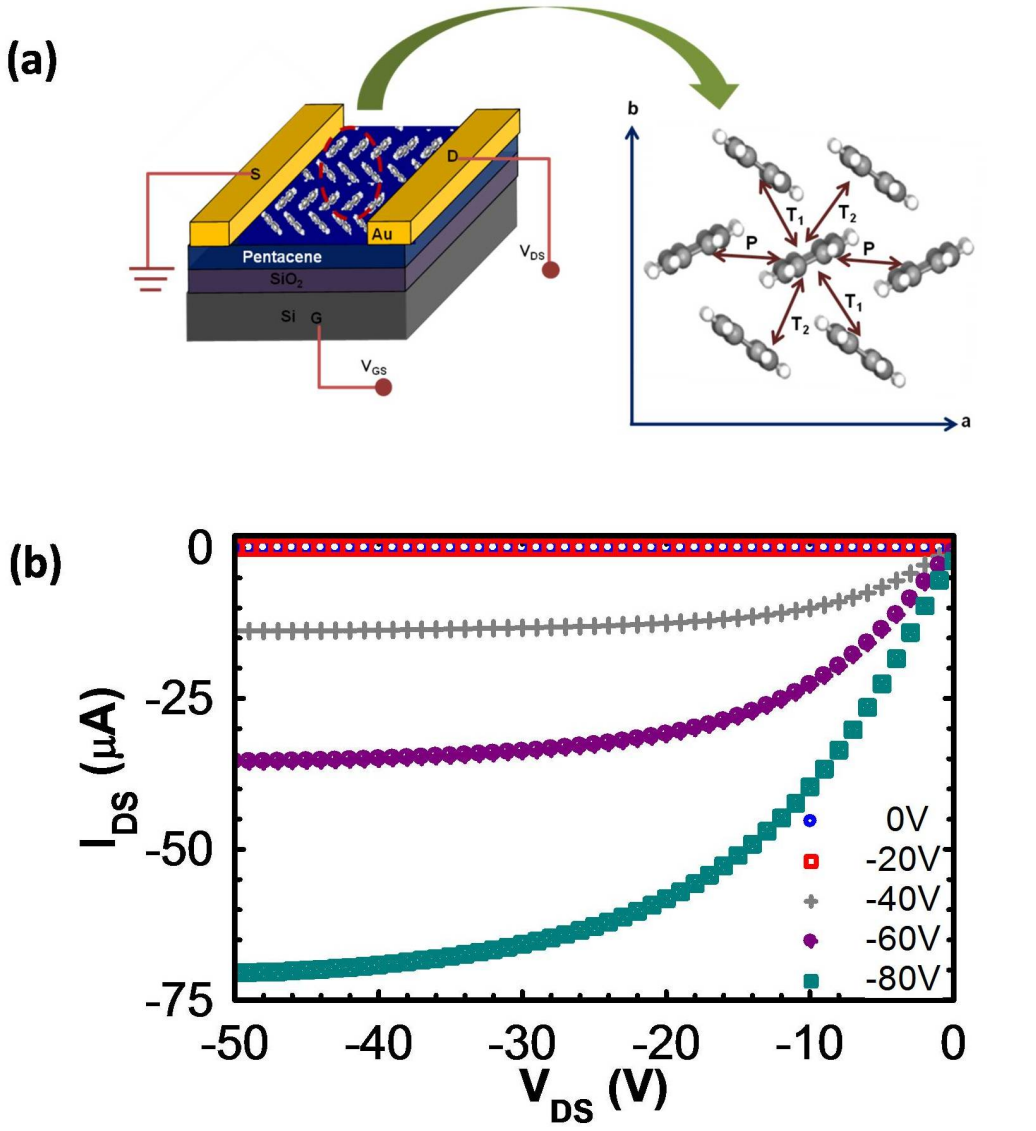


*Figure 3.7: (a) Schematic representation of pentacene thin film based OFET used to study charge transport in ab-plane. Right panel represents the different dimers that govern the charge transport in ab-plane; P dimers along a-axis, transverse dimers* $T_1$ *and* $T_2$ *, along diagonals. (b) Shows the room temperature* $I_{DS} - V_{DS}$ *characteristics at different gate bias varying from 0 to -80 V for a pentacene based OFET.*

characteristics ($I_{DS}$ – $V_{DS}$) for a pentacene based OFET. To estimate carrier mobility, $I_{DS}$ – $V_{DS}$ characteristics in linear region have been fitted according to the Eq. [23],

$$I_{DS} = \mu \frac{W}{L} C_i \left[ (V_G - V_T) V_{DS} - \frac{V_{DS}^2}{2} \right] \tag{3.44}$$

where $C_i$ is the dielectric capacitance per unit area, $W$ is the channel width, $L$ is the channel length and $V_T$ is the threshold voltage. Room temperature mobility estimated in this way has been found 0.3 $cm^2$/Vs, matching well with the typical mobilities observed in other studies [45, 46]. We observe that magnitudes of mobility in three terminal devices are higher by almost five orders than that in two terminal devices based on same pentacene thin film whereas the distance to be covered by charge carriers in two terminal devices is much less ($\approx$ 100 times) than that in three terminal devices. This anisotropy in mobility in different planes of pentacene thin film cannot be explained from experimental studies only and further microscopic investigations are required.

As discussed earlier, Marcus theory is used to study intrinsic charge transport in hopping regime [6]. This theory describes the charge transfer between neighboring molecular sites, $i$ and $j$ as a self exchange reaction process. First, $\lambda$ for a single pentacene molecule and $t_{ij}$ for all the dimers in ab-plane have been estimated, in order to estimate $k_{ij}$ using Eq. 3.2. Then diffusion coefficient ($D$) is calculated using $k_{ij}$ as [7],

$$D = \frac{1}{2n'} \sum_j r_j'^2 k_{ij} P_j \tag{3.45}$$

which further gives the hopping mobility, using the Einstein relation as [23],

$$\mu = \frac{eD}{k_B T} \tag{3.46}$$

where $n'$ is the space dimensionality, $r_j'$ is the length of hopping pathway $j$, $P_j (= k_{ij} / \sum k_{ij})$ is hopping probability of a charge carrier corresponding to the hopping pathway, $j$. Relevant hopping pathways for charge transport in pentacene thin film based two and three terminal devices can be viewed in Fig. 3.6(a) and 3.7(a), respectively. Thus, there are four unique dimers in unit cell of pentacene

*Table 3.1: Microscopic parameters; center of mass (CM) distance betwee the dimers [39], electronic coupling elements and intrinsic mobilities obtained from DFT calculations. Experimental mobilities are also liseted for comparison.*

| Dimer | CM distances (Å) | DIPRO Method | | Experimental |
|---|---|---|---|---|
| | | $t_{ij}$(meV) | $\mu$(cm$^2$/Vs) | $\mu$(cm$^2$/Vs) |
| P | 5.958 | 57.73 | Isotropic $\mu$ | |
| $T_1$ | 4.82 | 65.38 | in ab-plane | In OFET |
| $T_2$ | 4.83 | 68.46 | 1.8 | 0.3 |
| L | 15.60 | 2.60 | Along c-axis | In Two Terminal Devices |
| | | | $4.5 \times 10^{-5}$ | $5.4 \times 10^{-6}$ |

those decide charge transport in different directions; three dimers *P*, $T_1$ and $T_2$ in ab-plane, governing charge transport in three terminal devices i.e OFET and a single dimer (*L*) along c-axis of the unit cell and relevant for charge trasport in two terminal hole only devices. $t_{ij}$ along all of these directions have been estimated using DIPRO method and are listed in Table 3.1.

We observe that magnitudes of $t_{ij}$ between all the dimers lying in ab-plane are comparable whereas $t_{ij}$ between the dimers lying along c-axis is much lesser. It means that intrinsic anisotropy in electronic coupling elements between the dimers lying along different directions gives rise to anisotropy in charge transport in the devices fabricated with different configuration. Using the values of $\lambda$ and $t_{ij}$, $k_{ij}$ along different pathways have been estimated using Eq. 3.2. Average mobility in the ab-plane estimated, using Einstein relation is found to be 1.8 cm$^2$/Vs which corresponds to experimentally observed mobility in OFETs. Similarly charge transport in two terminal devices can be treated as unidirectional i.e. along c-axis of pentacene unit cell and intrinsic mobility along this direction has been found to be $4.5 \times 10^{-5}$ cm$^2$/Vs. Therefore, large difference in mobilities in two and three terminal devices can be interpreted in terms of efficient coupling between dimers in ab-plane and poor coupling between the dimers along c-axis.

Further, magnitude of field effect mobility in an OFET also depends on the direction of the transistor channel relative to specific hopping pathway in ab-plane of the pentacene. This orientational dependence in $\mu$ has been taken into

account by the following expression [47]

$$\mu_{\Phi} = \frac{e}{k_B T} \sum_{j} k_{ij} P_j \cos^2\gamma_j \cos^2(\theta_j - \Phi) \tag{3.47}$$

where $\Phi$ gives the orientation of the transistor channel relative to the some chosen reference axis . $\theta_j$ are the angles that different hopping pathways make with that chosen axis, so $\theta_j - \Phi$ are angles between different hopping pathways and transistor channel. All of these angles are defined in Fig. 3.8(a). $\gamma_j$ are the angles that different hopping pathways make with transport plane. All the other quantities are defined earlier and have the same meaning. For the dimers lying in ab-plane, $\gamma_j = 0$. Using Eq. 3.47 and taking a-axis as reference, $\mu_{\Phi}$ for pentacene in ab-plane can be written as

$$\mu_{\Phi} = 1.22\cos^2(\theta_P - \Phi) + 1.33\cos^2(\theta_{T_1} - \Phi) + 1.59\cos^2(\theta_{T_2} - \Phi) \tag{3.48}$$

Here, $\theta_p = 0^o$, $\theta_{T_1} = 51.74^o$ and $\theta_{T_2} = 128^o$ and define the angles of dimers $P$, $T_1$ and $T_2$ with the chosen axis, respectively. After putting the values of $\theta_p$, $\theta_{T_1}$ and $\theta_{T_2}$ in Eq. 3.48 and solving for $\mu_{\Phi}$, we got a plot for $\mu_{\Phi}$ versus $\Phi$ as shown in Fig. 3.8(b). Maximum mobility estimated in ab-plane has been found to be 3.6 $cm^2/Vs$, when $\Phi = 166^o$ i.e. when transistor channel is formed at an angle of $166^o$ from a-axis. This should be the maximum mobility that can be achieved in pentacene thin film based transistors. Theoretically predicted mobilities in ab-plane and along c-axis are somewhat larger than that experimentally measured in three and two terminal devices, respectively. This seems obvious, as thermal and energetic disorders of pentacene thin films have not been taken into account in theoretical calculations. Further, theoretically predicted mobilities using DFT along different planes and directions (ab-plane and c-axis ) also exhibit a large difference in magnitudes same as the mobilities in two and three terminal devices. Hence, large variation in mobilities in two and three terminal devices must be due to intrinsic anisotropy in intermolecular coupling along different directions.

Though, it is clear that anisotropy in the intermolecular coupling in pentacene dimers is due to variation in relative orientations of dimers (relative distances and angles between them) along different directions, however, intrinsic anisotropy of the pentacene molecule may also play a role in deciding the direction of charge

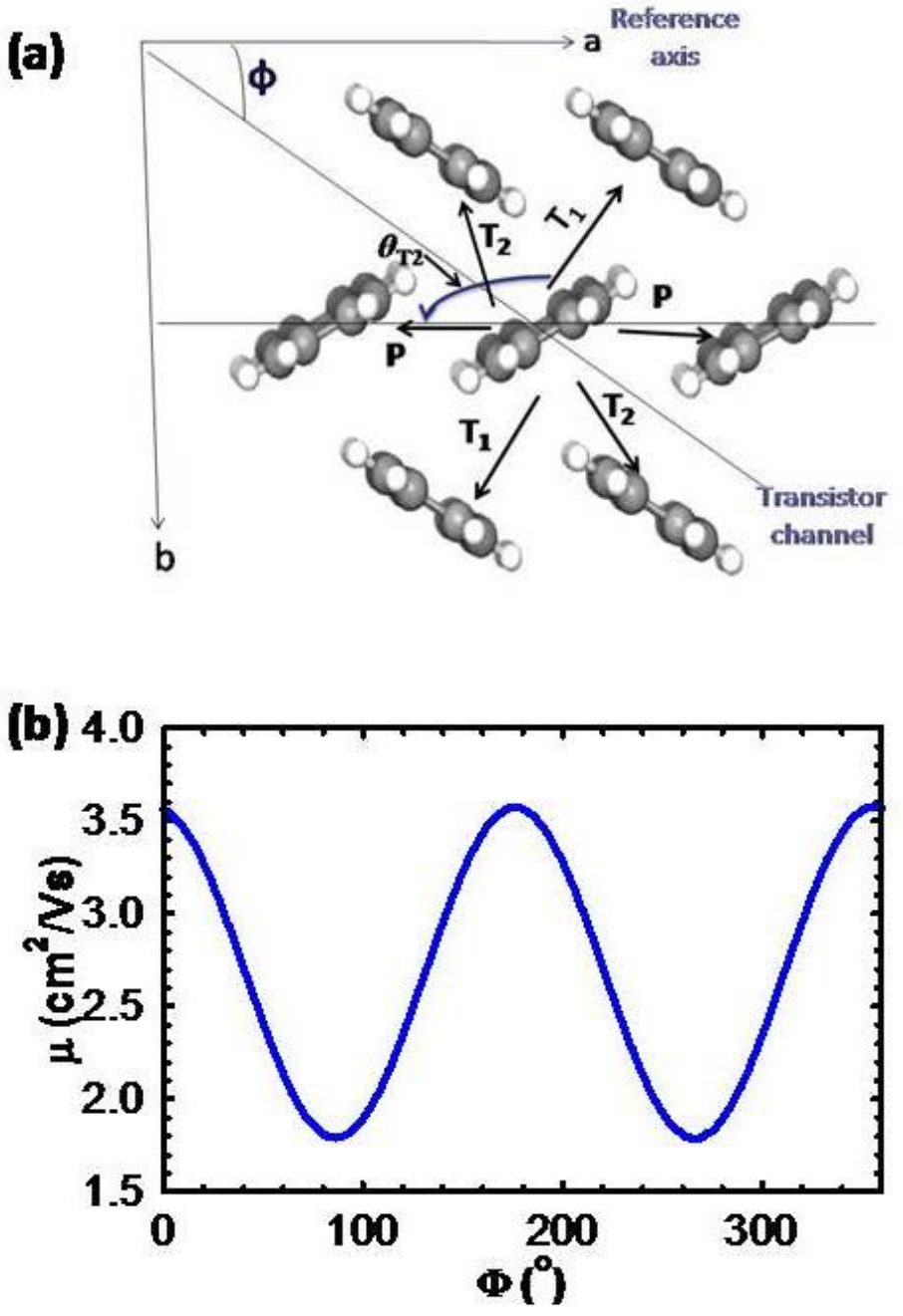


*Figure 3.8: (a) Schematic representation of different hopping pathway projections on the transistor channel and (b) estimated mobility as a function of orientation angle (Φ) of transistor channel with a-axis of the pentacene unit cell.*

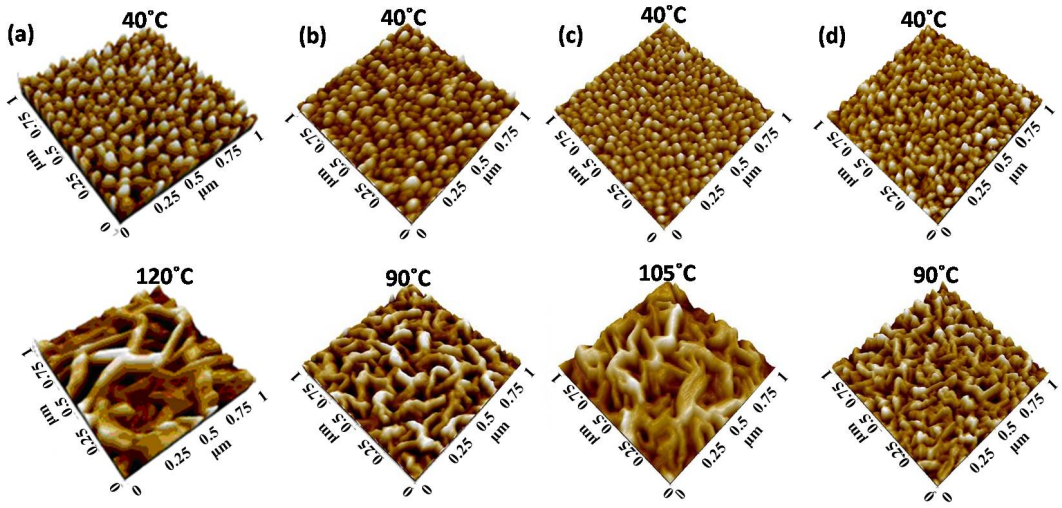


*Figure 3.9: AFM images of 100 nm thick films of (a) $H_2Pc$, (b) ZnPc , (c) CuPc and (d) $F_{16}CuPc$ at low substrate temperature ($T_G$) of $40^oC$ (upper panel) and at optimized $T_G$ ($120^oC$, $90^oC$, $105^oC$ and $90^oC$ for $H_2Pc$, ZnPc, CuPc and $F_{16}CuPc$, respectively) (lower panel).*

transport. Hence, it would be interesting to study whether this type of directional dependence of charge transport is observed in isotropic molecules such as Pcs, also.

## 3.12 Surface morphology of phthalocyanines thin films

Figure 3.9 shows the AFM images of 100 nm thick films of Pcs grown on $SiO_2$ at two different substrate temperatures ($T_G$); (i) at $40^oC$ and (ii) at optimized $T_G$ which is different for different Pc molecules and have been chosen by best surface morphologies. Variation in grain size and shape can be observed as we go from low to high $T_G$. When the molecules come closer to the substrate, they get adsorbed and diffuse on the substrate surface. Temperature given to the substrate determines the kinetic energy of the incoming molecules. Now depending on the kinetic energy, molecules either coalescence with the existing island or new nucleation centers form. At low $T_G$, as the kinetic energy of the molecules is too small to move and to meet the other island, they get adsorbed

at random sites resulting into polycrystalline grainy structure with almost equal sized grains (40-60 nm) distinguished by sharp grain boundaries. In other words, nucleation rate dominates the lateral growth at low $T_G$. However, at high $T_G$, diffusion of molecules on the surface increases and molecules get enough time to attach at a particular stable distance from another molecule due to weak Vander Waals interactions between them. Hence, grains show elongation and eventually lead to well interconnected rod-like nanowires due to the large lateral growth and less nucleation growth at higher temperatures, as discussed in Chapter 2 also.

## 3.13 Crystal structure of phthalocyanines thin films

Generally, when organic molecules are deposited on flat inert surface, they are supposed to stand almost vertically on the substrate, as we observed in pentacene. [48] Figure 3.10 shows the XRD spectra of Pcs thin films grown at optimized $T_G$ decided from the best surface morphology. XRD spectra of thin films grown at low $T_G$ ($40^oC$) show similar pattern but with low intensity peaks. Insets reveal the arrangement of the corresponding Pc molecules in the plane parallel to the substrate and relevant for charge transport in OFETs. The XRD pattern of $H_2Pc$ thin film exhibits a strong peak at $2\theta \sim 6.8^o$ (Fig. 3.10 (a)) which is attributed to the (200) plane and confirms the $\alpha$-phase monoclinic structure in $H_2Pc$ thin film [49]. From XRD, we can conclude that in $H_2Pc$ thin films grown on $SiO_2$, bc-plane lies parallel to the substrate and is relevant for charge transport in OFETs. Inset of Fig. 3.10 (a) shows the arrangement of $H_2Pc$ molecules in OFET geometry. In this plane $H_2Pc$ molecules adopt herringbone arrangement with a stacking along b-axis. XRD spectra of CuPc and ZnPc (Fig. 3.10(b)) are also similar to that of $H_2Pc$ and strong peaks at $2\theta \sim 6.8^o$ are also attributed to the $\alpha$-phase. However, in CuPc and ZnPc this peak corresponds to (100) plane [50] i.e. unit cell parameters for CuPc and ZnPc are different from that for $H_2Pc$. Though in CuPc and ZnPc thin films, bc-planes lie parallel to the substrate and these molecules also adopt stacking along b-axis but, no herringbone arrangement in bc-plane is there rather molecules adopt parallel arrangement (shown in the inset of Fig.3.10(b)). Figure 3.10(d) shows the XRD

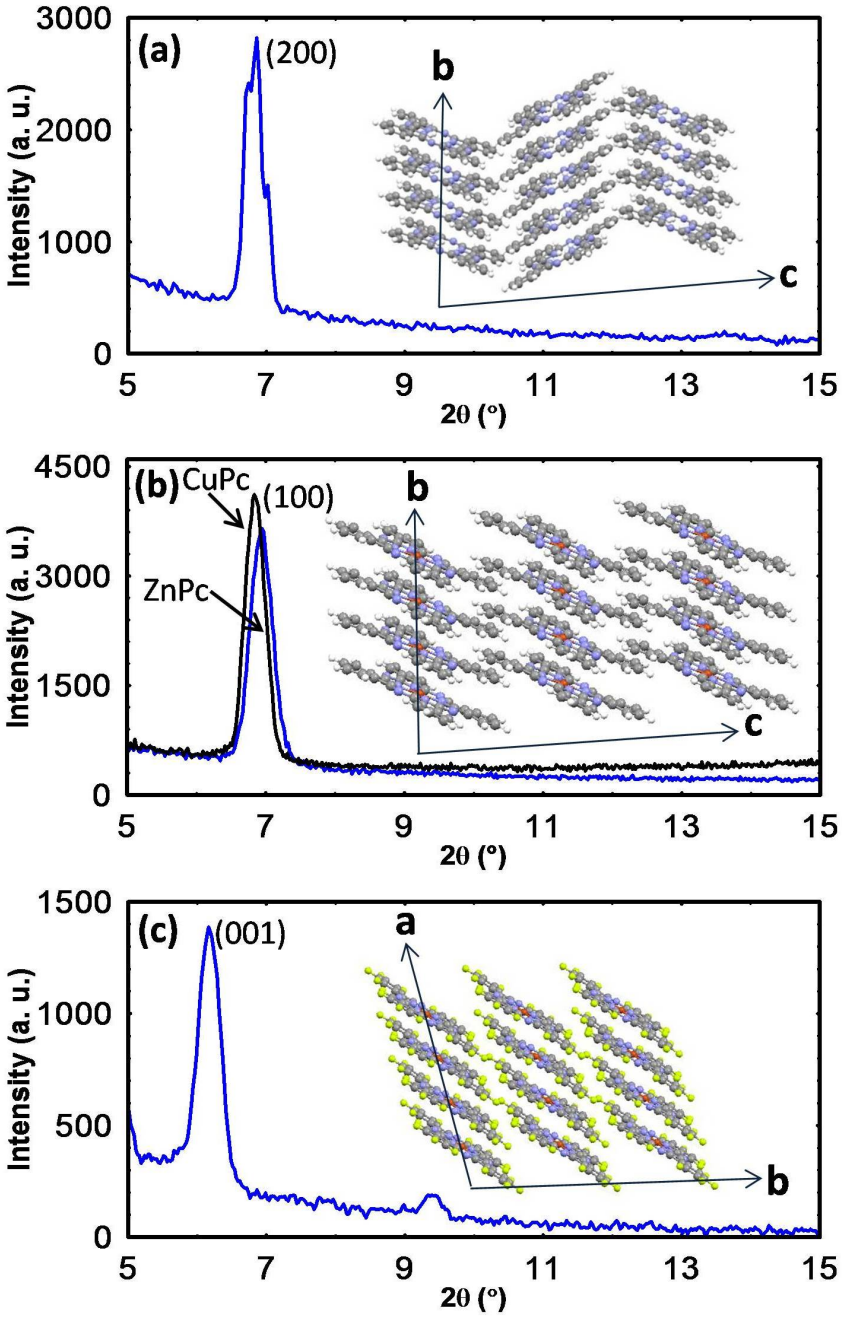


*Figure 3.10: XRD patterns for 100 nm thick films of (a) $H_2Pc$, (b) CuPc and ZnPc and (c) $F_{16}CuPc$ at optimized $T_G$, taken from surface morphology. Insets show the arrangement of Pcs molecules in a plane parallel to the substrate.*

*Table 3.2: Summary of lattice parameters of Pcs.*

| | space group | Z | a (Å) | b (Å) | c (Å) | $\alpha(^o)$ | $\beta(^o)$ | $\gamma(^o)$ |
|---|---|---|---|---|---|---|---|---|
| $H_2$Pc [55] | C2/c | 4 | 26.121 | 3.797 | 23.875 | 90 | 94.16 | 90 |
| ZnPc [56] | P1 | 1 | 12.886 | 3.769 | 12.061 | 96.22 | 90.62 | 90.32 |
| F16CuPc [51] | P1 | 1 | 4.86 | 10.22 | 14.80 | 74.14 | 87.14 | 80.75 |
| CuPc [50] | P1 | 1 | 12.886 | 3.769 | 12.061 | 96.22 | 90.62 | 90.32 |

of $F_{16}$CuPc thin films which exhibits a strong peak at $6.16^o$ and attributed to the (001) plane. [51] It means that in thin film of $F_{16}$CuPc ab-plane lies parallel and is relevant for charge transport in OFETs. By the analogy with a recent study performed on crystal structure of $F_{16}$CuPc, we can conclude that unit cell of $F_{16}$CuPc has triclinic structure with parallel stacking along a-axis (inset of Fig. 3.10(c)). Crystal structures of all of these Pcs have been summarized in Table 3.2. Next, to examine the effect of molecular parameters such as chemical and crystal structures of Pcs, on charge transport, we investigate the charge transport in OFETs based Pcs thin films.

## 3.14 Macroscopic view of charge transport in phthalocyanines thin films

To study the charge transport in Pcs thin films experimentally, we have used simple OFET structures with top contact configuration. Figure 3.11 shows the room temperature $I_{DS} - V_{DS}$ characteristics of $H_2$Pc, ZnPc, CuPc and $F_{16}$CuPc thin film based OFETs fabricated at two different $T_G$ i.e at $40^oC$ (left panel) and at optimized $T_G$ (right panel). OFETs show better performance as we go from low to high $T_G$. Currents obtained in OFETs grown at high $T_G$ are higher by one order of magnitude than that in OFETs grown at low $T_G$ ($40^oC$). This is attributed to the elongated nanowire like structure of thin films grown at high $T_G$ so that charge carriers don't have to face sharp grain boundaries between source and drain. Next, we estimate $\mu$ for Pcs fabricated at two different $T_G$, from linear regions of $I_{DS} - V_{DS}$ shown in Fig. 3.11, using the Eq. 3.44. [23] and are summarized in Table 3.3. We find that similar to $I_{DS}$, magnitudes of $\mu$ are also higher in the OFETs grown at high $T_G$ than that grown at low $T_G$.

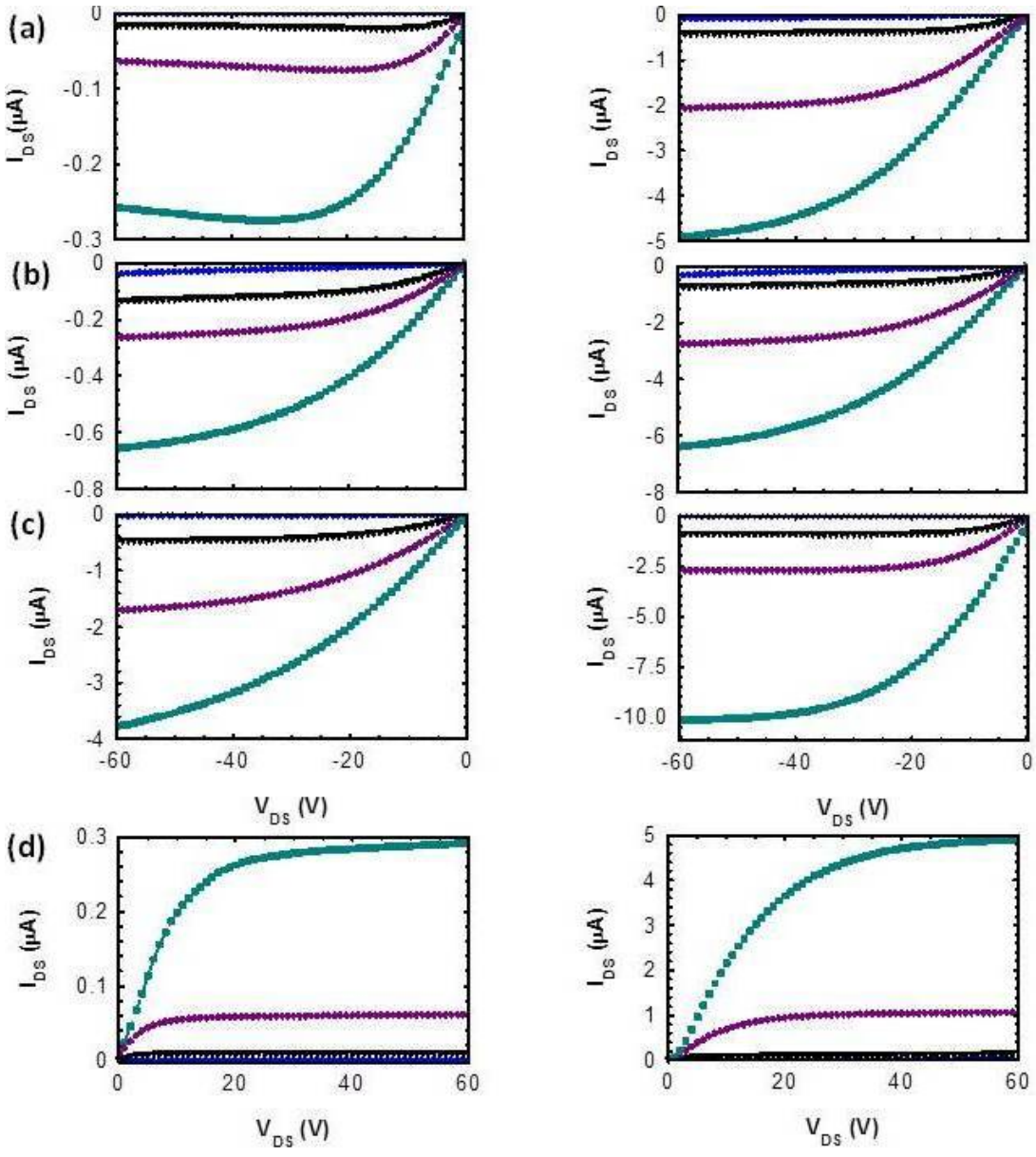


*Figure 3.11: Room temperature* $I_{DS} - V_{DS}$ *characteristics of (a)* $H_2Pc$*, (b) ZnPc, (c) CuPc and (d)* $F_{16}CuPc$ *based OFETs fabricated at* $T_G = 40^oC$ *(left panel) and at optimized* $T_G$ *(right panel). Gate voltages for all the OFETs have been varied from 0 to -60 V for p-type and from 0 to 60 V with a interval of 20 V.*

Further, we observe the difference in the magnitudes of mobility in different Pcs, in spite of similar surface morphologies and XRD patterns. In OFETs based on Pc thin films grown under optimized conditions, $\mu$ are found to follow the order: $H_2Pc < ZnPc < F_{16}CuPc < CuPc$, whereas in the OFETs in which thin films have been fabricated at low $T_G$, $\mu$ follows te order: $H_2Pc < F_{16}CuPc < ZnPc < CuPc$. Hence, to optimize the device performance, primarily surface morphology and crystallinity of organic thin films to get better $\pi - \pi$ overlap should be optimized by engineering different growth parameters. However, origin behind different magnitudes of mobility in Pcs thin film based OFETs cannot be explained on the basis of macroscopic parameters such as surface morphology and crystallinity of thin films. This led us to look into how important chemical structures and solid state packing of organic molecules are responsible in deciding the efficiency of charge transport in organic thin film. To answer this unresolved question, we have to investigate the charge transport microscopically, that will be totally based on the molecular parameters i.e. chemical structure of molecules and their arrangement in unit cell.

## 3.15 Microscopic view of charge transport in phthalocyanines

As discussed previously, intrinsic charge transport in organic semiconductors in hopping regime is studied by Marcus theory [6, 7]. All the microscopic parameters to study charge transport in hopping regime such as $\lambda$, $t_{ij}$, $k_{ij}$ and then resulting $\mu$ for Pcs have been estimated in the same way as for pentacene. All of these parameters are summarized in Table 3.3. We observe that all of these parameters vary from one Pc to other due to either difference in chemical structure or in solid-state packing.

$\lambda$ for different Pcs have been found to follow the order: $ZnPc < H_2Pc < CuPc < F_{16}CuPc$. It means that central atom as well as different substituents at the ligand in Pcs play a significant role in deciding their charge transport in thin films. But, as $\lambda$ for different Pcs do not follow the same trend what $\mu$ do. Hence, knowledge about chemical structure of the molecule is not sufficient in order to decide the efficiency of charge transport in different organic systems

and further investigation is required. Further, variation in $\lambda$ due to chemical structure of Pcs can be explained as follow. Figure 3.12 shows the charge density distribution of HOMO (for p-type) and LUMO (for n-type) of Pcs calculated using Gaussian 09 software. $H_2$Pc and ZnPc molecules exhibit very low values of $\lambda$ due to the absence of p-orbital and completely filled d-orbital in the central metal atom, respectively. In these molecules, HOMO is well delocalized over the Pc ring (Fig. 3.12(a), (b)), leading to very less coupling of the positive charge with the vibrations of the Pc macrocycle. In CuPc, although Cu atom does not show contribution to $\pi$-orbitals of HOMO (Fig. 3.12 (c)), larger $\lambda$ for CuPc must be attributed to the bonding nature of Cu atom which comes from the unpaired electron in unfilled d-orbital and results in larger geometry relaxation. Finally, we explain the largest $\lambda$ in $F_{16}$CuPc in which all the hydrogen atoms are replaced by fluorine atoms. These fluorine atoms increase the electron affinity of the molecule. As a consequence, p-type semiconducting behavior, observed for CuPc changes to n-type behavior in case of $F_{16}$CuPc. Also as these fluorine atoms take part in $\pi$-orbitals of LUMO (Fig. 3.12 (d)), there will be additional C-F bond relaxation when going from neutral to ionic states. Similar effect of fluorination on $\lambda$ for has been observed in previous studies also [12, 52].

Another key parameter deciding efficiency of charge transport is $t_{ij}$ [53] which measures the extent of overlapping between orbitals of adjacent molecules. As is clear from XRD (Fig.3.10), in $H_2$Pc, ZnPc and CuPc bc-plane and in $F_{16}$CuPc ab-plane lie parallel to the substrate and govern charge transport in OFETs. $t_{ij}$ between different dimers lying in relevant planes have been calculated using DIPRO (dimer projection) method [25, 54]. $t_{ij}$ in Pcs along stacking axis are found to be significantly larger than that in other directions, hence charge transport in OFETs based on Pcs thin films can be treated as one-dimensional and $t_{ij}$ for different Pcs calculated along stacking axis are summarized in Table 3.3 and make the trend: $H_2$Pc < ZnPc < CuPc < $F_{16}$CuPc. Now it is worth noting that though crystal structures of Pcs are different but all of these Pcs have $\pi$-$\pi$ stacking along short axis with almost same intermolecular distances. Hence, chemical structure of Pc molecules also should play an important role in deciding the efficiency of charge transport in devices based on Pcs thin films. This can also be explained by investigating charge distribution on frontier orbitals for Pcs dimers along stacking axis as shown in Fig. 3.13. For $H_2$Pc, HOMO is almost

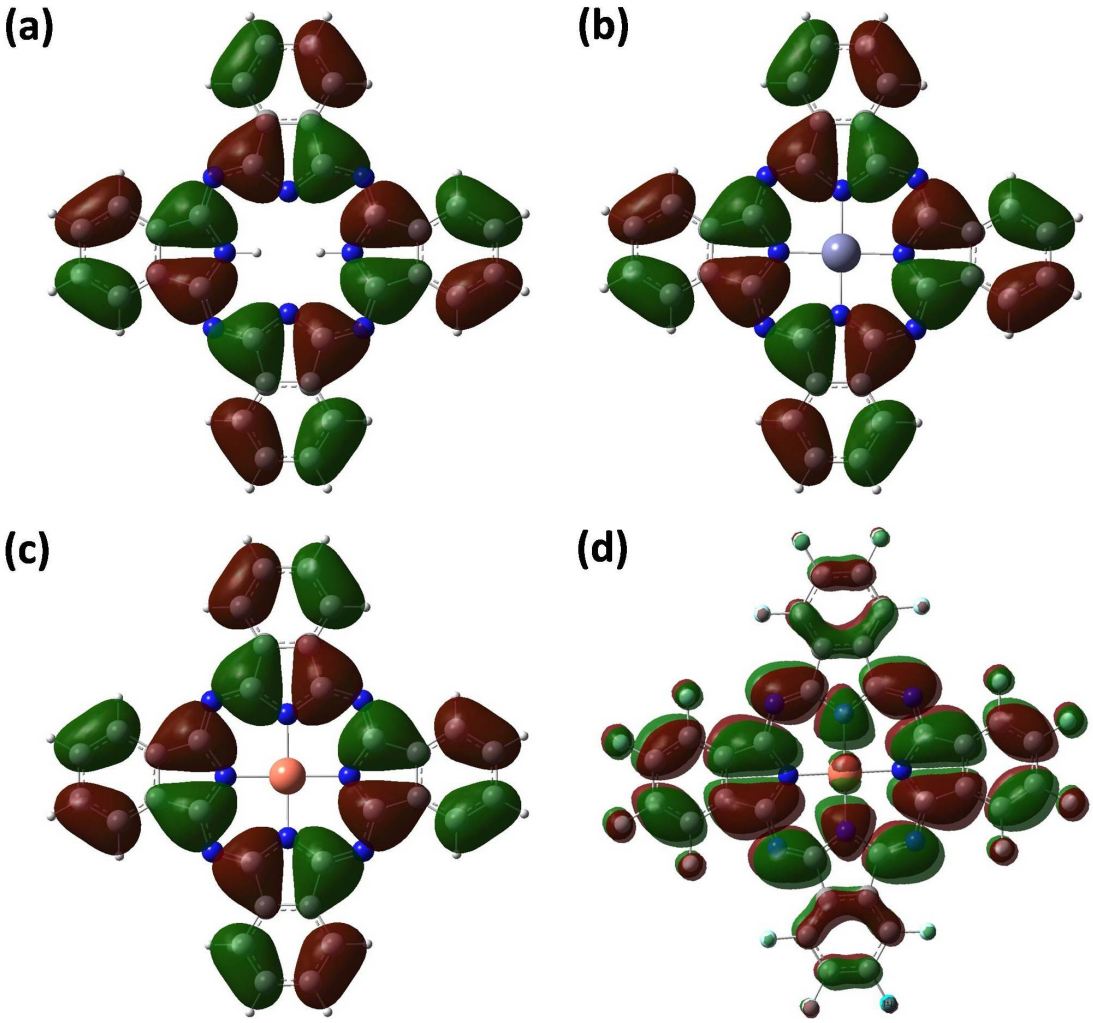


*Figure 3.12: Isosurfaces representing the charge density distribution on HOMO of (a) $H_2Pc$, (b) ZnPc and (c) CuPc and (d) LUMO of $F_{16}CuPC$ plotted using Gaussian 09.*

uniformly distributed on both the monomers and anti-bonding interaction between the $\pi$ orbitals of monomers can be seen in Fig. 3.13(a). Further as dimers in Pcs are not perfectly cofacial, effect of interaction is reduced. In ZnPc, both the monomers don't contribute equally to HOMO (Fig. 3.13(b)). In CuPc and $F_{16}$CuPc, though HOMO is almost uniformly distributed on the monomer, however, in dimer, HOMO gets localized mainly on the Cu atoms and N atoms and C-C bonds lying nearby the Cu-atoms. Further, bonding and anti-bonding interactions between the $\pi$-orbials of neighboring molecules in CuPc and $F_{16}$CuPc can be clearly observed in Fig. 3.13(c) and (d), respectively. As electronegativities of Cu and N atoms are higher than that of C and H atoms hence interaction between $\pi$ orbitals of monomers in CuPc and $F_{16}$CuPc should be stronger than that in $H_2$Pc where HOMO is delocalized over the whole molecule. Moreover, higher value of $t_{ij}$ in $F_{16}$CuPc in comparison to CuPc can be attributed to the the interaction of edge F-atoms of one monomer with $\pi$-orbitals of other due to the relative displacement of monomers. Similar interaction in CuPc is very weak due to H-atoms on the edge. $t_{ij}$ also do not follow the same trend what $\mu$ do. Hence, there are two competing factors that determine the efficiency of charge transport in organic semiconductors i.e localization of charge carrier on the molecule and degree of overlapping between the molecular orbitals.

Further, we observe that $k_{ij}$ and $\mu$ estimated using DFT exhibit the same order as $\mu$, determined experimentally in Pcs thin film based OFETs fabricated under optimized conditions (Table 3.3). However, at room temperature experimentally observed mobilities can follow the different trend. Hence, optimization of growth conditions is also required in order to examine the exact role of molecular parameters on charge transport properties in devices. Moreover, $\mu$ of all Pcs estimated using DFT calculations are higher by one order of magnitude than that observed experimentally. The lower magnitude of mobilities in experiments can be attributed to the thermal and energetic disorders in neighboring molecules that have not been taken into account in theory. Out of the above discussed Pcs, CuPc exhibits the highest mobility due to the highly interacting behavior of central Cu atom, coming from the unfilled d-orbital. Same effect of Cu atom must be be applicable to $F_{16}$CuPc, however additional relaxation of C-F bonds during the interaction with external charge diminishes the efficiency of charge transport in it.

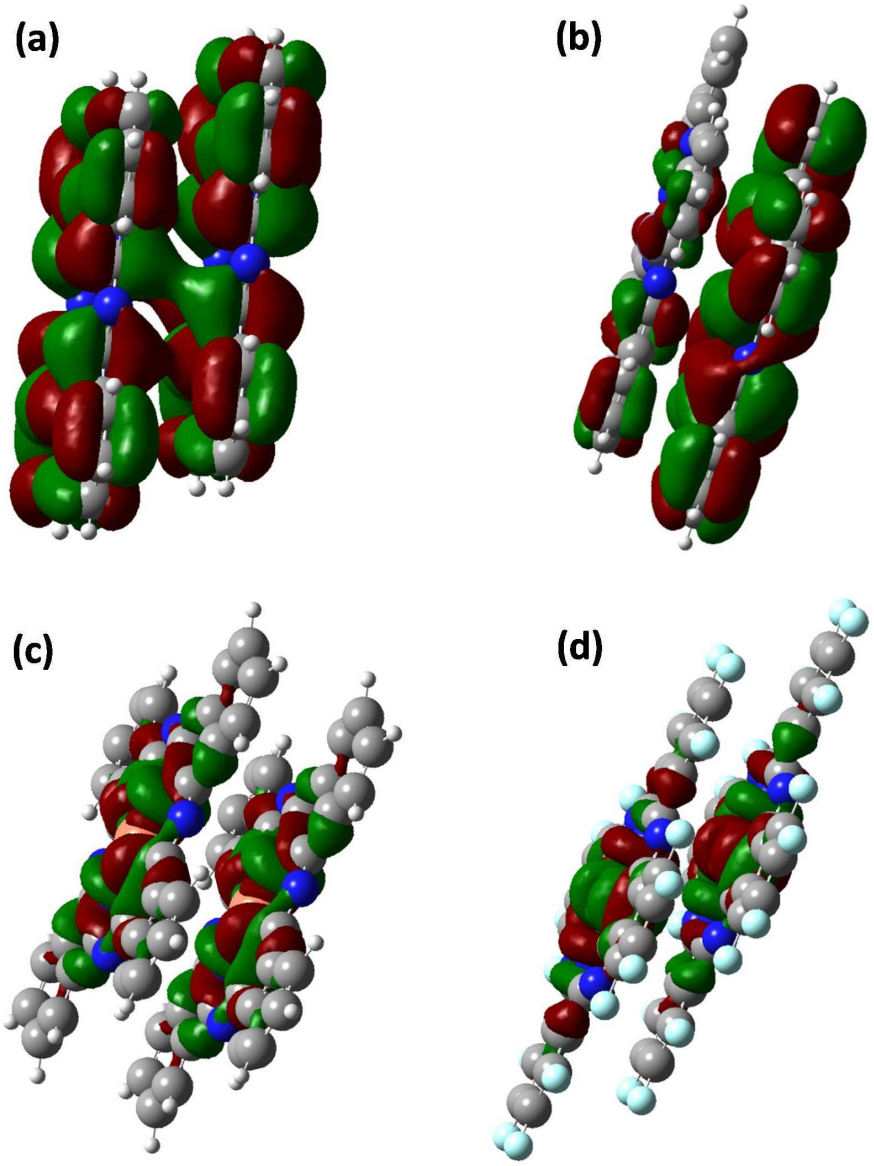


*Figure 3.13: Representation of charge density distribution on frontier orbitals of dimers of Pcs using Gaussian.*

*Table 3.3: Comparison of DFT calculated mobilities in hopping regime and experimentally observed mobilities in OFETs fabricated at two different* $T_G$ *i.e. 40* $^oC$ *and at optimized (opt.) temperature.*

| | $\lambda$ (meV) | $t_{ij}$ (meV) | $\mu$ (DFT) ($cm^2$/Vs) | $\mu$ (exp.) ($cm^2$/Vs) | |
|---|---|---|---|---|---|
| | | | | $T_G = 40^oC$ | Opt. $T_G$ |
| $H_2Pc$ | 40 | 11 | 2.8 x $10^{-2}$ | 7.6 x $10^{-5}$ | 1.8 x $10^{-3}$ |
| ZnPc | 35 | 14 | 9.9 x $10^{-2}$ | 6.2 x $10^{-4}$ | 9.2 x $10^{-3}$ |
| $F_{16}CuPc$ | 239 | 44.2 | 1.20 x $10^{-1}$ | 5.8 x $10^{-4}$ | 1.8 x $10^{-2}$ |
| CuPc | 136 | 33.6 | 1.87 x $10^{-1}$ | 1.2 x $10^{-3}$ | 3.4 x $10^{-2}$ |

In Marcus theory, mobility is determined by a dimer i.e. charge transport is governed by the electronic structure of the constituent molecules. However, charge transport in organic semiconductors also depends on the electronic structures of molecules in solid state. Actually, Marcus theory gives the estimate of maximum mobility that can be achieved in hopping regime where charge carriers are localized in the tail of the GDOS. However, it does not give idea about maximum mobility that can be achieved in an organic semiconductor. As is well known, mobility in OFETs increases with respect to the background charge carrier concentration. Because, with increasing background carrier concentration, charge carriers start occupying the higher energy states in GDOS and need less activation energy to hop to neighboring sites. Hence, as Fermi level is moved from tail to the center of GDOS, density of localized states increases and in the vicinity of the center of GDOS density of localized states is so high that charge carriers should not need any activation energy to transport to neighboring sites. Then charge carriers can be treated similar to a delocalized wave and maximum mobility in OFETs should be achieved. Mechanism of charge transport also seems to be different and band-like transport [21] seems to be the dominating mechanism. Experimentally, to access the central region of the GDOS is not so trivial, primarily due to the dielectric breakdown. Theoretically, to have an idea about the maximum mobilities that can be achieved in Pcs thin films based OFETs, we need to perform band structure calculations. Dispersions in valence and conduction band primarily decide the efficiency of hole and electron transport in organic semiconductor. The band structure and density of states for Pcs have been estimated using periodic DFT calculations with the help of Quantum

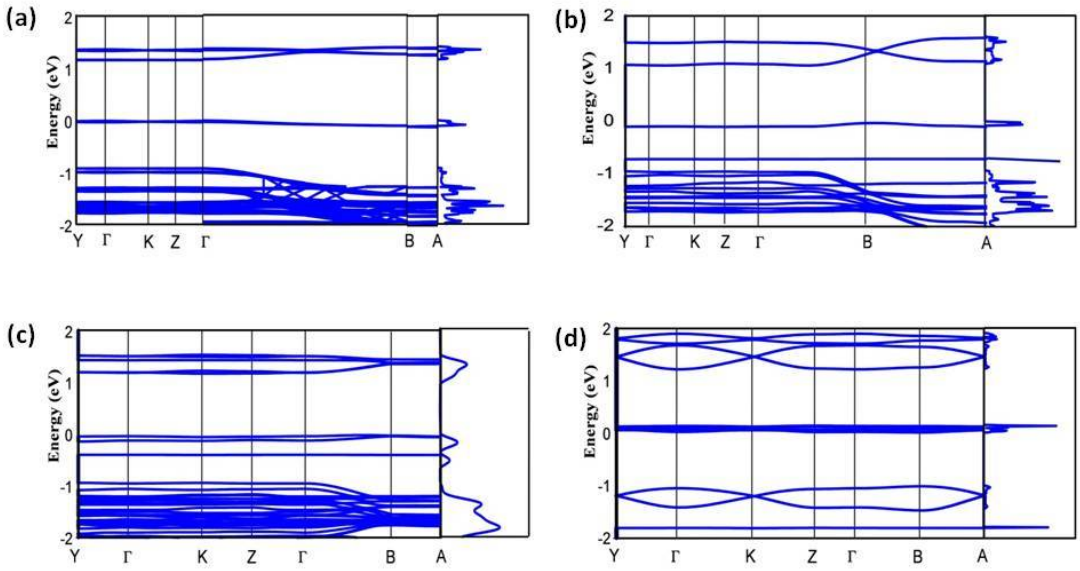


*Figure 3.14: Band structures and DOS plots of (a) $H_2Pc$, (b) ZnPc, (c) CuPc and (d) $F_{16}CuPc$ estimated using periodic DFT calculations. Different k-points used in the calculation of band structure are Y = (0.5, 0, 0), Γ = (0, 0, 0), K = (0.5, 0, 0.5), Z = (0, 0, 0.5), B = (0, 0.5, 0) and A = (0.5, 0.5, 0). Zero of energy has been set at the valence band maximum for p-type and at conduction band minimum for n-type Pcs*

Espresso package [29].

Figure 4.5 shows the band structure and density of states of Pcs. Unit cell of $H_2$Pc consists of four molecules and that of ZnPc, CuPc and $F_{16}$CuPc have one molecule (Table (3.2)). After zooming valance and conduction bands of $H_2$Pc, we find that each of them consists of four subbands due to four molecules in the unit cell. Valence and conduction bands of ZnPc represent no subband as there is only one molecule in unit cell of ZnPc. Further, due to the unfilled d-orbital in Cu atom, spin polarized calculations with dispersion correction have been performed for CuPc and $F_{16}$CuPc, resulting in a magnetic moment of $\sim 1\mu_B$ per Cu atom. Antiferreomagnetic (AF) state is found to be energetically more stable than the ferromagnetic (FM) state which is consistent with the previous study [57]. As there are two molecules per unit cell of CuPc and $F_{16}$CuPc in AFM state, valence and conduction bands consist of two subbands.

Next, we calculate the mobilities from band structure of Pcs as [21],

$$\mu = \frac{e\tau}{m_e} \tag{3.49}$$

where $m_e$ is the effective mass and $\tau$ is the relaxation time [58]. As can be seen in Fig. 4.5 that significant dispersion in valence (for p-type) and conduction (for n-type) bands of Pcs is found only along the stacking direction, consistent with concept of the unidirectionality of charge transport in Pcs. $m_e$ for Pcs have been estimated from the parabolic fitting of the top or bottom of valence or conduction band for p and n-type Pcs, respectively and given as, $m_e = \hbar^2|\frac{\delta^2 E}{\delta k^2}|^{-1}$ [59, 60]. Next, as acoustic phonon scattering is found to be around three times stronger than that for optic phonon in organic semiconductors [61], deformation potential has been used to calculate $\tau$ in Pcs. In the deformation potential approximation [62], $\tau$ for one-dimensional systems can be written as,

$$\tau = \frac{\hbar^2 C_1}{(2\pi|m_e|k_B T)^{1/2} E_1^2} \tag{3.50}$$

where $C_1$ and $E_1$ represent the elastic constant and deformation potential, respectively. To calculate $C_1$, we have followed the procedure, discussed in a study by Huang *et. al.* [63]. $C_1$ for different Pcs along stacking direction have been calculated by stretching and compressing the unit cells along that direction and then relaxing it at different volumes. Then $C_1$ is estimated by fitting total energy $E$ vs. lattice constant $l$ curve according to

$$C_1 = a_0 \left(\frac{\partial^2 E}{\partial a^2}\right)|_{a=a_0} \tag{3.51}$$

$a_0$, being the equilibrium lattice constant. $E_1$ for Pcs have been calculated through the relation

$$E_1 = \frac{\partial\,(E_{VBM} - E_{core})}{\partial\,(\Delta a/a_0)} \tag{3.52}$$

$E_{VBM}$ and $E_{CBM}$ represent the energy corresponding to valence band maximum and conduction band minimum, respectively and are relevant to hole and electron transport, respectively. Using the values of $C$, $E_1$ and $m_e$, $\mu$ have been estimated using Eq. 3.49 with all the parameters listed in Table 3.4.

From Table 3.4, we observe that maximum possible mobilities in Pcs are higher

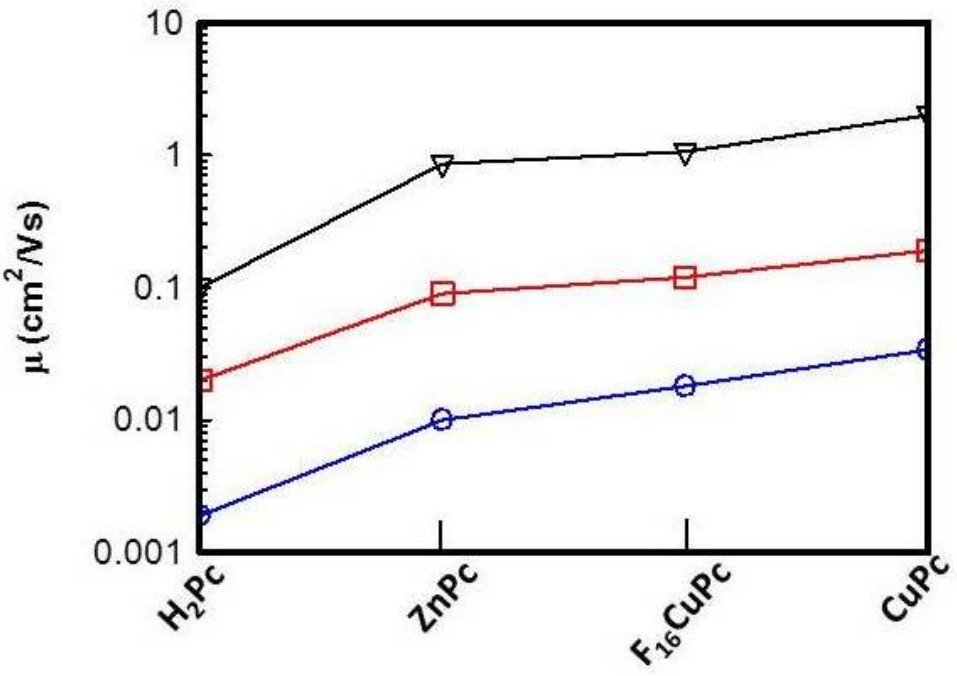


*Figure 3.15: Mobilities of Pcs estimated by different techniques i.e by characterizing OFETs (empty circle), Hopping (empty square) and band mobilities (empty triangle) using Marcus theory and periodic DFT calculations, respectively. Mobilities vary almost parallely in all Pcs when moving from one method to other.*

than the hopping mobilities. Further, maximum mobility in Pc also depends on the chemical structure of the molecule. From Table 3.3 and 3.4, we find that $\mu$ for Pcs estimated using different methods exhibit the same trend as: $H_2Pc$ < ZnPc < $F_{16}$CuPc < CuPc and also similar to that followed by inverse effective mass ($1/m_e$). For comparison, $\mu$ for Pcs estimated from three different methods i.e experimental, Marcus theory and band structure, have been plotted in Fig. 3.15. Same trends in $\mu$ obtained using different methods seem obvious. Whether charge carriers are treated localized or delocalized, interaction between orbitals of adjacent molecules determines the efficiency of charge transport. Since, $m_e$ is determined from the curvature of bands i.e. depends on the dispersion of bands near the Fermi level and dispersion in bands is further decided by the interaction between adjacent molecules. Hence, $m_e$ has the effect of both the molecular parameters i.e chemical structure of the molecule and their relative displacement.

*Table 3.4: Summary of different parameters: deformation potential ($E_1$), elastic constant (C), effective mass ($m_e$), band width (BW) and mobility estimated for Pcs, using periodic DFT calculations.*

| | $E_1$(eV) | $C_1$(eV/ang) | $m_e$ | $\mu$ $cm^2$/Vs | BW (eV) |
|---|---|---|---|---|---|
| H2Pc | 0.89 | 34 | 228 | 9.95 x $10^{-2}$ | 0.12 |
| ZnPc | 0.96 | 19.9 | 34 | 8.58 x $10^{-1}$ | 0.11 |
| F16CuPc | 1.35 | 16.13 | 16.4 | 1.06 | 0.15 |
| CuPc | 1.05 | 11.99 | 12 | 2.09 | 0.348 |

$m_e$ can be considered as a crucial parameter that governs the charge transport in band-like regime, however, $C_1$ and $E_1$ also play important roles. Further in Fig. 3.15, we observe that all three mobility curves are parallel. It means that intrinsic mobilities in hopping regime are higher than experimentally observed ones by almost same proportion for all Pcs. Similarly, band mobilities for all pcs are found to increase in a proportion to intrinsic hopping mobilities. After analyzing, we find that intrinsic hopping mobilities for Pcs are proportional to those observed experimentally and average proportional constant has been found to be 7.2 . Similarly a proportional constant of 9.5 has been estimated between hopping and band mobilities using DFT. Hence, we can write: $\mu_{\text{Marcus}} \simeq 7.2\mu_{\text{exp.}}$ and $\mu_{\text{Band}} \simeq 9.5\mu_{\text{Marcus}}$ i.e. $\mu_{\text{Band}} \simeq 68.4\mu_{\text{exp.}}$.

Finally, from discussion on the macroscopic and microscopic view of charge transport in Pcs, we conclude that intrinsic anisotropy of the molecule is not important for the anisotropy in the efficiency of charge transport along different dimers, rather, there relative arrangements are responsible.

## 3.16 Conclusion

In conclusion, a detailed and systematic investigation on the charge transport properties of organic semiconductors have been presented using both macroscopic and microscopic approaches. It has been realized that performance of devices based on organic thin films needs to be optimized by engineering various growth parameters in order to examine the exact impact of microscopic molecular parameters on charge transport properties. We conclude that directional dependence of charge transport in devices having different structures, based on the same organic

thin film, is due to the anisotropy in the electronic coupling between the dimers lying along different directions in unit cell. Intrinsic anisotropy of the molecule is not responsible for the anisotropy in electronic coupling. Finally, we have established a correlation between macroscopic and microscopic charge transport in organic semiconductors.

# Bibliography


[1] V. Coropceanu, J. Cornil, D. A. da Silva Filho, Y. Olivier, R. Silbey, and J.-L. Bredas, Chem. rev. **107**, 926 (2007).

[2] H. Bassler, Phys. Status Solidi B **175**, 15(1993).

[3] P. W. M. Blom and M. C. J. M. Vissenberg, Mater. Sci. Eng. **27**, 53 (2000).

[4] S. D. Baranovskii, Phys. Stat. sol. (b) **251**, 487-525 (2014).

[5] A. Miller and E. Abrahams, Phys. Rev. **120**, 745 (1960).

[6] R. A. Marcus, Rev. Mod. Phys. **65**, 599 (1993).

[7] G. R. Hutchison, M. A. Ratner, and T. J. Marks, J. Am. Chem. Soc. **127**, 2339 (2005).

[8] Z. Shuai, L. Wang, and Q. Li, Adv. Mater. **23**, 1145 (2011).

[9] P. Kumar, A. Sharma, S. Yadav, and S. Ghosh, Org. Electron **14**, 1663 (2013).

[10] A. D. Carlo, F. Piacenza, A. Bolognesi, B. Stadlober, and H. Maresch, Appl. Phys. Lett. **86**, 263501 (2005).

[11] C. Lee, W. Yang, and R. G. Parr, Phys. Rev. B **37**, 785 (1988).

[12] Z. Y. Zhang, X. Chen, M. G. Lagally, Phys. Rev. Lett. **73**, 1829 (1994).

[13] Y.-H. Park, Y.-H. Kim, S.-K. Kwon, I.-S. Koo, and K.Y. Yang, Bulletin of the Korean Chemical Society **31**, 1649 (2010).

[14] J. L. Brdas, J. P. Calbert, D. A. da Silva Filho, and J. Cornil, Proceedings of the National Academy of Sciences **99**, 5804 (2002).

[15] A. Troisi and G. Orlandi, J. Phys. Chem, B **109**, 1849 (2005).

[16] C. Pramanik and G. P. Miller Molecules **17**, 4625-4633 (2012,).

[17] K. Sakamoto and E. Ohno-Okumura, Materials **2**, 1127 (2009).

[18] L. Edwards and M. Gouterman, Journal of Molecular Spectroscopy **33**, 292 (1970).

[19] T. N. Sokolova, T. N. Lomova, M. E. Klueva, E. E. Suslova, V. E. Mayzlish, and G. P. Shaposhnikov, Molecules **5**, 775 (2000).

[20] M. J. Frisch, G. W. Trucks, H. B. Schlegel, G. E. Scuseria, M. A. Robb, J. R. Cheeseman, G. Scalmani, V. Barone, B. Mennucci, G. A. Petersson, et al., Gaussian09 Revision A.02, Gaussian Inc. Wallingford CT (2009).

[21] S. O. Kasap, Principles of electronic materials and devices (McGraw-Hill, 2006).

[22] Ashcroft, Neil W., and N. David Mermin. "Solid State Physics (Holt, Rinehart and Winston, New York, 1976)".

[23] S. M. Sze and K. K. Ng., Physics of Semioconductor Devices, 3rd edition. (Wiley-Interscience, 2006).

[24] S. V. Novikov, D. H. Dunlap, V. M. Kenkre, P. E. Parris, A. V. Vannikov, Phys. Rev. Lett. **81**, 4472 (1998).

[25] B. Baumeier, J. Kirkpatrick, and D. Andrienko, Phys. Chem. Chem. Phys. **12**, 11103 (2010).

[26] P. Hohenberg and W. Kohn, Phy. reV. **136**, 864 (1964).

[27] W. Kohn and L. J. Sham, Phy. Rev. **140**, 1133 (1965).

[28] V. Ruhle, C. Junghans, A. Lukyanov, K. Kremer, and D. Andrienko, Journal of chemical theory and computation **5**, 3211 (2009).

[29] P. Giannozzi, S. Baroni, N. Bonini, M. Calandra, R. Car, C. Cavazzoni, D. Ceresoli, G. L. Chiarotti, M. Cococcioni, I. Dabo, et al., J. Phys.: Condensed Matter **21**, 395502 (2009).

[30] A. D. Becke, Phys. Rev. A **38**, 3098 (1988).

[31] V. A. Rassolov, J. A. Pople, M. A. Ratner, and T. L. Windus, J. Chem. Phys. **109**, 1223 (1998).

[32] J. P. Perdew, K. Burke, and M. Ernzerhof, Phys. Rev. Lett. **78**, 1396 (1997).

[33] S. Grimme, J. Comput. Chem. **27**, 1787 (2006).

[34] S. Grimme, J. Antony, S. Ehrlich, and H. Krieg, J. Chem. Phys. **132**, 154104 (2010).

[35] Z. Zhang and M. G. Lagally Science **276**, 377 (1997).

[36] Frank-J. Meyer zu Heringdorf, M. C. Reuter & R. M. Tromp Nature **412** , 517 (2001).

[37] R. Ruiz, B. Nickel, N. Koch, L.C. Feldman, R.F. Haglund, A. Kahn, F. Family, and G. Scoles, Phys. Rev. Lett. **91**, 136102 (2003).

[38] R. L. Schwoebel and E. J. Shipsey, J. Appl. Phys. **37**, 3682 (1966).

[39] H. Yoshida, K. Inaba, and N. Sato, Appl. Phys. Lett. **90**, 181930 (2007).

[40] J. Gotzen, D. Kafer, C. Woll and G. Witte, Phys. Rev. B **81**, 085440 (2010).

[41] R. B. Campbell, J. M. Robertson, and J. Trotter, Acta Crystallogr. 15, 289 (1962).

[42] R. Agrawal, and S. Ghosh, Appl. Phys. Lett. **89**, 222114 (2006).

[43] N. F. Mott and R. W. Gurney, Electronic Processes in Ionic Crystals (Oxford University Press, Oxford, 1940).

[44] W. F. Pasveer, J. Cottaar, C. Tanase, R. Coehoorn, P. A. Bobbert, and P. W. M. Blom, D. M. de Leeuw, and M. A. J. Michels, Phys. Rev. Lett. **94**, 206601 (2005).

[45] J. H. Na, M. Kitamura, D. Lee, and Y. Arakawa, Appl. Phys. Lett. **90**, 163514 (2007).

[46] W.-Y. Chou, C.-W. Kuo, H.-L. Cheng, Y.-R. Chen, F.-C. Tang, F.-Y. Yang, D.-Y. Shu, and C.-C. Liao, Appl. Phys. Lett. **89**, 112126 (2006).

[47] Shu-Hao Wen, An Li, Junling Song, Wei-Qiao Deng, Ke-Li Han, and William A. Goddard III, J. Phys. Chem. B **113**, 8813 (2009).

[48] E. Mikayelyan, I. Vladimirov, D. Wesner, L. Grodd, A. I. Rodygin, H. Schonherr, S. A. Ponomarenko, U. Pietsch, D. A. Ivanov, and S. Grigorian, RSC Adv. 6, 115085 (2016).

[49] S. M. Bayliss, S. Heutz, G. Rumbles, and T. S. Jones, Phys. Chem. Chem. Phys. **1**, 3673 (1999).

[50] A. Hoshino, Y. Takenaka, and H. Miyaji, Acta Crystallographica Section B **59**, 393 (2003).

[51] P. A. Pandey, L. A. Rochford, D. S. Keeble, J. P. Rourke, T. S. Jones, R. Beanland, and N. R. Wilson, Chemistry of Materials **24**, 1365 (2012).

[52] M. C. R. Delgado, K. R. Pigg, D. A. da Silva Filho, N. E. Gruhn, Y. Sakamoto, T. Suzuki, R. M. Osuna, J. Casado, V. Hernndez, J. T. L. Navarrete, et al., Journal of the American Chemical Society **131**, 1502 (2009).

[53] J. L. Brdas, J. P. Calbert, D. A. da Silva Filho, and J. Cornil, Proceedings of the National Academy of Sciences 99, 5804 (2002).

[54] E. F. Valeev, V. Coropceanu, D. A. da Silva Filho, S. Salman, and J.-L. Bredas, J. Am. Chem. Soc. **128**, 9882 (2006).

[55] J. Janczak and R. Kubiak, Journal of Alloys and Compounds **190**, 121 (1992).

[56] S. Yanagisawa, K. Yamauchi, T. Inaoka, T. Oguchi, and I. Hamada, Phys. Rev. B **90**, 245141 (2014).

[57] G. Giovannetti, G. Brocks, and J. van den Brink, Phys. Rev. B **77**, 035133 (2008).

[58] D. Wang, W. Shi, J. Chen, J. Xi, and Z. Shuai, Phys. Chem. Chem. Phys. **14**, 16505 (2012).

[59] R. C. Hatch, D. L. Huber, and H. Hochst, Physical Review B **80**, 081411 (2009).

[60] N. Ueno and S. Kera, Progress in Surface Science **83**, 490 (2008).

[61] L. Tang, M. Long, D. Wang, and Z. Shuai, Science in China Series B: Chemistry **52**, 1646 (2009).

[62] H. Kobayashi, N. Kobayashi, S. Hosoi, N. Koshitani, D. Murakami, R. Shirasawa, Y. Kudo, D. Hobara, Y. Tokita, and M. Itabashi, J. Chem. Phys. **139**, 014707 (2013).

[63] Y. Zhu, H. Bai, and Y. Huang, Chemistry Open **5**, 78 (2016).

# Chapter 4

# Field driven hopping to band-like transport in organic thin film

In the Chapter 1, we discussed how structural disorder induced traps in organic thin films can be reduced substantially, by optimizing the different growth parameters. However, due to the inherent spatial disorder in polycrystalline organic thin films, charge carriers are localized in the tail states of Gaussian density of states (GDOS) and charge transport in these devices is described by the hopping of charge carriers among neighboring sites, leading to low values of mobility in organic devices based on polycrystalline thin films. Hence, it seems that engineering of growth parameters is not sufficient to get the high mobilities in polycrystalline organic thin films comparable to their pure single crystal and further investigations are required. In this chapter, we have studied a field-driven crossover from localized charge transport with low mobilities to delocalized transport with mobilities comparable to that obtained in their single crystals.

## 4.1 Introduction

Thermally activated hopping is the dominant mechanism of charge transport in organic thin film based devices where localization of charge carriers in the tail of Gaussian density of states (GDOS) results into low carrier mobilities [1]. In this regime, charge carriers require some activation energy to hop between neighboring sites leading to positive temperature coefficient of mobility. Low mobilities in organic thin films is the fundamental issue limiting their applications in integrated circuits, displays and memory devices where much fast processing is required [2]. Further, devices based on organic light emitting diodes (OLEDs), such as electronic displays, electronic paper etc. require organic field effect transistors (OFETs) for active matrix backplanes [3–5]. Hence, understanding the mechanism behind the localization of charge carriers in organic thin films is required. Although, delocalized charge transport with high mobilities has been observed in pure organic single crystals [2, 6] however, organic single crystals cannot be used in large area, rolable and foldable electronic devices. Poor device integration and cross-talk between devices are also the drawbacks of single crystals. The real challenge with polycrystalline organic thin films lies in achieving high mobility in comparable with pure organic single crystals, typically associated with delocalized band-like transport. Considerable efforts have been put [7, 8] towards improving the performance of organic thin film based devices by engineering the growth parameters, substrate/organic interface and device parameters but, high mobilities comparable with that in single crystals could not be achieved. Observations of negative temperature coefficient in polycrystalline organic thin films have previously been observed and interpreted in terms of large thermal fluctuations in electronic coupling rather than band transport [9–11]. Hence, an understanding of the crossover from localized to delocalized band-like transport in polycrystalline organic thin film is required.

In this chapter, we present an experimental and theoretical investigation of both, the hopping and the band-like transport in the same organic system. We investigate conduction in pentacene thin film in the presence of injected charge so that Fermi level can be varied. We find that the temperature coefficient of mobility changes from positive to negative corresponding to a transition from hopping to band-like transport as the Fermi level is modulated using the gate voltage.

The observed values of carrier mobilities in the band transport regime are two orders of magnitude higher than those in the hopping regime. Our experimental results are supported by theoretical calculations for hopping mobility estimates using Marcus theory [12, 13] and periodic density functional theory (DFT) based estimates for the band mobility.

## 4.2 Methodology

### 4.2.1 Computational details

To estimate different charge transport parameters in hopping regime, we have used Gaussian 09 package [14]. All parameters for hopping mobility have been calculated, by employing ground state energy calculations on pentacene monomer and dimers using B3LYP (Becke, three-parameter, Lee-Yang-Parr) functional [15, 16] and 631-G (d,p) basis set [17]. To estimate $\lambda$, geometries of neutral and ionic molecules are optimized and the single point energy are run on optimized geometries. Transfer integrals have been calculated from the output of Gaussian calculations using versatile Object-oriented Toolkit for Coarse-graining Applications (VOTCA) package [18–20].

The band mobility has been estimated using periodic DFT calculations using Quantum Espresso package [21]. To study band transport, experimentally determined lattice parameters of pentacene bulk phase [22] have been taken as initial point. Atomic coordinates have been relaxed on $4 \times 4 \times 3$ MonkhorstPack k-mesh. Non scf calculation for density of states have been performed on denser k mesh of $6 \times 6 \times 4$. We use generalized gradient approximatin (GGA) with the Perdew-Burke-Ernzerhol (PBE) [23] exchange correlation function and ultrasoft pseudopotentials. Dispersion interactions between organic molecules have been taken into account by using London type pairwise empirical atomic interactions as implemented by DFT-D2 method [24, 25].

### 4.2.2 Experimental details

We use pentacene for our experimets, for its relatively high carrier mobility in polycrystalline thin film and single crystal form, [13, 23]. We grow thin film of

pentacene using thermal evaporation of high purity (> 99.999%), triple sublimed pentacene at a base pressure of $5 \times 10^{-6}$ mbar. Very low evaporation rate of 0.1 Åwas maintained throughout the growth, in order to minimize structural disorder. [8] We fabricate three terminal organic field effect transistors (OFETs) with a 100 nm thick pentacene film grown on $n^{++}$ $Si/SiO_2$ substrate. Au source and drain contacts are fabricated on the top of pentacene thin film with the channel length, $L$ and width, $W$ of 20 $\mu$m and 3 mm, respectively. The electrical measurements are performed in rough vacuum ($10^{-2}$ mbar) using Keithley picoammeter, Agilent and Keithley voltage sources.

## 4.3 Working of a p-type OFET in negative and positive $V_{DS}$ regime

Figure 4.1 shows the output characteristics ($I_{DS}$ – $V_{DS}$) of pentacene thin film based OFET in negative as well as positive source-drain bias ($V_{DS}$) regime. Working of a p-type OFET in negative $V_{DS}$ regime has been discussed thoroughly in Chapter 2. Lets discuss here in brief. In a p-type OFET, a negative source-gate bias ($V_G$) accumulates a layer of holes at organic/dielectric interface. On applying a negative $V_{DS}$, charge carriers flow from source to drain and two different regions; accumulation region near source and depletion region due to the pinch off the channel near drain exist (schematically show in Fig. 4.1(a)). However, in positive $V_{DS}$ regime, working of the OFET is different from that in negative $V_{DS}$ regime. When a positive instead of a negative bias is applied at drain, device structure becomes quite similar to a hole only two terminal device (Fig. 4.1(b)). There are however two key differences; (i) organic thin film is sandwiched laterally between two metal electrodes whereas it is sandwiched vertically in two terminal devices. (ii) An additional gate voltage is used to control the density of background charge carriers in the device. Figure 4.1(b) schematically represents the working of the same OFET in positive $V_{DS}$ regime. In positive $V_{DS}$ regime, as drain is at higher potential than source, holes are injected at the drain electrode and move towards source i.e source and drain are interchanged. Further, in this regime, as there is no pinch-off, no depletion region is observed within the channel rather only accumulation region exists for the whole channel.

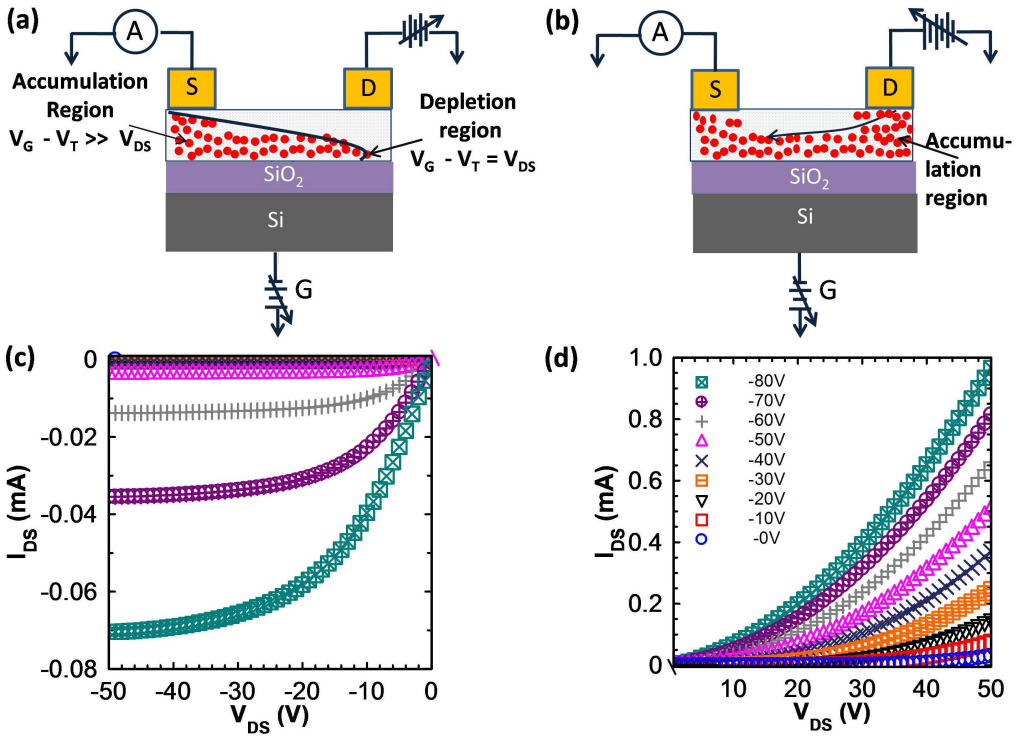


*Figure 4.1: Schematic representation of the working of a p-type OFET in (a) negative* $V_{DS}$ *regime and (b) positive* $V_{DS}$ *regime. In negative* $V_{DS}$ *regime, two regions exist within the channel; accumulation region and depletion region. However, in positive* $V_{DS}$ *regime, there is no depletion region rather only accumulation region exists for the whole channel. (c) and (d) show the room temperature output characteristics (*$I_{DS}$–$V_{DS}$*) of pentacene thin film based OFET in negative and positive* $V_{DS}$ *regime, respectively. Mechanisms of charge transport in negative and positive* $V_{DS}$ *regime seem different.*

Figure 4.1(c) and (d) represent the resulting output characteristics ($I_{DS}$–$V_{DS}$) characteristic of pentacene thin film based OFET in negative and positive $V_{DS}$ regime, respectively. As discussed in chapter 1, in negative $V_{DS}$ regime, $I_{DS}$–$V_{DS}$ exhibits two regions; linear region at small $V_{DS}$ and saturation region at high $V_{DS}$ due to the pinch-off the channel. However, in positive $V_{DS}$ region, as there is no pinch-off, no saturation is observed in $I_{DS}$ – $V_{DS}$ characteristics rather $I_{DS}$ increases non-linearly with $V_{DS}$ (Fig. 4.1(d)). $I_{DS}$ increases with $V_G$ in both, negative as well as positive $V_{DS}$ regime due to an increase in density of free holes. Hence, charge transport mechanism in the OFET in positive $V_{DS}$ regime seems different from that in negative $V_{DS}$ regime. Detailed comparative study on charge transport mechanism in negaive and posive $V_{DS}$ regimes has been represented in forthcoming sections.

## 4.4 Charge transport mechanism in negative $V_{DS}$ regime

Figure 4.2(a) shows the $I_{DS}$ – $V_{DS}$ on a log-log scale in negative $V_{DS}$ regime. Two regions; linear and saturation are observed clearly in $I_{DS}$ – $V_{DS}$. $\mu$ has been estimated by fitting the $I_{DS}$ – $V_{DS}$ characteristics in linear region as [26],

$$I_{DS} = \mu \frac{W}{L} C_i \left[ (V_G - V_T) V_{DS} - \frac{V_{DS}^2}{2} \right] \tag{4.1}$$

where $C_i$ is the dielectric capacitance per unit area and $V_T$ is the threshold voltage. The room temperature mobility has been found to be 0.3 $cm^2/Vs$, matching well with the typical mobilities observed in other studies [27–30]. To understand the charge transport mechanism in negative $V_{DS}$ regime, $\mu$ from $I_{DS}$ – $V_{DS}$ acquired at different temperatures have been estimated and have been plotted in Fig. 4.2(b). $\mu$ at all gate voltages increase with temperature exhibiting Arrhenius behavior, ($\mu \sim \exp(-E_a/k_BT)$). Hence, charge transport in this regime may be described by the thermally activated hopping of charge carriers within the localized states in GDOS. Inset of Fig. 4.2(b) shows that activation energy decreases as $V_G$ increases which is obvious. As gate voltage increases, injected charge carriers first fill the interface states if present and lower energy states that give rise

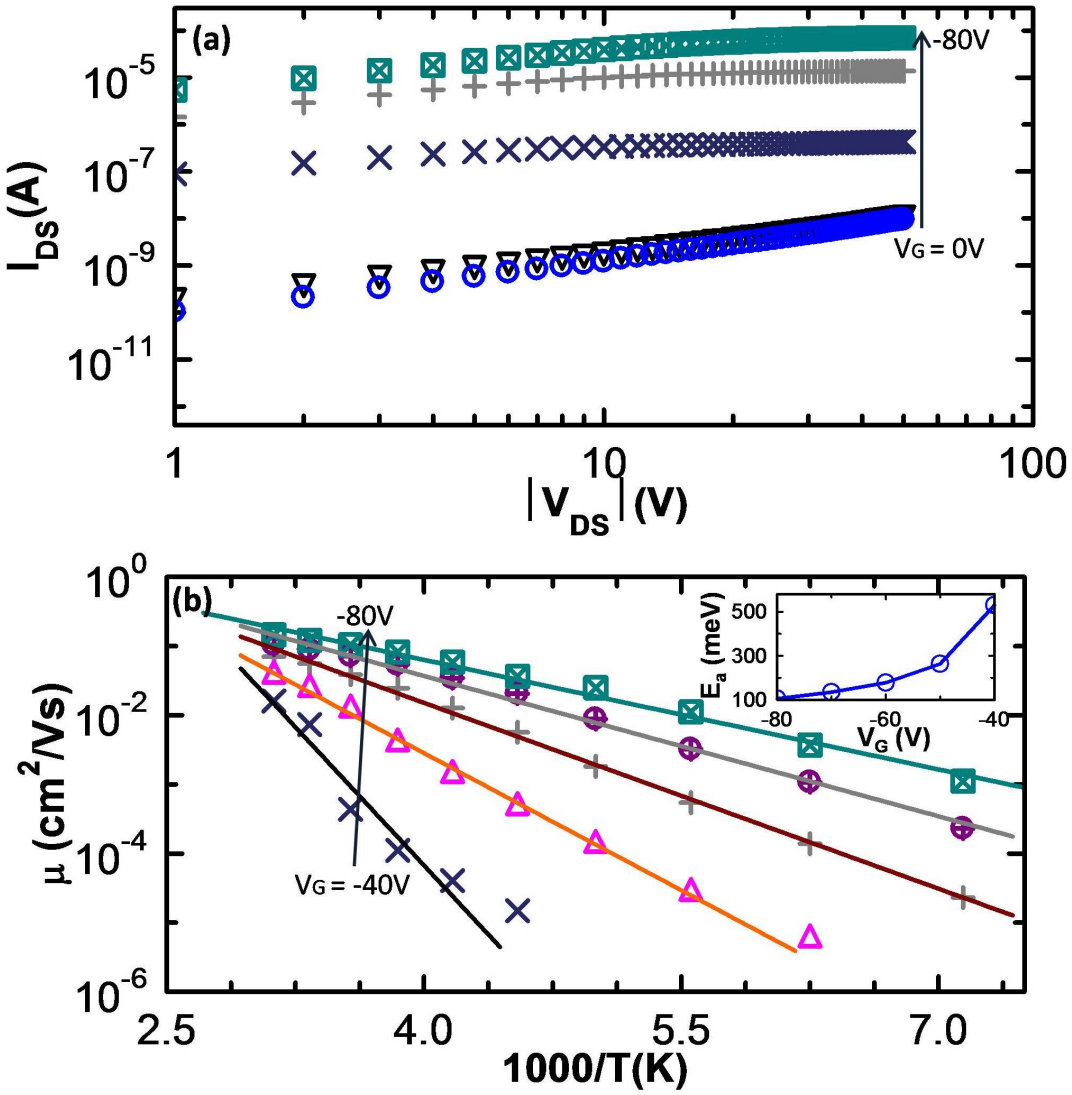


*Figure 4.2:* ***Negative source-drain bias regime:*** *(a)* $I_{DS}$-$V_{DS}$ *on a log-log plot for a pentacene thin film based OFET. Here, linear and saturation regions are clearly distinguishable. (b) Arrhenius temperature dependence of charge carrier mobility measured at different* $V_G$*. Inset shows the variation of activation energy with the gate voltage. Different symbols represent different values of the applied gate voltage,* $V_G$*.*

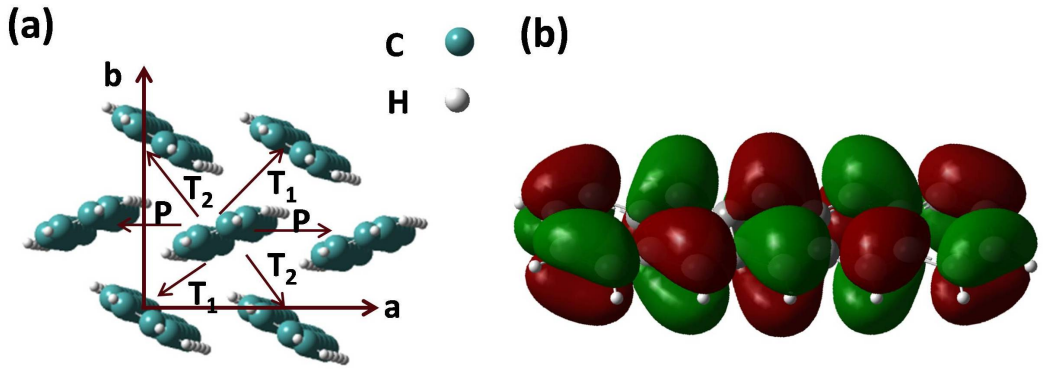


*Figure 4.3: (a) Schematic representation of different dimers in ab-plane; P dimers along a-axis,* $T_1$ *and* $T_2$*, transverse dimers along digonals and (b) isosurface representing the charge density distribution on HOMO of pentacene*

to a threshold voltage. Then additional charge carriers start filling higher energy states in the GDOS shifting the Fermi level ($E_F$) towards the center of the GDOS. Since, density of localized states increases as Fermi level shifts from tail towards the center of GDOS, charge carriers occupying higher energy states need less activation energy.

Next, we compare the experimentally observed mobility in negative $V_{DS}$ regime with the intrinsic mobility of pentacene in hopping regime. As discussed in previous chapter, Marcus theory [12] is used to study intrinsic charge transport in hopping regime. This theory describes the charge transfer between neighboring molecular sites, $i$ and $j$ as a self exchange reaction process and the rate of this reaction $k_{ij}$ is given by,

$$k_{ij} = \frac{t_{ij}^2}{\hbar}\sqrt{\frac{\pi}{4\lambda k_B T}}\exp\left(-\frac{\lambda}{k_B T} - \frac{(E_j - E_i)}{2k_B T} - \frac{(E_j - E_i)^2}{16k_B T\lambda}\right) \tag{4.2}$$

where $\lambda$ represents the strength of coupling of external charge with the lattice phonon and is known as reorganization energy, $t_{ij}$, the transfer integral, represents the strength of electronic coupling between neighboring molecules which further depends on the overlapping of orbitals of neighboring molecules. Hence, according to Marcus theory, in order to calculate $k_{ij}$, two parameters $t_{ij}$ and $\lambda$ have to be calculated. If both the molecules involved in charge transfer are equivalent, term

($E_i - E_j$) can be neglected. From $k_{ij}$, hopping mobility can be estimated using the Einstein relation as [26],

$$\mu = \frac{eD}{k_B T} \tag{4.3}$$

where

$$D = \frac{1}{2n} \sum_j r_j^2 k_{ij} P_j \tag{4.4}$$

and $n$ is the space dimensionality, $P_j (= k_{ij} / \sum k_{ij})$ is hopping probability of a charge carrier corresponding to the hopping pathway, $j$.

Detailed discussion on the estimation of $t_{ij}$ and $\lambda$ has been presented in Chapter 3. $\lambda$ is intrinsic property of a single molecule and is estimated by performing single point energy calculation on optimized geometries of neutral and ionic molecule as [31]

$$\lambda = [(E_{\pm}^{'} - E_{\pm}) + (E^{'} - E)] \tag{4.5}$$

where $E$ and $E_{\pm}$ are the ground state energies of the molecule in the neutral state and in the ionic state ('+' and '-'signs represent the cation and anion, respectively ) respectively. $E^{'}$ is the energy of the neutral molecule in the optimized geometry of the charged molecule and $E_{\pm}^{'}$ is the energy of the charged molecule in the optimized geometry of the neutral molecule. As it is related to the coupling of external charge with the lattice phonon, it is preferred to be small. $\lambda$ has been found to be 97 meV for a pentacene molecule.

Since, energy splitting in dimer method overestimates the magnitudes of intermolecular electronic coupling (as discussed in Chapter 3), because of ignoring the non orthonormality of monomer orbitals. Dimer projection (DIPRO) [20] method has been employed to estimate $t_{ij}$, along all different dimers, lying in ab-plane of pentacene ( 4.3(a)). In this method, $t_{ij}$ is directly estimated from the orbitals of dimers and monomers, by projecting monomer orbitals on the dimer orbitals [20]. Thus non-orthonormality of frontier orbitals of monomers is taken into account. $t_{ij}$ estimated along dimers, $P$, $T_1$ and $T_2$ are listed in Table 4.1. Figure 4.3(b) shows the distribution of charge density on the HOMO of pentacene. We observe that HOMO is uniformly distributed over the all the benzene rings in pentacene. Further, as H-atoms have no $p$-orbitals, they do not contribute to the $\pi$-orbitals of HOMO. Further, using Eq. 4.2, 4.4 and 4.3, average mobility in ab-plane has

*Table 4.1: Summary of experimentally observed and DFT calculated mobilities of pentacene in hopping regime and different parameters that decide the efficiency of hopping transport.*

| Hopping Transport | | | | | |
|---|---|---|---|---|---|
| $\lambda$ | $t_{ij}$(meV) | | | $\mu$ (exp.) | $\mu$ (DFT) |
| | P | $T_1$ | $T_2$ | | |
| 97 | 57.74 | 65.38 | 68.46 | 0.15 | 1.8 |

been found to be 1.8 $cm^2$/Vs. Predicted magnitudes of $\lambda$ , $t_{ij}$ and $\mu$ are comparable with that estimated in previous studies in pentacene [32–34]. This should be the highest mobility that can be achieved in hopping regime. The theoretically calculated mobility estimates are higher than the experimentally observed values. This can possibly be attributed to the thermal and energetic disorder in neighboring molecules that have not been taken into account in theory.

## 4.5 Charge transport mechanism in positive $V_{DS}$ regime

Figure 4.4(a) represents $I_{DS}$ as a function of applied positive $V_{DS}$ on a log-log plot. At small $V_{DS}$, charge carriers injected from one electrode redistribute themselves in such a way that they replace the holes flowing at the other. Hence charge transport is contact limited and $I_{DS}$ is governed by the thermally generated free charge carriers in device, resulting in an Ohmic region in $I_{DS}-V_{DS}$. At high bias, density of injected carriers increases and accumulation of holes creates a space charge region. $I_{DS}$ then increases non-linearly with $V_{DS}$ due to space charge limited conduction (SCLC) [35, 36]. In SCLC regime, current exhibits a power law dependence on voltage and power law exponent eventually increases with bias due to field dependent mobility as proposed by Bassler et. al. [1].

$$\mu\left(F,T\right)=\mu\left(0,T\right)\exp\left[\gamma\left(T\right)\sqrt{F}\right] \tag{4.6}$$

where $\mu(0,T)$ is the zero field charge carrier mobility and $\gamma(T)$ is the field activation factor. Hence, in positive $V_{DS}$ regime too, there are two regions in $I_{DS}-V_{DS}$;

Ohmic and SCLC.

Further, with increasing gate voltage, the background carrier concentration in device increases. At higher gate bias more charge carriers need to be injected from source to create a space charge, resulting into the weakening of SCLC at higher $V_G$. Hence, as $V_G$ increases, crossover from Ohmic to SCLC takes place at higher $V_{DS}$ and eventually, only Ohmic region is observed for the whole range of $V_{DS}$, high $V_G$. In SCLC region, mobility is estimated by solving the following set of equations self consistently [37],

$$I_{DS} = ep\,(x)\,\mu\,[T, F\,(x)]\,F\,(x)\,A \tag{4.7}$$

$$\frac{dF\,(x)}{dx} = \frac{ep\,(x)}{\epsilon_s} \tag{4.8}$$

$$V_{DS} = \int_0^L F\,(x)\,dx \tag{4.9}$$

Here $A$ is the effective area of cross-section, *p(x)* is the density of charge carriers at a distance $x$ from the injecting electrode and $\epsilon_s$ is the dielectric constant of organic semiconductor. Room temperature mobility estimated in this way has been found to be 48.3 $cm^2/Vs$ at a gate voltage of -80 $V$ which is almost two orders of magnitude higher than that in the negative source-drain bias regime and also higher than the hopping mobility limit set by Marcus theory. Surprisingly, the order of magnitude matches well with mobilitiy values observed in ultrapure single crystals of pentacene [38].

Next, to understand the charge transport mechanism in positive $V_{DS}$ regime, we have estimated $\mu$ at different temperatures and different gate voltages. Fig. 4.4(b) shows the $T$ and $V_G$ dependence of zero field mobility $\mu(0, T)$. We observe that in positive source-drain bias regime, mobilities increase with temperature up to $\sim$ 280 K, beyond which mobilities start decreasing with temperature. Below $\sim$ 280 K, charge transport must be limited by impurity scattering [26, 39]. As thermal energy of charge carriers increase with temperature, they spend less time in the vicinity of the impurity and impurity scattering is reduced, resulting in the improved charge transport at high temperature. Beyond $\sim$ 280 K, the decrease in mobility with the increase in temperature can be explained on the basis of phonon scattering [26, 39]. As the amplitudes of thermal vibrations (i.e phonon

*Table 4.2: Summary of experimentally observed and DFT calculated mobilities of pentacene in band transport regime and different parameters that decide the efficiency of band transport.*

| Band Transport | | | | |
|---|---|---|---|---|
| $D_p$ eV | B GPa | $m_e/m_0$ | $\mu$ (exp) $cm^2/Vs$ | $\mu$ (DFT) $cm^2/Vs$ |
| 1.24 | 12.5 | 1.23 | 48.3 | 55.5 |

concentration) of lattice increase with temperature, scattering of charge carriers with phonons also increases resulting a decrease in mobility at higher temperatures. After fitting the mobility curves in the high temperature range according to $\mu(T) \sim T^{-\gamma}$, $\gamma$ has been found to be in the range 2.1 - 2.4. These values of $\gamma$ match well with those obtained for pure organic crystals, [2, 40] highlighting the role of phonon scattering in polycrystalline organic thin films. The role of thermal fluctuations in intermolecular electronic coupling as suggested by *Troisi et al.* [9] is ruled out by carrying out molecular dynamics simulations and evaluating the temperature dependence of mobility in pentacene thin film phase. We observe no signature of band-like transport from these simulations.

Further, room temperature mobility estimated from $I_{DS}$ – $V_{DS}$ in positive $V_{DS}$ regime is consistent with the band mobility values expected for single crystals [38]. To support our experimental observations of band transport, we have theoretically estimated the band mobilities of pentacene bulk phase [22] using periodic DFT based calculations. Brillouin zone of pentacene with high symmetric $k$-points used in the calculation of band structure are shown in Figure 4.5(a). Brillouin zone is the primitive cell in reciprocal space equivalent to the unit cell in real space. Figure 4.5(b) shows the distribution of charge density in the surrounding of molecules in pentacene unit cell. Figure 4.5(c) shows the band structure and density of states for pentacene bulk phase [41]. The band structure calculations have been carried out in Brillouin zone connecting the different high symmetry points, X, M, Y, Z with the internal coordinates being (0,0,0), (0.5,0,0), (0.5,0.5,0), (0,0.5,0) and (0,0,0.5) in units of $(2\pi/a; 2\pi/b; 2\pi/c)$, respectively. As there are two molecules in equivalent configuration in pentacee unit cell, each band in band structure is composed of two subbands. Pentacene shows a direct band gap at $\Gamma$ to be 0.70 eV which is lower than the experimentally observed one

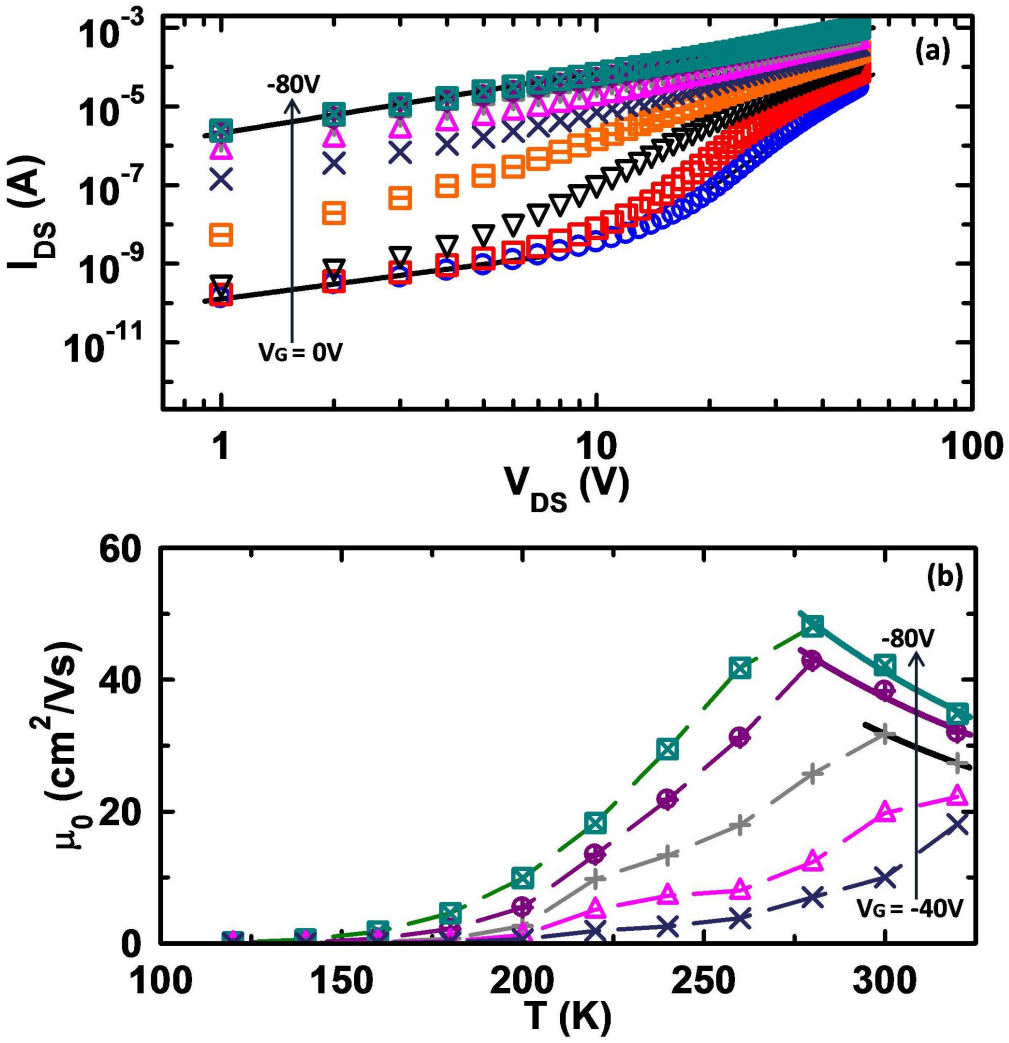


*Figure 4.4:* ***Positive source-drain bias regime:*** *(a)* $I_{DS}$-$V_{DS}$ *on a log-log plot for a pentacene thin film based OFET.* $I_{DS}$-$V_{DS}$ *characteristics are similar to two terminal devices i.e. initial Ohmic region and then field dependent SCLC. However as* $V_G$ *increases SCLC starts weakening and approaches Ohmic region for the entire range of* $V_{DS}$*. (b) Temperature dependence of charge carrier mobility measured at different* $V_G$ *in positive source-drain bias regime. Dashed lines are used to connect the different data points at same* $V_G$ *and solid lines represent fitting according to the power-law* ($\mu \sim T^{-\gamma}$) *at high temperatures. Different colored symbols represent different values of the gate voltage,* $V_G$*.*

(2.2 eV) [42]. This is a common drawback of DFT however, it does not affect the accuracy of transport parameters estimated from band structure because, transport parameters are estimated from the slope of the valence or conduction band and not from the band gap.

From band structure, carrier mobility can be estimated as [34],

$$\mu = \frac{e\tau}{m_e} \tag{4.10}$$

So there are two main parameters to be determined; effective mass ($m_e$) and relaxation time ($\tau$). Effective mass has been calculated from band structure as [34], $m_e = \hbar^2 \left( \frac{d^2E(k)}{dk^2} \right)$. The relaxation time has been estimated using the acoustic deformation potential and follows as [43],

$$\tau = \frac{\hbar^2 B}{(2\pi k_B T)^{1/2} m^{1/2} D_p} \tag{4.11}$$

where $B$ is the bulk modulus and $D_p$ is the accoustic deformation potential. $B$ and $D_p$ can be given by [43],

$$B = V_0 \left( \frac{\partial^2 E}{\partial V^2} \right)_{V_0} \tag{4.12}$$

$V_0$ being the equilibrium volume of the unit cell and

$$D_p = \frac{1}{V_0} \frac{\partial E_{VC}}{\partial(\Delta V)} \tag{4.13}$$

where $\Delta V$ represents the change in the volume of pentacene unit cell and $E_{vc}$ is the energy difference between the core level and top of maximum valence band for hole transport. As localized 1s level is not sensitive to the slight lattice deformation, it can be used as energy reference to obtain the absolute band energy change for valence band maximum (VBM). This energy difference between the VBM and 1s level is plotted against the fratcional change in volume to obtain $D_p$. Then band mobility, estimated using Eq. 4.10 has been found to be 55.5 $cm^2/Vs$ and is listed in Table 4.2, with all the other parameters. This should be highest band mobility that can be achieved in pentacene. This crossover from

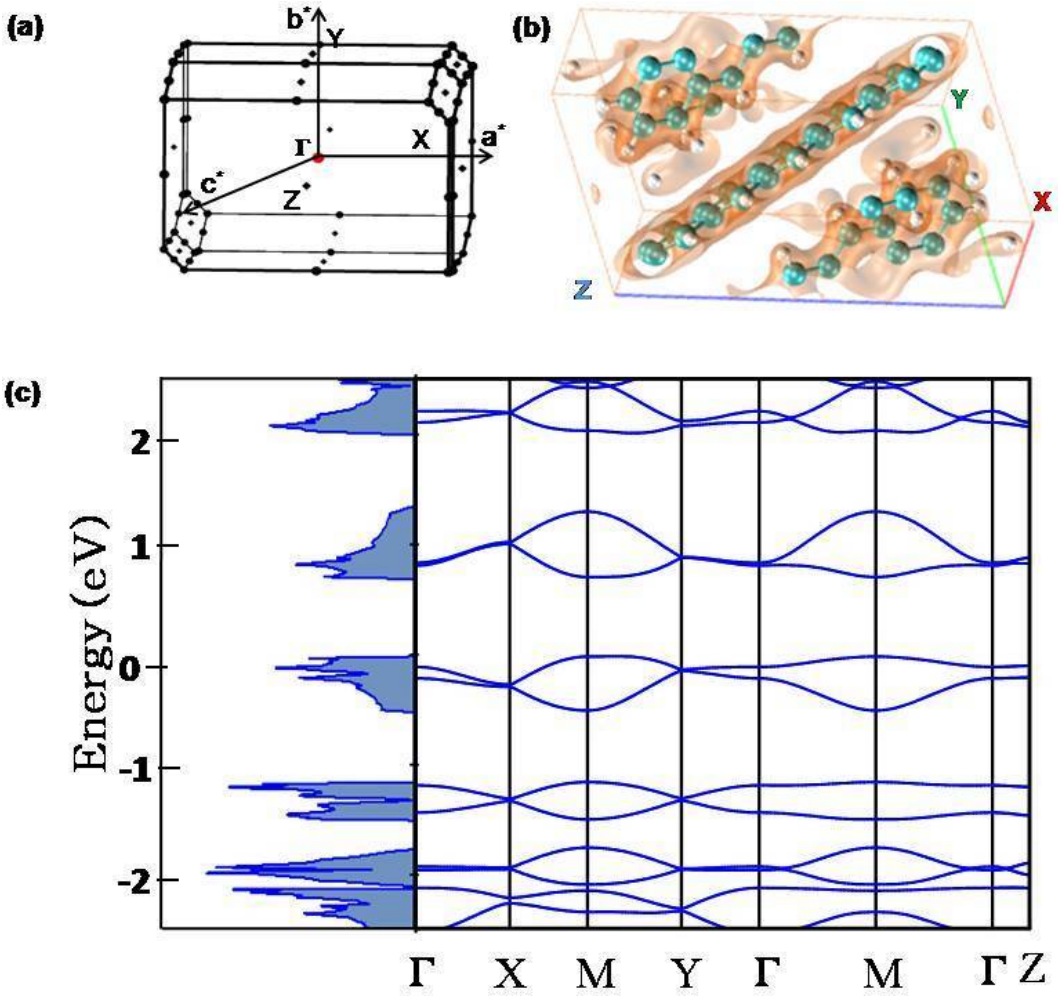


*Figure 4.5: (a) First Brillouin zone for crystal structure of pentacene in reciprocal lattice. (b) Distribution of charge density in the surrounding of molecules in pentacene unit cell. (c) Calculated band structure and density of states of pentacene using periodic DFT calculations. Different high symmetry points are represented in units of* $(2\pi/\mathrm{a}, 2\pi/\mathrm{b}, 2\pi/\mathrm{c})$ *along certain directions as* $\Gamma$ *= (0, 0, 0), X = (0.5, 0, 0), M = (0.5, 0.5, 0), Y = (0, 0.5, 0) and Z = (0, 0, 0.5). Zero of energy has been set at the valence band maximum.*

hopping transport in negative $V_{DS}$ regime to band-like transport in positive $V_{DS}$ regime can be attributed to the shifting of the Fermi level (explained below) from tail towards the center of GDOS. This can be further shown by analytically estimating the positions of $E_F$ in negative as well as positive $V_{DS}$ regime.

## 4.6 Estimation of $E_F$

The positions of the Fermi level in both regimes can be analytically estimated as follow. The total charge concentration in the channel at a spatial position $x$ (distance from the injecting electrode) can be written as:

$$p_{tot}(x) = p_f + p_G + p_{DS}(x) \tag{4.14}$$

where $p_f$ is the concentration of thermally generated free charge carriers and $p_G$ and $p_{DS}(x)$ are the charge carrier concentrations injected by the gate and source-drain bias, respectively. In the negative source-drain bias regime, when the gate bias is larger than the source-drain bias, $p_{tot}$, using gradual channel approximation can be written as [44],

$$p_{tot}(x) = p_f + C_i \left( V_G - \frac{x}{L} V_{DS} \right) / et \tag{4.15}$$

where $t$ is the thickness of the accumulation layer and has been take to be 10 nm. When source-drain bias approaches the gate voltage, channel is depleted and the Fermi level lies in the deep localized states below the equilibrium level ($-\sigma^2/k_BT$, $\sigma$ being the width of GDOS), resulting into low values of mobility.

In the positive source-drain bias regime, at low bias, injected carrier concentration is equal to the extracted one and the transport is injection limited. Then total carrier concentration and position of the Fermi level is decided by the gate voltage i.e.

$$p_{tot} = p_0 + C_i V_G / eh \tag{4.16}$$

At high bias, all the charge carriers injecting at one electrode are not balanced by those extracting at the other, resulting accumulation of charge carriers. Then $p_{DS}(x)$ may be estimated as follows [26, 45]. From Eqs. 4.7 and 4.8, at a spatial position, $x'$ from source, it can be written that

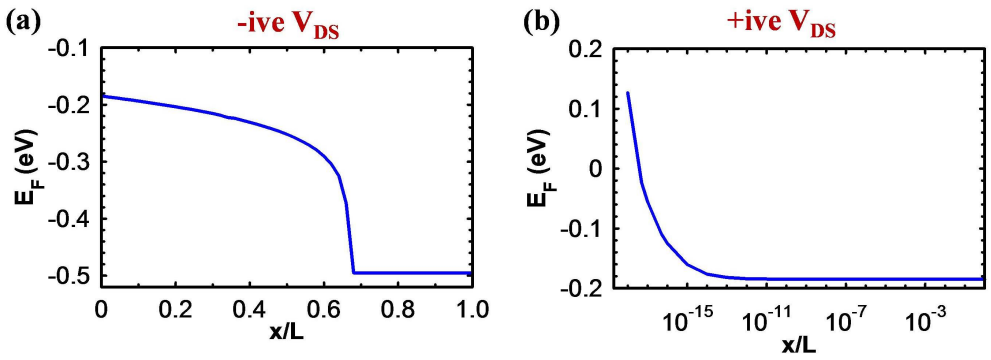


*Figure 4.6: Estimated Fermi level ($E_F$) within the channel as a function of the distance taken from the source in (a)negative $V_{DS}$ regime and (b)positive $V_{DS}$ regime. $|V_G|$ and $|V_{DS}|$ have been kept fixed at 40 V and 60 V, respectively.*

$$I_{DS} = \mu\left[T, F\left(x'\right)\right]\epsilon_s A F\left(x'\right)\frac{F\left(x'\right)}{dx'} \tag{4.17}$$

after integrating spatially from 0 to x and putting boundary condition ($F(0) = 0$), we get,

$$F\left(x\right) = \sqrt{\frac{2I_{DS}x}{\mu\left[T, F\left(x\right)\right]\epsilon_s}} \tag{4.18}$$

Now, in SCLC regime $I_{DS}$ can be given as

$$I_{DS} = \frac{9}{8}\mu\left[T, F\left(x\right)\right]\epsilon_s\frac{V_{DS}^2}{L^3} \tag{4.19}$$

putting this value of $I_{DS}$ in Eq. 4.19 and solving for *F(x)*, we get,

$$F\left(x\right) = \frac{3}{2}x^{1/2}\frac{V_{DS}^2}{L^3} \tag{4.20}$$

Finally, putting the value of F(x) in Eq. 4.8, p(x) can be given as

$$p(x) = 3V_{DS}\epsilon_s x^{-1/2}/4L^{3/2} \tag{4.21}$$

This is actually the $P_{DS}$ that is defined in Eq. 4.14

$$p_{DS}(x) = \epsilon_s 3 V_{DS} x^{-1/2} / 4 L^{3/2} \tag{4.22}$$

and total carrier concentration is given by Eq. 4.14. Dependence of the Fermi level on the carrier concentration is given by [37],

$$\int_{-\infty}^{\infty} f\,(E, E_F)\, g\,(E)\, dE = p_{tot} \tag{4.23}$$

where $f(E, E_F) = [1 + \exp(E_F - E)/k_B T]^{-1}$, is Fermi function, exhibiting the energetic distribution of the charge carriers at thermal equilibrium. g(E) represents the GDOS in HOMO of the organic semiconductor given by [37],

$$g(E) = \left(N_V / \sqrt{2\pi}\sigma\right) \exp(-\frac{E^2}{2\sigma^2}) \tag{4.24}$$

$N_V$ is effective density of states in the HOMO. Hence, position of $E_F$ depends on three parameters; (i) spatial position (x) between source and drain (ii) magnitude of negative or positive $V_{DS}$ i.e. $|V_{DS}|$ and (iii) magnitude of $V_G$. Lets examine the effect of each of these parameters separately.

### 4.6.1 Dependence of $E_F$ on $x$ when $V_{DS}$ and $V_{GS}$ are fixed

If $V_{DS}$ and $V_G$ are fixed then positional dependence of $E_F$ in positive and negative $V_{DS}$ regime can be estimated as follow. In negative $V_{DS}$ regime, there are two regions: linear (for $V_{DS} < V_G$) and saturation (For $V_{DS} > V_G$). In linear region, for a fixed $V_G$ and $V_{DS}$, total carrier density as a function of $x$ can be estimated using Eq. 4.15 and corresponding $E_F$ can be estimated from Eq. 4.23. Variation in $E_F$ as a function of $x$ in linear region has been shown in Fig. 4.6(a). In saturation regime, Fermi level enters into the deep localized states in GDOS and becomes almost constant (also shown in Fig. 4.6(a)).

As can be seen, in Fig. 4.6(a), in negative $V_{DS}$ regime, Fermi level decreases from source to drain gradually in accumulation region and becomes constant in depletion region. However, in positive $V_{DS}$ regime, $E_F$ varies in some different manner with x when $V_{DS}$ and $V_{GS}$ are fixed. In positive $V_{DS}$ regime too, there are two regions: linear and space charge region. Carrier concentration in positive

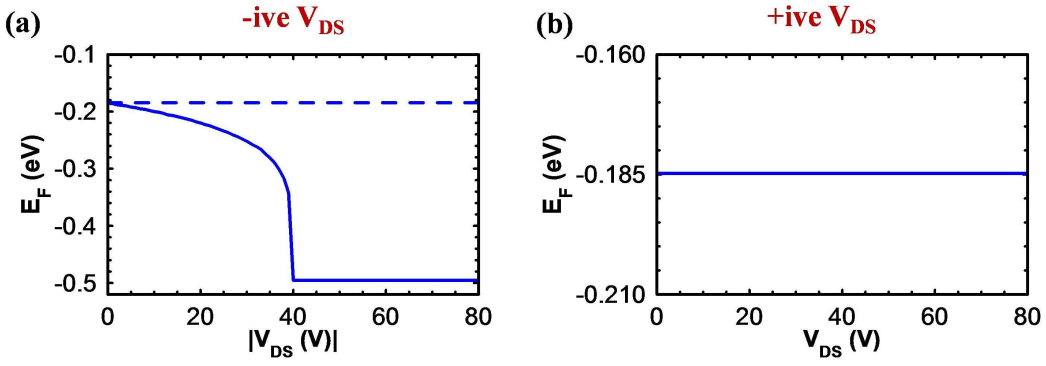


*Figure 4.7: Estimated Fermi level ($E_F$) at source and drain as a function of source-drain bias for a fixed $|V_G|$ in (a) negative $|V_{DS}|$ regime and (b) positive $V_{DS}$ regime. Dashed and solid lines in (a) represent the positio of Fermi level at source and drain, respectively.*

$V_{DS}$ can be estimated from Eqs.4.14, 4.16 and 4.22 and then Fermi level using Eq. 4.23. Fermi levels in both regions as a function of x have been shown in Fig 4.6(b).

### 4.6.2 Dependence of $E_F$ on $V_{DS}$ when x and $V_G$ are fixed

To examine the effect of source-drain bias on Fermi level, we estimate position of $E_F$ at two positions i.e. at source (x=0) and at drain (x=L) for a fixed $V_G$. As source is grounded in negative $V_{DS}$ regime i.e. $V = 0$ or $V_{DS}=V$, at source contact, $E_F$ does not depend on $V_{DS}$ and remains constant for a fixed $V_G$ (Fig.4.7 ). At drain contact (x=L), position of Fermi level depends on the relative values of $V_{DS}$ and $V_G$ and can be estimated using Eq. 4.15 and 4.23. For a fixed $V_G$, variation in $E_F$ with respect to $V_{DS}$ have been shown in Fig. 4.7. In positive $V_{DS}$ regime, voltage is applied at source (as discussed in Section 4.5). In Ohmic region, as no accumulation of charge carrier takes place, Fermi level should remain constant between source and drain for a fixed $V_G$. In space charge region, source contact acts as a infinite source of charge carriers and hence Fermi level is quite high, also obvious from Eq. 4.22. At drain contact, $E_F$ as a function of $V_G$ has been shown in Fig. 4.7(b).

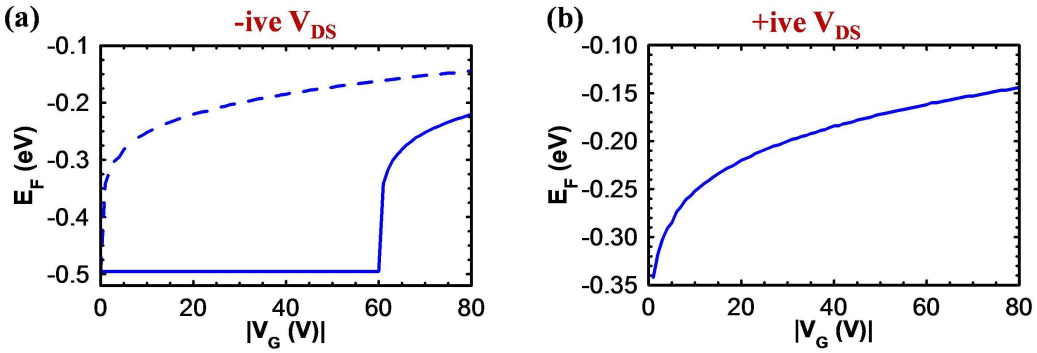


*Figure 4.8: Estimated Fermi level ($E_F$) at source and drain as a function of $|V_G|$ for fixed $V_{DS}$ in (a) negative $|V_{DS}|$ regime and (b) positive $V_{DS}$ regime. Dashed and solid lines in (a) represent the Fermi level at source ad drain respectively.*

### 4.6.3 Dependence of $E_F$ on $V_G$ when $x$ and $V_{DS}$ are fixed

Finally, we investigate the effect of $V_G$ i.e. background carrier concentration at source and drain when a fixed $V_{DS}$ is applied. For negative $V_{DS}$ regime, positions of Fermi level with respect to $V_G$ have been plotted in Fig. 4.8(a) at source and drain contact. Dashed lines represet the fermi level at sourec wheras solid line shows the position of Fermi level at drain. For positive $V_{DS}$ regime, as source can provide infinite carriers, it is not possible to draw a Fermi level there. Fermi lavel at drain has been plotted in Fig. 4.8(b).

We observe that in all the cases discussed above Fermi level in positive $V_{DS}$ regime lies above than that in negative $V_{DS}$. The density of occupied states is high in the accumulation region and low in the depletion region, resulting in the current being controlled by the low mobility region i.e. the tail of the GDOS. In the positive source-drain bias regime, as there is no depletion region, the Fermi level across the entire channel remains near the center of the GDOS. As Fermi level moves from tail to the center of GDOS, density of localized states increases continuously. Near the center of GDOS density of localized states is so high that charge carriers require no activation energy to move to neighboring sites and move like a wave. This would explain the band-like transport with higher mobilities in positive source-drain bias regime in pentacene thin film based OFETs. Hopping and band-like transport governed by two different sections of the GDOS have

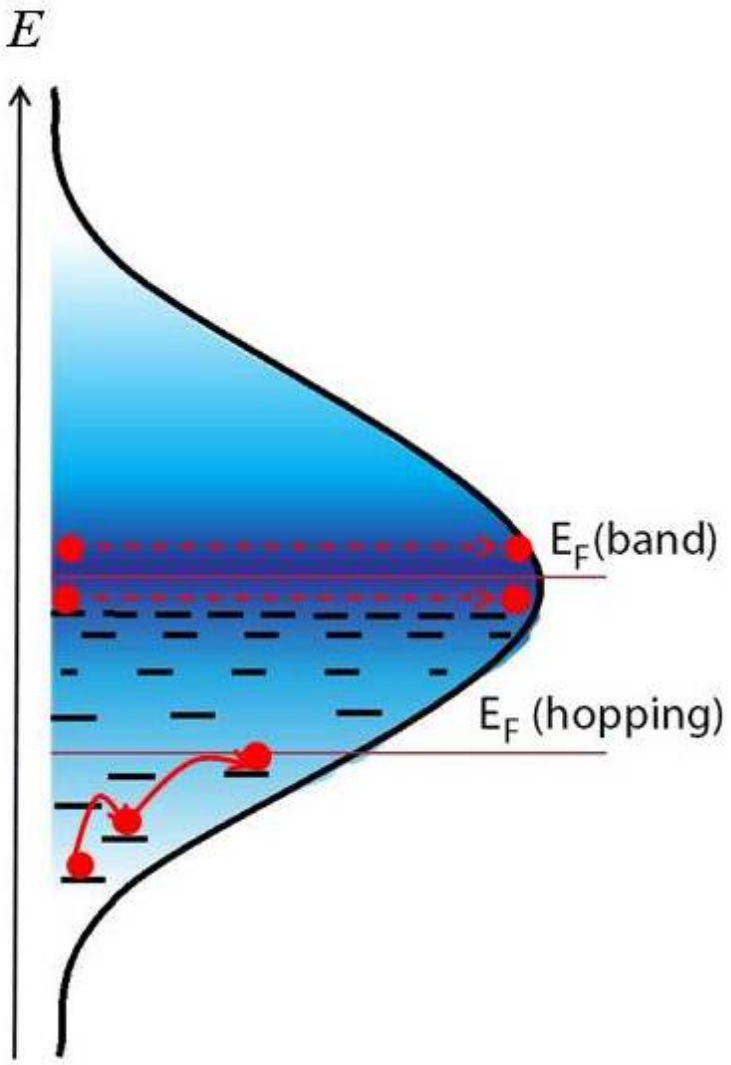


*Figure 4.9: Schematic illustration of charge transport governed by two different sections of the GDOS. When the Fermi level lies near the tail of the GDOS, transport is described by thermally activated hopping. As the Fermi level moves towards the central region, band-like transport becomes possible.*

been schematically represented in Fig. 4.9.

## 4.7 Conclusion

In conclusion, by studying the characteristics of a pentacene thin film based OFET in both negative and positive source-drain bias regime, we have shown that different transport regimes can be observed in the same organic system. The large difference in mobilities in positive and negative source-drain bias regime has been explained on the basis of position of the Fermi level. In positive source-drain bias regime, mobilities comparable with single crystal of pentacene have been obtained due to the Fermi level lying near the center of the GDOS for the whole channel. The above observations suggest that it is possible to observe band like conduction in polycrystalline films provided that the Fermi level can be moved into a region of high density of states.

# Bibliography


[1] H. Bassler, physica status solidi (b) **175**, 15 (1993).

[2] M. Gershenson, V. Podzorov, and A. Morpurgo, Rev. Mod. Phys. **78**, 973 (2006).

[3] G. H. Gelinck et al., Nature Materials 3, 106 (2004); T. Sekitani, U. Zschieschang, H. Klauk and T. Someya, Nature Materials **9**, 1015 (2010).

[4] T. Lei, and J. Pei, J. Mater. Chem. **22**, 785 (2012).

[5] G. Gelnick, P. Heremans, K. Nomoto, T. D. Anthopolous, Adv. Mater. **22**, 3778 (2010).

[6] J. Takeya, M. Yamagishi, Y. Tominari, R. Hirahara, Y. Nakazawa, T. Nishikawa, T. Kawase, T. Shimoda, S. Ogawa, Appl. Phys. Lett. **90**, 102120 (2007).

[7] D. Boudinet, M. Benwadih, S. Altazin, J.M. Verilhac, E.D. Vito, C. Serbutoviez, G.Horowitz, A. Facchetti, J. Am. Chem. Soc. **133**, 9968 (2011).

[8] P. Kumar, A. Sharma, S. Yadav, and S. Ghosh, Org. Electron **14**, 1663 (2013).

[9] A. Troisi and G. Orlandi, Phys. Rev. Lett. **96**, 086601 (2006).

[10] S. Fratini and S. Ciuchi, Phys. Rev. Lett. **103**, 266601 (2009).

[11] T. Sakanoue and H. Sirringhaus, Nat. Mater. **9**, 736 (2010).

[12] R. A. Marcus, Rev. Mod. Phys. **65**, 599 (1993).

[13] A. Afzali, C. D. Dimitrakopoulos, and T. L. Breen, J. Am. Chem. Soc. **124**, 8812 (2002).

[14] M. J. Frisch, G. W. Trucks, H. B. Schlegel, G. E. Scuseria, M. A. Robb, J. R. Cheeseman, G. Scalmani, V. Barone, B. Mennucci, G. A. Petersson, et al., Gaussian09 Revision A.02, Gaussian Inc. Wallingford CT (2009).

[15] A. D. Becke, Phys. Rev. A **38**, 3098 (1988).

[16] C. Lee, W. Yang, and R. G. Parr, Phys. Rev. B **37**, 785 (1988).

[17] V. A. Rassolov, J. A. Pople, M. A. Ratner, and T. L. Windus, J. Chem.l Phys. **109**, 1223 (1998).

[18] V. Ruhle, C. Junghans, A. Lukyanov, K. Kremer, and D. Andrienko, J. Chem. Theory Comput. **5**, 3211 (2009).

[19] V. Ruhle, A. Lukyanov, F. May, M. Schrader, T. Veho, J. Kirkpatrick, B. Baumeier, and D. Andrienko, J. Chem. Theory Comput. **7**, 3335 (2011).

[20] B. Baumeier, J. Kirkpatrick, and D. Andrienko, Phys. Chem. Chem. Phys. **12**, 11103 (2010).

[21] P. Giannozzi, S. Baroni, N. Bonini, M. Calandra, R. Car, C. Cavazzoni, D. Ceresoli, G. L. Chiarotti, M. Cococcioni, I. Dabo, et al., J. Phys.: Condensed Matter **21**, 395502 (2009).

[22] J. Gotzen, D. Kafer, C. Woll and G. Witte, Phys. Rev. B **81**, 085440 (2010).

[23] J. P. Perdew, K. Burke, and M. Ernzerhof, Phys. Rev. Lett. **78**, 1396 (1997).

[24] S. Grimme, Journal of Computational Chemistry **27**, 1787 (2006).

[25] S. Grimme, J. Antony, S. Ehrlich, and H. Krieg, J. Chem. Phys. **132**, 154104 (2010).

[26] S. M. Sze and K. K. Ng., Physics of Semioconductor Devices, 3rd edition. (Wiley-Interscience, 2006).

[27] C.-M. Chen, C.-M. Liu, M.-C. Tsai, H.-C. Chen, and K.-H. Wei, J. Mater. Chem. C **1**, 2328 (2013).

[28] J. H. Na, M. Kitamura, D. Lee, and Y. Arakawa, Appl. Phys. Lett. **90**, 163514 (2007).

[29] S. E. Fritz, T. W. Kelley, and C. D. Frisbie, The J. Phys. Chem. B **109**, 10574 (2005).

[30] W.-Y. Chou, C.-W. Kuo, H.-L. Cheng, Y.-R. Chen, F.-C. Tang, F.-Y. Yang, D.-Y. Shu, and C.-C. Liao, Appl. Phys. Lett. **89**, 112126 (2006).

[31] Y.-H. Park, Y.-H. Kim, S.-K. Kwon, I.-S. Koo, and K.Y. Yang, Bulletin of the Korean Chemical Society **31**, 1649 (2010).

[32] I. Yavuz, B. N. Martin, J. Park, and K. N. Houk, J. Am. Chem. Soc. **137**, 2856 (2015).

[33] T. P. Nguyen, J. H. Shim, and J. Y. Lee, J. Phys.l Chem. C **119**, 11301 (2015).

[34] H. Kobayashi, N. Kobayashi, S. Hosoi, N. Koshitani, D. Murakami, R. Shirasawa, Y. Kudo, D. Hobara, Y. Tokita, and M. Itabashi, J. Chem. Phys. **139**, 014707 (2013).

[35] Agrawal, R.; Kumar, P.; Ghosh, S.; Mahapatro, A. K. Appl. Phys. Lett. **93**, 073311 (2008).

[36] Lampert, M. A.; Mark, P. Current injection in solids; Electrical science series; Academic Press, 1970.

[37] S. D. Baranovskii, physica status solidi (b) **251**, 487 (2014).

[38] O. D. Jurchescu, J. Baas, and T. T. M. Palstra, Appl. Phys. Lett. **84**, 3061 (2004).

[39] S. O. Kasap, Principles of electronic materials and devices (McGraw-Hill, 2006).

[40] A. Heck, J. J. Kranz, and M. Elstner, J. Chem. l Theory Comput. **12**, 3087 (2016).

[41] R. B. Campbell, J. M. Robertson, and J. Trotter, Acta Crystallogr. **15**, 289 (1962).

[42] L. Brehmer, Acta Polymerica **32**, 665 (1981).

[43] D. Wang, W. Shi, J. Chen, J. Xi, and Z. Shuai, Phys. Chem.Chem. Phys. **14**, 16505 (2012).

[44] M. Weis, J. Appl. Phys. **111**, 054506 (2012).

[45] Y. B. Zhu and L. K. Ang, J. Appl. Phys. **110**, 094514 (2011).

# Chapter 5

# Diffusion in organic thin film

Generally, charge carriers in organic semiconductors are localized in the tail of the Gaussian density of states (GDOS) and make jump via thermal activation to neighboring sites. Non-uniform distribution of charge carriers in GDOS is quite possible. Due to density gradient, charge carriers start diffusing along with drifting. Hence, diffusion of charge carriers should also be taken into account while studying charge transport in organic semiconductors. However, estimation of diffusion coefficient ($D$) in organic semiconductors is a non trivial task. Here, we present a direct approach to determine $D$ in disordered organic semiconductors, using a metal/semiconductor/metal device structure with one ohmic and other Schottky contact. First principle density functional theory (DFT) calculations have also been employed to check the consistency of this approach.

## 5.1 Introduction

Applications of organic semiconductors in modern electronics [1] necessitates deeper understanding of the charge carrier transport mechanism in them. Typically charge carrier mobility ($\mu$) has been considered a key parameter [2, 3] that characterizes the charge transport in organic semiconductors. However the physics of organic semiconductors and organic devices cannot be explained on the basis of mobility alone. Diffusion [4, 5] of charge carriers is another crucial phenomenon that needs to be investigated in order to understand the transport properties of organic systems and devices physics, thoroughly. In contrast to inorganic semiconductors where ordered valence and conduction band exist, the physics of organic semiconductors is governed by the positional and energetic disorders in Gaussian density of states (GDOS). In disordered organic semiconductors, charge carriers are localized in the tail of GDOS and charge transport in these systems is understood in terms of discrete hopping events among these localized states [6, 7]. Due to the immobilization of charge carriers in these localised states, significant non-uniform carrier distribution exists, resulting diffusive transport which may also affect the drift velocity of charge carriers. Hence investigation on the process of carrier diffusion is essential for not only to achieve deeper understanding on the device physics but also for developing new theoretical models. Further, as hopping transport in organic semiconductors is described by the incoherent jumps of charge carrier from one site to other site, by absorbing a phonon, it is a relatively slow process and charge carriers can take very long time to equilibrate. Thus disordered organic semiconductors must be treated as systems under non-equilibrium conditions [8]. It has been accepted previously [8, 9] that for disordered semiconductors under non-equilibrium conditions, an enhancement factor depending upon charge carrier density ($p$) and temperature ($T$) should be included in classical Einstein relation [10]. There are several theoretical and experimental methodologies to extract mobility [2, 11, 12] however, determination of $D$ is independently a complex problem as it is related to the temporal distribution of the charge carriers.

Although some efforts have been gone experimentally and theoretically towards evaluating the diffusion coefficient of charge carriers by; (i) Monte Carlo simulation [4], (ii) fitting of experimental time-of-flight (TOF) data using dif-

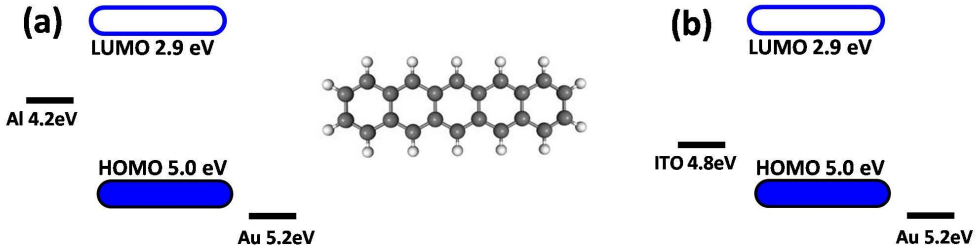


*Figure 5.1: Schematic representation of energy level diagram in (a) Al/pentacene/Au and (b) ITO/pentacene/Au based two terminal devices. In the middle, optimized structure of pentacene molecule has been shown.*

ferent models for photo-current transient equation [13], (iii) using the shape of electro luminescence transients in organic semiconductors [14]. Each of these methods has its own limitation as follow; (i) active layer thickness required for TOF experiments is typically several micrometers where as the film used in any realistic devices are often two order of magnitude less than that, (ii) no sharp TOF signal is observed in disordered organic semiconductor because of the presence of deep traps and large distribution of transport energy levels, (iii) the value of $\mu$ depend on the distance traveled by the photo-carriers excited by a UV light pulse under an external dc field, (iv) at high value of the dc field applied, the $\mu$ and $D$ become field dependent and as a result it is difficult to separate the effects due to the material disorder from those induced by the field itself, (v) specific injection contacts are needed in transient current technique, (vi) not all organic semiconductor show electro luminescence, (vii) the typical electric field needed in these cases are different than that of an operating devices. Moreover, most of these methods are indirect and model based, forbidding the direct determination of $D$, particularly in disordered systems.

Here, we present a relatively easy, nevertheless a powerful technique to determine $D$, using the most fundamental device i.e. metal/organic/metal based Schottky diode. Essentially, this method is based on current-voltage ($J$-$V$) and capacitance-frequency ($C$-$f$) characteristics of organic Schottky diode.

The absence of metallurgical Ohmic contact and limited success in doping of organic semiconductors [15] make organic devices critically depend on the efficiency of current injection [16–18] from metal electrodes to organic layers.

However in contrast to inorganic Schottky diode to achieve an organic Schottky junction, following issues have to be considered; (i) the electronic energy levels of the organic molecule and their relative position with respect to work function of metal electrodes [19], (ii) chemical and electronic interactions [20] between organic semiconductor and metal electrodes and (iii) the band bending [21, 22] at metal/organic interfaces. It has been shown that except in few cases, [23, 24] vacuum level alignment (VLA), known as Mott-Schottky limit [19], is a good approximation for determining the barrier for holes and electrons at metal/organic interfaces. Evidences of band bending by photoemission measurements remains controversial [23,24] due to several reasons, such as surface charging, buried interfaces and ambiguity with thickness dependence. Further, rectification in current when moving from reverse to forward bias does not confirm conclusively, the band bending and formation of Schottky barrier in organic diode [25]. Modulation of capacitance with bias in metal/organic/metal structure i.e. presence of Mott-Schottky capacitance [26] which is observed due to band bending is also essential.

## 5.2 Experimental details

We have chosen pentacene for our study. Due to simple chemical structure and increasing applications in commercial electronics [27], pentacene can be considered as a representative for molecular organic semiconductor family. However, similar techniques and analysis can be applied to other molecules also. The devices in our study consist of a single layer of pentacene sandwiched between pair of metal electrodes, Al and Au or ITO and Au. High purity ($> 99.999\%$), triple sublimed pentacene, procured from Sigma Aldrich Chemical Co. USA have been used for this study. Organic layers were deposited in an oil free evaporation system at a base pressure of $2 \times 10^{-6}$ Torr. All pentacene thin films have been deposited at very low deposition rate of 0.1 Å/s, in order to avoid structural disorder induced defects as much as possible, as discussed before. Impact of growth parameters on the trap concentration has been studied in Chapter 2 also. It is extremely important to optimize structural disorders while fabricating Schottky diode as they impede severely in achieving desirable $J$-$V$ and capacitance-voltage ($C$-$V$) characteristics. The $J$-$V$, $C$-$V$ and $C$-$f$ characteristics are measured in rough vac-

uum ($10^{-2}$ mbar) using Keithley picoammeter, voltage sources and Wayne Kerr LCR meter.

Here, we have considered two hole only sandwiched devices, based on pentacene i.e. Al/pentacene/Au and ITO/pentacene/Au. Pentacene is a hole transport material with highest occupied molecular orbital (HOMO) and lowest occupied molecular orbital (LUMO) at 5.0 eV and 2.9 eV, respectively [28]. The work functions of ITO, Al and Au are 4.8, 4.2 eV and 5.2 eV, respectively. According to Mott-Schottky VLA, there would be no barrier or negligible barrier at Au/pentacene and ITO/pentacene interfaces, respectively but a significant barrier of 0.8 eV exists for holes at Al/pentacene interface. Energy level diagram for Al/pentacene/Au and ITO/pentacene/Au based two terminal devices have been shown in Fig. 5.1.

## 5.3 *J-V* and *C-V* characteristics of two terminal sandwiched devices

Figure 5.2(a) shows the room temperature characteristics of *J-V* and *C-V* characteristics of Al/pentacene/Au based two terminal device under forward as well reverse bias i.e when voltage applied at Au is positive and negative, respectively. We observe high rectification of the order of $\approx 10^4$ in current when voltage applied at Au is changed from negative to positive. In reverse bias (V < 0) current is very low. *J-V* characteristics exhibit three different regions (Fig. 5.2(a)), for different ranges of *V*. Region I: when *V* lies within the range, –3 < V < 0.3. In this region, current increases with the magnitude of applied bias. Region II lies in the range, 0.3 < V < 1, in which device shows diode like behavior i.e. current shows exponential dependence on applied bias. Actually, V = 1.0 is the built-in potential ($V_{bi}$) due to the difference in the work functions of two metal electrodes. Region III starts from V ≥ 1 where dependence of current on voltage changes from exponential to power-law type. As shown before in Chapter 2, power law dependence of current on voltage is generally attributed to space charge limited conduction (SCLC) [17, 28]. Now, let us characterize the J – V characteristics in different regions. As in region I, currents are only parasitic, this region can be omitted. In region II, *J-V* characteristics could be well fitted

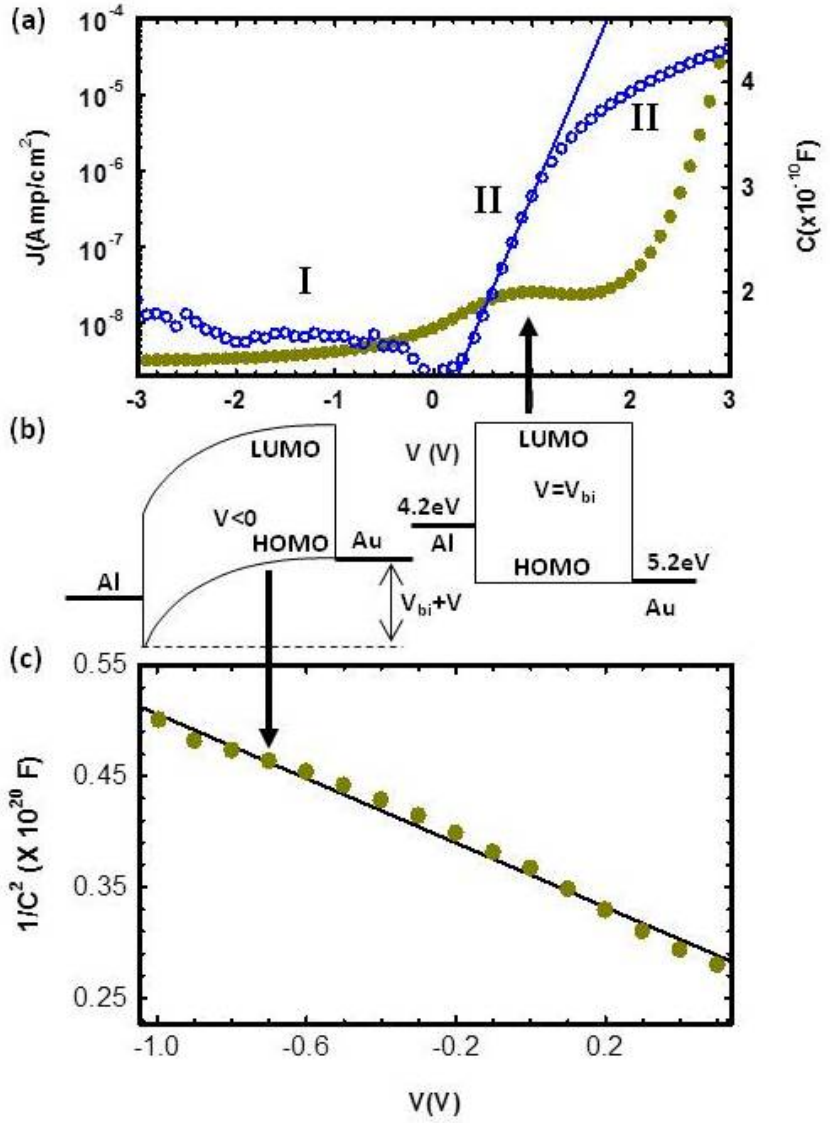


*Figure 5.2: (a) Room temperature J-V (empty circle) and C-V (filled circle) characteristics of Al/pentacene/Au based devices in which pentacene thin film has been sandwiched between metal electrodes with one Ohmic and other non-Ohmic. Measuring frequency of capacitance has been kept fixed at 200 Hz. In both, J-V and C-V characteristics, there are three distinct regions, I, II and III. Solid line in region II represents fitting with Mott Schottky relation (Eq. 5.1) for Schottky diode. (b) Illustration of band bending in depletion region (left). Flat band condition is observed when V approaches* $\mathrm{V_{bi}}$ *(right). (c) Shows* $1/\mathrm{C}^2-\mathrm{V}$ *characteristics in region II. Linear dependence of* $1/\mathrm{C}^2$ *on Vreflects the formation of depletion region in reverse bias.*

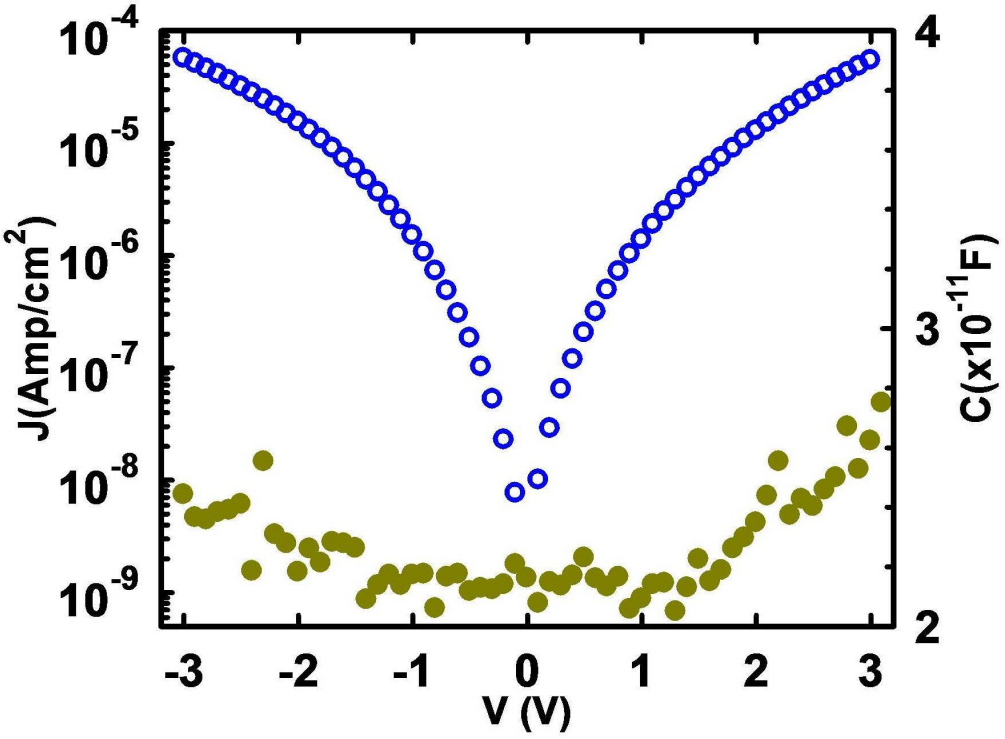


*Figure 5.3: Room temperature J-V (empty circle) and C-V (filled circle) characteristics of ITO/pentacene/Au based devices in which pentacene thin film has been sandwiched between metal electrodes with both the contacts Ohmic. Measuring frequency of capacitance has been kept fixed at 200 Hz.*

according Mott-Schottky relation [10]

$$J_{II} = J_0 \left[ \exp\left( \frac{eV}{gk_BT} - 1 \right) \right] \tag{5.1}$$

where $J_0 = A^*T^2\exp(-\phi_B/k_BT)$ and known as saturation current, $A^*$ is called the effective Richardson constant, $\phi_B$ is the Schottky barrier height, $k_B$ is Boltzmann's constant, $e$ is the electronic charge and $g$ is the enhancement factor that discussed in Section 1.1 and known as ideality factor in organic semiconductors [9]. Value of $g$ is *1* in the thermionic theory of Schottky diode [10]. From fitting the *J-V* characteristics in region II, according to Eq. 5.1, we get $g = 1.8$ in Al/pentacene/Au diode. In region III, J – V characteristics exhibits non-linear behavior due to SCLC and could be fitted with Mott Gurneys square law [28]

$$J_{III} = \frac{9}{8}\mu(T)\epsilon_s\frac{(V - V_{bi})^2}{d^3} \tag{5.2}$$

where $\mu(T)$ is the mobility of charge carriers and depends strongly on temperature due to hopping transport, $d$ is the thickness of the pentacene thin film and $\epsilon_s$ is the dielectric constant of organic semiconductor. Hence, in region III, current follows SCLC showing the power law dependence on applied bias with an exponent of *2* for low bias but the exponent increases at high bias due to field-dependent mobility [6]. $\mu(T)$, estimated by fitting *J-V* characteristics in region III, has been found to be $1.3 \times 10^{-5}$cm$^2$/Vs. Further, $g$ has been found to be greater than *1* in Al/pentacene/Au diode. It has been observed [8] in previous studies also that in hopping transport in disordered organic semiconductors, $g$ can deviate from unity due to the broad distribution of localized states in GDOS. Hence, classical Einstein relation, $D/\mu = k_BT/e$ is needed to be modified as [8, 9, 29],

$$D/\mu = gk_BT/e \tag{5.3}$$

should be applied in order to estimate $D$. Room temperature diffusion coefficient, estimated in this way has been found to be 3.4 $\times 10^{-7}$ cm$^2$/s.

Hence, we are able to obtain $D$ for disordered organic semiconductors. However, these parameters would give accurate results provided the formation of depletion region due to band bending at metal/organic interface can be estab-

lished. As discussed earlier, asymmetry in *J-V* characteristics can be observed without the formation of depletion region also. To confirm the formation of depletion region, *C-V* characteristics of the same Al/pentacene/Au diode has also been shown in Fig. 5.2(a). Similar to *J-V* characteristics, three distinct regions can also be observed in *C-V* characteristics. For *C-V* characteristics, we define the range of applied voltage for region I to be $-3 \geq V \leq 1$. In the reverse bias ($V < 0$), capacitance decreases as the magnitude of the applied bias ($|V|$) increases. In forward bias region ($0 < V < 1$), capacitance increases with voltage. This decrease and increase in capacitance with reverse and forward bias, respectively, confirms the presence of depletion region due to band bending [30]. In this region, capacitance $C_I$ of a Schottky diode as a function of $V$ can be written as [10],

$$C_I = \left( \frac{0.5 A^2 e \epsilon_s N_A}{V_{bi} \pm V} \right)^{1/2} \tag{5.4}$$

where $N_A$ is the acceptor concentration. Positive and negative signs give the capacitance in reverse and forward bias, respectively. When $V$ becomes equal to $V_{bi}$ depletion region is collapsed and the situation is known as the flat band condition. Under this condition depletion capacitance diminishes. Then a peak in *C-V* characteristics should be observed at $V_{bi}$, due to the combined effect of dropping off the depletion capacitance and subsequently increase of the diffusion capacitance [31] (will be discussed in forthcoming section). In Fig. 5.2(a), a peak due to the collapse of depletion region has been observed at $V = 1 \pm 0.05V$ in *C-V* characteristics. Hence, from *C-V* characteristics $V_{bi}$ is obtained to be $1.0 \pm 0.05V$ which is equal to the difference in work functions of two metal, Au and Al. This further illustrates that intrinsic properties of organic molecules (chemical structure etc.) do not play any role in determining the $V_{bi}$. Except, electronic energy levels (HOMO and LUMO) of organic molecules and metal work functions need to be engineered, in order to fabricate a perfect Schottky diode. Also, growth conditions of thin film need to be optimized, to avoid the extra localization of charge carriers by structural disorder induced defects and metal/molecule interface. Further, in region I, if we plot $1/C^2$ as a function of applied bias, it should be a straight line (Eq. 5.4). $1/C^2 - V$ plot has been shown in Fig. 5.2(b) and a straight line also confirms the band bending and presence of

depletion region in Al/pentacene/Au diode. Hence, we conclude from this section that organic Schottky diodes can be successfully used to determine $D$.

For comparison, we have also fabricated ITO/pentacene/Au based hole only devices with both the contacts Ohmic. Resulting $J$-$V$ and $C$-$V$ characteristics have been presented in Fig 5.3. In ITO/pentacene/Au based device, both the contacts act as Ohmic, due to either no barrier at Au/pentacene or negligible potential barrier of 0.2 eV at ITO/pentacene interface for hole injection. We observe that $J$-$V$ characteristics does not show rectification in forward bias region ($V > 0$), rather they are symmetric. Three distinct regions which we observed in asymmetric device (Al/pentacene/Au) are not exhibited in symmetric device (ITO/pentacene/Au). There is no distinguishable region in which current shows exponential dependence on $V$. Rather, for both positive and negative applied bias at Au, current shows the power law dependence on $V$, due to SCLC. Further, slope increases with bias for both positive and negative $V$, due to the field and carrier concentration dependence mobility ($\mu[T, P, F]$), suggested by Pasveer et al. [32]. $J$-$V$ characteristics to determine $\mu[T, P, F]$ have been discussed in Chapter 3 and need not to be solved here again. SCLC is generally exhibited by low mobility semiconductors when metal electrode supplies more charge carriers than that can be transported by the semiconductor in device. Then a space charge is created due to accumulation of charge carriers injected by metal electrode and leads to SCLC in semiconductors. Similar to current, capacitance also show symmetry with respect to forward and reverse bias and three regions disappear in $C$-$V$ also. No peak in $C$-$V$ characteristics is observed, rather, capacitance increases with bias for the whole range of $V$ which further shows that no depletion region is formed when both the contacts are Ohmic. Hence, accumulation of charge for both positive and negative applied bias on Au, gives the capacitance in this region which increases with bias and is known as diffusion capacitance [31].

Further, $J$-$V$ and $C$-$V$ characteristics in symmetric devices (ITO/pentacene/Au) for the whole range of positive and negative voltage, can be considered to be equivalent to those in region III (SCLC region) in asymmetric devices (Au/pentacene/Au) and contribution to capacitance comes from the diffusion capacitance also. Diffusion capacitance ($C_{diff}$) is correlated with corresponding $J$-$V$ characteristics as [31]

$$C_{diff} = \tau \frac{d(J_{III})}{dV} \tag{5.5}$$

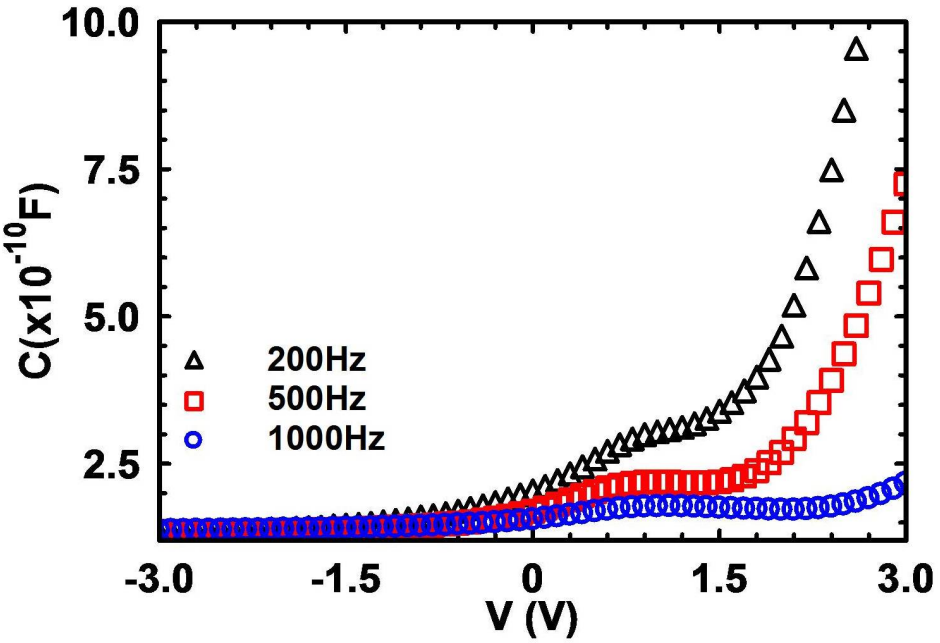


*Figure 5.4: Room temperature C-V characteristics of Al/pentacene/Au based Schottky diodes measured at different frequencies. In SCLC region, capacitance decreases with increasing frequency whereas in depletion region, no significant variation in capacitance with respect to frequency has been observed.*

This explains the origin of capacitance in SCLC region in asymmetric and symmetric devices.

Finally, as there is no exponential dependent region in *J-V* characteristics, it is not possible to estimate $g$ for symmetric devices and hence, these devices cannot be used to estimate $D$. This discussion further demands the Schottky barrier at one contact and consequently formation of depletion region due to band bending. It has been shown [33] in previous study that space charge created due to the accumulated charge gives rise to the frequency dependence of electrical characteristics. This may be helpful in investigating charge carrier dynamics in organic devices. Hence, to study how $C$ in SCLC region depends on frequency ($f$), we have investigated *C-V* characteristics at different $f$.

## 5.4 Dependence of *C-V* characteristics on frequency

To observe the frequency dependence of C-V characteristics for depletion and diffusion capacitance, we have shown C-V characteristics of Al/pentacene/Au at different frequencies in Fig. 5.4. It can be observed in Fig. 5.4 that diffusion capacitance decreases as the frequency increases whereas depletion capacitance does not show significant variation with frequency. Reduction in diffusion capacitance with increasing frequency can be explained as follow. At high frequency, relaxation time of charge carriers in organic semiconductors increases due to low mobility, hence organic devices cannot respond as well at high frequencies, leading to low value of capacitance. In reverse bias, contribution to capacitance comes from the depletion region, hence capacitance does not get affected by frequency of ac signal. Further, as the frequency increases, height of the peak in *C-V* characteristics decreases but the position of peak remains same.

Till now, we have estimated $D$ in organic semiconductors from *J-V* characteristics using generalized Einstein relation and formation of a perfect Schottky diode is also shown in previous sections. In next section, we will show that *C-f* characteristics in SCLC region individually can be employed, to estimate $D$. However, in depletion region, as capacitance does not change significantly with frequency, it is not possible to determine $D$ from *C-f* characteristics in this region.

## 5.5 Frequency dependence of *C-f* characteristics in depletion and SCLC region

*C-f* characteristics of Al/pentacene/Au diode for a fixed bias of 2 $V$ (empty squares) and -2 $V$ (empty circles) have been shown in Fig. 5.5, in order to investigate the variation of capacitance with frequency in SCLC and depletion region, respectively. At a applied bias of 2 $V$ i.e. in SCLC region, capacitance decreases as the frequency increases upto a characteristic frequency $f_t \approx 3 \times 10^3 s^{-1}$, beyond that it becomes almost constant. However, in depletion region (V = –2V), capacitance remains almost same for the whole range of frequency. This has been explained in previous section that decrease in diffusion capacitance at higher fre-

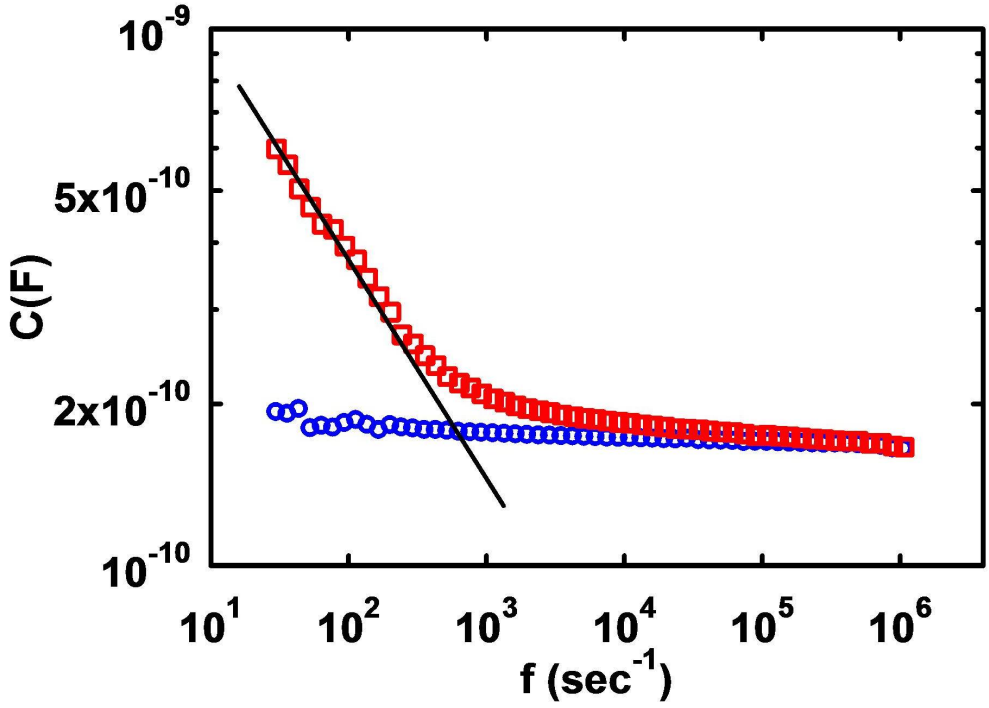


*Figure 5.5: Frequency dependence of capacitance in depletion region (empty circle) and in SCLC region (empty square). Solid line is to show the variaion of C with f clearly.*

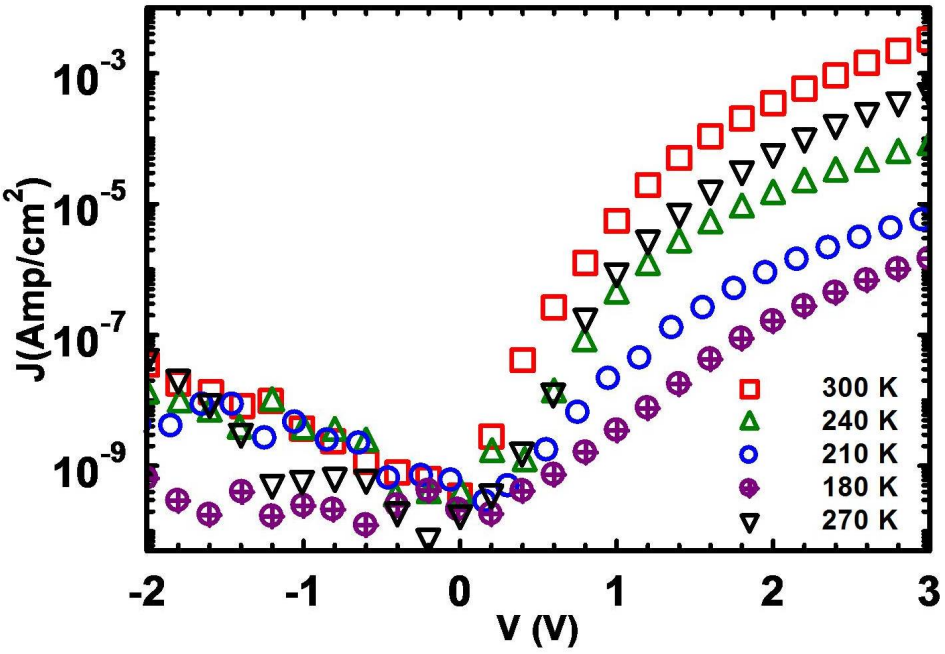


*Figure 5.6: Temperature dependence of J-V characteristics of Al/pentacene/Au Schottky diodes fabricated at 0.1 Å/s.*

quency is attributed to the increase in relaxation time in organic semiconductor and injected charge carriers are not able to rearrange themselves in order to follow the frequency of the ac signal. As in SCLC region, significant contribution to capacitance comes from diffusion capacitance, the frequency at which the capacitance in forward region becomes constant i.e. $f_t$ should correspond to the charge carrier relaxation time $\tau$ in pentacene. If $\tau$ is known, $D$ can be determined using a very fundamental formula of diffusion coefficient [34],

$$D = d^2/\tau \tag{5.6}$$

$d$, being the thickness of pentacene thin film. $f_t \approx 3\times10^3 s^{-1}$ gives $\tau = 3.3\times10^{-4}$s and then using Eq. 5.6, $D$ has been found to be $8\times10^{-7}cm^2/s$, consistent with the vlaue obtained from $J$-$V$ characteristics.

Next, we investigate how $D$ varies with temperature. For this we performed temperature dependent measurements for $J$-$V$ characteristics.

## 5.6 Evaluation of temperature dependence of *D*

To understand the carrier dynamics in organic Schottky diode and to estimate the temperature dependence of $D$, we have plotted $J$-$V$ characteristics of Al/pentacene/Au diode at different temperatures in Fig. 5.6. We observe that the two regions, II and III exhibiting diode-like characteristics and SCLC, respectively, can be distinguished clearly at high temperatures. However, as temperature decreases, II region starts merging with the III region. It means that Schottky junction starts weakening as we go to lower temperatures i.e depletion region does not form at sufficiently low temperatures because as the thermal energy of holes is low, they get neutralized by the acceptors in organic semiconductor. Further, $g$ and $\mu$ at different temperatures have been estimated independently from II and III regions of $J$-$V$ characteristics, respectively and then $D$ using generalized Einstein relation have also been estimated at different temperatures. Variations of $g$, $\mu$ and $D$ with temperature have been shown in Fig. 5.7. $\mu$ and $D$, decrease with temperature but $g$ increases i.e. the ratio $D/\mu$ increases.

Decrease in $\mu$ and $D$ with temperature is obvious due to the decrease in thermal energy of charge carriers. However, increase in $D/\mu$ can be explained as follows. Charge transport in organic semiconductors is characterized by two energy levels i.e. equilibrium level ($E_{eq} = -\sigma^2/k_BT$, $\sigma$, being the width of GDOS) and a transport level ($E_{tr} = -5/9\sigma^2/k_BT$) [35]. $E_{eq}$ and $E_{tr}$ are the levels to which charge carries relax and hop, respectively. At high temperature, a small deviation from unity in $D/\mu$ is observed because charge carriers have sufficient thermal energy to hop to $E_{tr}$. Hence, a number of charge carriers contribute to drift transport, resulting in small deviation in $D/\mu$. However, as temperature decreases, $D/\mu$ increases continuously, due to the enhanced diffusion of charge carriers. Because, at low temperature, $E_{eq}$ lies deeper in the tail of GDOS than that at high temperature. Hence, less number of charge carriers hop to $E_{tr}$ and accumulation of charge carriers having non-uniform distribution takes place in the tail of GDOS. Due to the charge density gradient, large fraction of charge carriers contributes to diffusive transport, leading to a high value of $D/\mu$ . It means that as the temperature is lowered, diffusive transport relative to drift starts dominating. $E_{eq}$ and $E_{tr}$ for low and high temperatures have been shown in Fig 5.8.

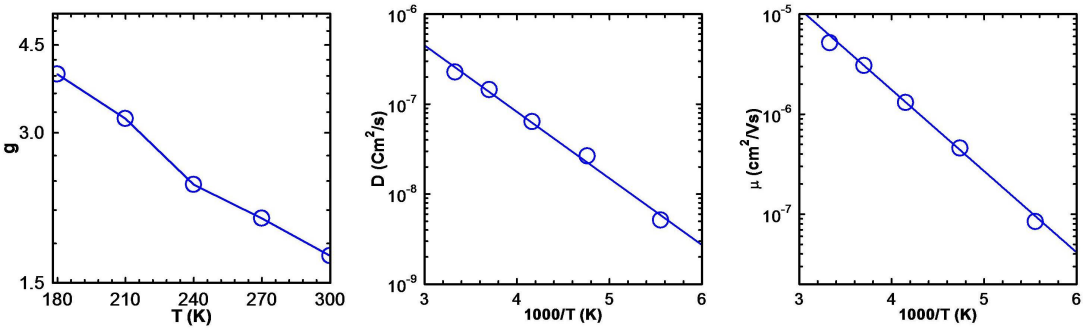


*Figure 5.7: Temperature dependence of (a) g, (b) D and (c) μ, in Al/pentacene/Au device.*

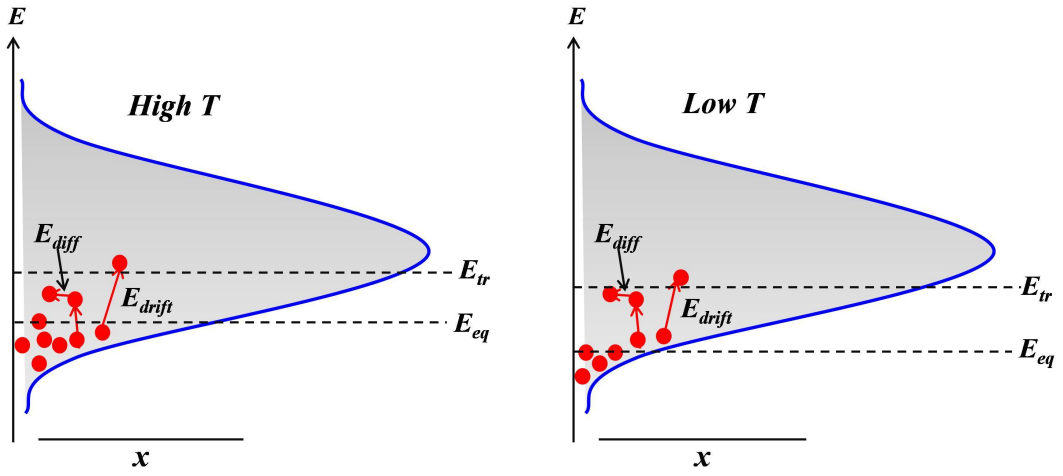


*Figure 5.8: Schematic representation of two charge transport governing energy levels, $E_{eq}$ and $E_{tr}$ in GDOS, at high and low temperatures. Both levels move towards the tail of the GDOS at low temperatures.*

Further, $D$ and $\mu$ show the Arrhenius-type temperature dependence, as shown in Fig. 5.7. Activation energies for diffusion ($E_{diff}$) and drift ($E_{drift}$) have been estimated to be 114 meV and 122 meV, respectively. Activation energies for drift and diffusion are found to be comparable with each other however, $E_{drift}$ is little bit higher than $E_{diff}$ and this also reflects the significance of diffusive transport in organic semiconductors.

Although, two methods have been presented to estimate the diffusion coefficient in organic semiconductors and congruence of the values of $D$ from these two methods also establishes the significance of this simple method. To corroborate the experimental results, Marcus theory [36, 37] is used to estimate charge transfer rates ($k_{ij}$) and intrinsic mobilities ($\mu$ )in hopping regimes. Surprisingly, it can be efficiently used to estimate $D$. For this, we have used the first-principle density functional theory (DFT) in the same manner as discussed in Chapter 3, to estimate $k_{ij}$. As, we have used two terminal sandwiched devices to estimate $D$, it corresponds to diffusion of charge carriers along c-axis. Along this direction, as there is only one significant dimer, that decides charge transport in two termial devices. Hence $k_{ij}$ and $D$ have been estimated along this direction only and have been found to be 1.43 $\times 10^{11} s^{-1}$ and 1.02 $\times 10^{-6} cm^2/Vs$. Intrinsic $D$ estimated in this way is little higher in magnitude than that observed experimentally and attributed to the non inclusion of thermal and energetic disorders in theoretical calculations.

## 5.7 Conclusion

In summary, diffusion of charge carriers is a crucial phenomenon and cannot be ignored when studying and modeling charge transport in organic semiconductors. *J-V* and *C-f* characteristics of a two terminal device can be independently employed to determine $D$ in disordered organic semiconductors provided one of the two terminals of the device should provide a near perfect Schottky barrier by the presence of depletion region due to band bending. Consistency in the magnitudes of $D$ estimated using two methods establishes that generalized Einstein relation is required for organic semiconductors having broad distribution of density of states. Theoretically estimated $D$ using DFT is also found to be consistent with those observed experimentally.

# Bibliography


[1] S. R. Forrest, Nature **428**, 911, (2004).

[2] V. Coropceanu, A. Demetrio, S. Filho, Y. Olivier, R. Silbey, and J. Bre, Chem. Rev. **107**, 926 (2007).

[3] G. Horowitz, Adv. Mater. **10**, 365 (1998).

[4] R. Richert, L. Pautmeier, and H. Bassler, Phys. Rev. Lett. **63**, 547 (1989).

[5] S. R. Mohan, M. P. Singh, M. P. Joshi, and L. M. Kukreja, J. Phys. Chem. C **117**, 24663 (2013).

[6] H. Bassler, Phys. Status Solidi B **175**, 15 (1993).

[7] A. A. Berezin, Phys. Lett. **86A**, 480 (1981).

[8] Y. Roichman and N. Tessler, Appl. Phys. Lett. **80**, 1948 (2002).

[9] G. A. H. Wetzelaer, L. J. A. Koster, and P. W. M. Blom, Phys. Rev. Lett. **107**, 066605 (2011).

[10] S. M. Sze and K. K. Ng, Physics of Semiconductor Devices, 3rd ed.; Wiley India, 2010.

[11] R.J. Chesterfield, J.C. Mckeen, C.R. Newman, P.C. Ewbank, S. Filho, J. Bre, L.L. Miller, K.R. Mann, and C.D. Frisbie, J. Phys. Chem. B **108**, 19281 (2004).

[12] Wei-Qiao Deng and William A. Goddard, J. Phys. Chem. B **108**, 8614 (2004).

[13] Hao-En Tseng, Tzu-Hao Jen, Kang-Yung Peng, and Show-An Chen, Appl. Phys. Lett. **84**, 1456 (2004).

[14] A. K. Tripathi, D. C. Tripathi, and Y. N. Mohapatra, Phys. Rev. B **84**, 041201R (2011).

[15] I. Salzmann, G. Heimel, S. Duhm, M. Oehzelt, P. Pingel, B.M. George, A. Schnegg, K. Lips, R.-P. Blum, A. Vollmer, and N. Koch, Phys. Rev. Lett. **108**, 035502 (2012).

[16] Y. Shen, M. Klein, D. Jacobs, J. Campbell Scott, and G. Malliaras, Phys. Rev. Lett. **86**, 3867 (2001).

[17] A.K. Mahapatro and S. Ghosh, Appl. Phys. Lett. **80**, 4840 (2002).

[18] W. Silveira and J. Marohn, Phys. Rev. Lett. **93**, 116104 (2004).

[19] Novikov, S.V. and Malliaras, G.G., Phys. Status Solidi B **243**, 391 (2006).

[20] T. Hosokai, H. Machida, a. Gerlach, S. Kera, F. Schreiber, and N. Ueno, Phys. Rev. B **83**, 195310 (2011).

[21] Z. Zhang and J.T. Yates, Chem. Rev. **112**, 5520 (2012).

[22] R. Schlaf, P.G. Schroeder, M.W. Nelson, B. a. Parkinson, P. a. Lee, K.W. Nebesny, and N.R. Armstrong, J. Appl. Phys. **86**, 1499 (1999).

[23] Y. Harima, K. Yamashita, H. Ishii, and K. Seki, Thin Solid Films **366**, 237 (2000).

[24] R. Agrawal, and S. Ghosh, Appl. Phys. Lett. **89**, 222114 (2006).

[25] B.N. Pal, J. Sun, B.J. Jung, E. Choi, A.G. Andreou, and H.E. Katz, Adv. Mater. **20**, 1023 (2008).

[26] T. Kirchartz, W. Gong, S. a. Hawks, T. Agostinelli, R.C.I. MacKenzie, Y. Yang, and J. Nelson, J. Phys. Chem. C **116**, 7672 (2012).

[27] C. Pramanik and G. P. Miller, Molecules **17**, 4625 (2012).

[28] R. Agrawal, P. Kumar, S. Ghosh, and A.K. Mahapatro, Appl. Phys. Lett. **93**, 073311 (2008).

[29] K. Harada, A. G. Werner, M. Pfeiffer, C. J. Bloom, C. M. Elliott, and K. Leo, Phys. Rev.Lett. **94**, 036601 (2005).

[30] A. Sharma, P. Kumar, B. Singh, S.R. Chaudhuri, and S. Ghosh, Appl. Phys. Lett. **99**, 39 (2011).

[31] D. A. Neamen, Semiconductor Physics and Devices, 3rd ed. (Tata McGraw-Hill, New Delhi, 2007).

[32] W. F. Pasveer, J. Cottaar, C. Tanase, R. Coehoorn, P. A. Bobbert, and P. W. M. Blom, D. M. de Leeuw, and M. A. J. Michels, Phys. Rev. Lett. **94**, 206601 (2005). Chem. Soc. **127**, 16866 (2005).

[33] H. Campbell, P. S. Davids, and D. L. Smith, Appl. Phys. Lett. **72**, 1863 (1998).

[34] A. Einstein, Ann. Phys. **17**, 549 (1905).

[35] T. V. Woudenbergh, Charge injection into organic semiconductors. Diss. University of Groningen, 2005.

[36] R. A. Marcus, Rev. Mod. Phys. **65**, 599 (1993).

[37] G. R. Hutchison, M. A. Ratner, and T. J. Marks, J. Am.

# Chapter 6

# Conclusions

Understanding the elementary process behind the complex charge transport in organic semiconductors is essential to optimize the performance of organic devices. In this thesis, we have presented systematic experimental and theoretical investigations on charge transport mechanism in organic molecular semiconductors and tried to correlate the macroscopic charge transport parameters with microscopic molecular parameters. It seems that current classification of mechanism of charge transport on the basis of degree of crystallinity of the semiconductors is not valid and a generalized theory based on degree of localization of charge carriers should be developed.

## 6.1 Summary

The work presented in this thesis is motivated by emerging research in organic semiconductors due to their several advantages such as large area fabrication, low cost, easy processing, possibility of fabrication on flexible and transparent substrates etc. These properties of organic semiconductors lead to their enormous applications in electronic and opto-electronic devices. Despite the phenomenal progress in organic semiconductor based electronics in last few years, considerable debate is going on very fundamental issues regarding the charge carrier transport in these materials. This thesis is focused on a comprehensive investigation on the charge transport in organic semiconductors from both macroscopic and microscopic views. Systematic experimental and theoretical studies have been performed to pursue the purpose.

In **Chapter 2**, we have systematically investigated the charge transport mechanism in copper phthalocyanine (CuPc) based polycrystalline organic thin films, with and without traps. Density of trap in CuPc thin films has been controlled by engineering different growth conditions. Surface morphology of CuPc thin films grown at low substrate temperatures ($T_G$) of 40$^o$C exhibits polycrystalline grainy structure with almost equal sized grains (40-60 nm) and a large number of grain boundaries. These grain boundaries act as traps for charge carriers and hinder the charge transport in organic thin films. On the other hand, surface morphology of thin films grown at high $T_G$ of 120$^o$C shows anisotropic nanowire like structure with very less or negligible grain boundaries, hence provides a smooth path for charge carriers to move in thin film. To investigate the charge transport in CuPc thin films with and without traps, we have fabricated two terminal and three terminal based devices. Current-Voltage ($J$-$V$) characteristics of two terminal devices (ITO/CuPc/Au) fabricated at low $T_G$ could be well fitted to trap charge limited conduction (TCLC). Further, to confirm the existence of traps in CuPc thin films grown at low $T_G$, capacitance-frequency ($C$-$f$) and capacitance-temperature ($C$-$T$) characteristics of Al/CuPc/Au based Schottky diodes have been measured. A step in ($C$-$f$) and ($C$-$T$) characteristics confirms the existence of trap in CuPc thin films grown at low $T_G$. On the other hand, $C$-$f$ and $C$-$T$ characteristics of Al/CuPc/Au based Schottky diodes in which CuPc thin films are grown at high $T_G$, don't show any peak and hence no distribution of trap

has been obtained. Further, *J-V* characteristics of ITO/CuPc/Au two terminal devices based on CuPc thin films grown at high $T_G$ follows field-dependent space charge limited conduction (SCLC), rather than TCLC. This further supports for the absence of traps in CuPc thin films grown at high $T_G$. Next, to study charge transport mechanism thin film parallel to film surface, we have fabricated organic field effect transistors (OFETs) with CuPc thin films with and without traps. To study the conduction mechanism, we have plotted the charge carrier mobilities ($\mu$) as a function of temperature ($T$) and gate voltage ($V_G$), separately, for the OFETs with and without traps. Dependence of $\mu$ on $V_G$ and $T$ shows that multiple trapping and release (MTR) model can be applied to explain the charge transport in OFETs based on polycrystalline CuPc thin films with traps whereas percolation model (PM) can explain charge transport in OFETs without traps. Finally, we conclude that chareg transport mechanism in polycrystalline thin films of CuPc with and without traps are completely different whether charge transport is considered parallel or perpendicular to the substrate.

It is extremely important to investigate the trap and their role on charge transport thoroughly, because to investigate the role of microscopic parameters on the charge transport would be a futile exercise unless the thin films have negligible traps.

In **Chapter 3** we have shown that though, optimization of surface morphology and crystalline quality of organic thin films is required, in order to get the maximum mobility in devices however, physics of charge transport cannot be understood on the basis of surface morphology and crystalline quality dependence of mobility. Here, we have investigated charge transport in anisotropic (pentacene) and isotropic (phthalocyanines) molecules using both macroscopic and microscopic approaches. To study charge transport from macroscopic view, we have fabricated devices in different configurations with the same organic thin film of pentacene grown under optimized conditions and then devices in same configuration but with different organic thin films of phthalocyanines. Large difference in magnitudes of mobility in pentacene thin film, parallel and perpendicular to the film surface has been observed. Similarly, difference in mobilities in different phthalocyanines thin films parallel to the surface have been observed in spite of identical surface morphologies and X-ray diffraction patterns. To explain the origin behind this anisotropy in mobility, we have performed first principles den-

sity function theory (DFT) calculations for the different dimers in unit cells of pentacene and phthalocyanines. Anisotropy in the mobility of pentacene in two terminal and three terminal devices has been explained on the basis of strong coupling between dimers in the plane parallel to the thin film surface and weak coupling between the dimers along the perpendicular to the film. Difference in mobilities in different phthalocyanine based OFETs has been attributed to the different chemical structures of phthalocyanines. Thus a correlation between macroscopic mobility and microscopic molecular parameters has been established.

In **Chapter 4** we have investigated the fundamental mechanism behind the localization of charge carriers in organic thin films that leads to thermally activated hopping of charge carriers in polycrystalline thin film based OFETs. For this we have studied the conduction in pentacene thin film based OFETs in both negative as well as positive source-drain bias ($V_{DS}$) regime. In the negative $V_{DS}$ regime, room temperature mobility is found to be 0.3 $cm^2$/Vs consistent with the mobility of pentacene in hopping regime. Arrhenius-like temperature dependence of mobility in negative $V_{DS}$ regime also confirms the hopping transport in pentacene thin films. Surprisingly, when a positive instead of negative $V_{DS}$ is applied, OFETs become identical to the two terminal device with the difference that background carrier concentration can be controlled by an additional $V_G$ in OFETs. $I_{DS}$ – $V_{DS}$ characteristics at different $V_G$ are also found to be similar to that of a hole only device i.e initially Ohmic and then SCLC. Room temperature mobility has been found by fitting the $I_{DS}$ – $V_{DS}$ characteristics according to field dependent SCLC and found to be 48.3 $cm^2$/Vs consistent with band mobilities in pentacene. Further, in positive $V_{DS}$ regime mobilities exhibit negative temperature coefficient at high temperature, confirming charge transport limited by phonon scattering. The mechanism behind a crossover from localized charge transport in the negative $V_{DS}$ regime to delocalized charge transport in positive $V_{DS}$ regime can be explained by the position of Fermi level. In the negative $V_{DS}$ regime, Fermi level lies in the tail of the Gaussian density of states (GDOS) due to the depletion region formed from pinching off the channel near drain contact however, Fermi level lies near the center of GDOS in positive $V_{DS}$ regime due to absence of depletion region. As density of localized states increase as Fermi level moves from tail towards the center of GDOS, charge carriers need lesser activation energy to hop to neighboring sites. In the center of GDOS density of

localized states is so high that charge carriers need no activation energy and they move as a delocalized wave. Hence, it is possible to observe, both the hopping and the band-like transport in the same organic system.

In **Chapter 5**, a simple and direct method to estimate diffusion coefficient ($D$) of charge carriers in organic semiconductors has been presented, by using simple two terminal sandwiched devices. As, in organic semiconductors charge carriers are localized in the tail of GDOS and move to neighboring site by phonon assisted tunneling, non-uniform charge distribution exists leading to diffusive charge transport along with the drift motion. $J$-$V$ and $C$-$f$ characteristics of a two terminal device can be independently employed to determine $D$ in disordered organic semiconductors provided one of the two terminals of the device should provide a Schottky barrier by the presence of depletion region due to band bending. Consistency in the magnitudes of $D$ estimated using two methods establishes that generalized Einstein relation is required in organic semiconductors having broad distribution of density of states. Theoretically estimated $D$ using DFT is also found to be consistent with those observed experimentally.

## 6.2 Scope for future work

Although, we have presented a detailed investigation on charge transport in organic semiconductors and tried to correlate charge transport with microscopic molecular parameters, there are still some issues regarding the basic mechanism of charge transport in these systems and should be further debated.

**(i)** Development of a generalized theory that classifies the different regimes of charge transport on the basis of degree of localization of charge carriers rather than on the degree of crystallinity of organic semiconductors. As the mobility is measured in plane and perpendicular to plane, similar anisotropy in diffusion coefficients needs to be carried out.

**(ii)** More investigation on the diffusion of charge carriers in organic semiconductors is required as two terminal devices used in this study estimates the diffusion coefficients along the direction perpendicular to the film surface.

**(iii)** Detailed molecular dynamics simulations at different temperatures need to be carried out to find out diffusion barrier to compare with experimental values.